AD NUMBER

AD117710

NEW LIMITATION CHANGE

TO

Approved for public release, distribution unlimited

FROM

Distribution authorized to U.S. Gov't. agencies and their contractors; Administrative/Operational Use; Sep 1956. Other requests shall be referred to Air Weather Service [Air Force], Military Air Transport Service, Washington, DC.

AUTHORITY

AFWA ltr, 19 Apr 2005

AD117710

AWSM 105-47

AIR WEATHER SERVICE MANUAL

~~FOR OFFICIAL USE ONLY~~

~~(AFR 190-16)~~

CONSTANT-PRESSURE TRAJECTORIES

REDESIGNATED

AWS TECHNICAL REPORT 227

SEPTEMBER 1956

HEADQUARTERS
AIR WEATHER SERVICE
MILITARY AIR TRANSPORT SERVICE
UNITED STATES AIR FORCE
Washington 25, D.C.

AWS MANUAL
No. 105-47

HEADQUARTERS
AIR WEATHER SERVICE
MILITARY AIR TRANSPORT SERVICE
UNITED STATES AIR FORCE
Washington 25, D. C.
September 1956

FOREWORD

1. Purpose. To aid AWS personnel in constructing trajectories for constant-pressure-balloon flights.

2. Scope.

a. Several current methods for obtaining the trajectories from the usual upper-level, constant-pressure contour charts or flow charts are described. Also included is a new, so-called "AWS Method" developed by Dr. Karl R. Johannessen in this headquarters. The merits of the various methods are presented with directions for selecting the method most suitable for a given problem.

b. Since the trajectory problem is intimately connected with analysis and forecasting of the upper-level contour field or flow field, comment is made on the special requirements imposed on the analysis and forecasting of these fields when they are to be used for obtaining trajectories.

c. The Manual is divided into two primary sections: 1) operational, and 2) theoretical. Although they are complementary with frequent cross references, the operational portion is written to stand alone for procedural use. The theoretical portion has been added only for those who desire a more complete understanding of the entire trajectory problem.

d. Although techniques similar to those used for determining constant-pressure trajectories are used also in solving problems of atmospheric diffusion and dispersion, this Manual does not include atmospheric dispersion of particulate matter within its scope. The manner in which methods described in this Manual may be applied to dispersion problems is outlined in AWS TR 105-62 [13].

3. Supply of Manuals. This Manual is stocked at Headquarters MATS, Command Adjutant, Publishing Division. Additional copies may be requisitioned from Headquarters Air Weather Service, ATTN: AWSAD, in accordance with AWSR 5-3, as amended.

BY ORDER OF THE COMMANDER:

OFFICIAL:

Richard E. Bell

RICHARD E. BELL
Major, USAF
Adjutant

RICHARD M. GILL
Colonel, USAF
Chief of Staff

DISTRIBUTION:
"S" augmented to 3 copies for each forecast center and 5 copies for each weather central (less the 20% overage for stock) plus "Z".

TABLE OF CONTENTS

TABLE OF CONTENTS (Cont'd)

LIST OF TABLES

LIST OF ILLUSTRATIONS

LIST OF ILLUSTRATIONS (Cont'd)

LIST OF ILLUSTRATIONS (Cont'd)

Section I

OPERATIONAL ASPECTS OF CONSTANT-PRESSURE TRAJECTORIES

1.1. Introduction and Definitions.

The trajectory of any object is the locus of the successive positions it occupies in space. If we further place marks along this geometric curve and denote the times when the object coincides with these marks, the trajectory completely describes the motion of the object. Specifically, when the object is a parcel of the atmosphere, we speak about an air trajectory. Since the air generally moves vertically as well as horizontally, an air trajectory is a three-dimensional curve.

By a constant-pressure-surface trajectory or in short a constant-pressure trajectory, is meant the trajectory of an object that at all times stays in a constant-pressure surface and moves with the wind in this surface. Such a trajectory is approximated by a balloon that is controlled to float at a constant pressure, i.e., a constant-pressure balloon.

This Manual is mainly concerned with constant-pressure-surface trajectories.

A constant-pressure trajectory will usually not coincide with the air trajectory originating from the same point in time and space. Only when the flow is isobaric (i.e., the air does not ascend or descend through the pressure surface in question) will this be the case.

Also, the horizontal projection of the air trajectory through a point is usually different from the constant-pressure trajectory through the same point. The difference between the two types of trajectories is well illustrated by an interesting study by Wexler [31]. Wexler attempted to trace the smoke pall that occurred in September 1950 over locations in the eastern United States back to the forest fires in Canada that originated the smoke. Constant-pressure trajectories at various pressure levels failed to lead back to the correct origin. The air and the smoke with it followed air trajectories which, because of the vertical displacement of the air, had horizontal projections considerably different from any of the constant-pressure trajectories. Only when the trajectory was computed on isentropic surfaces did it lead back to the correct origin.

In routine forecasting meteorologists are only indirectly concerned with the question, "Where does the air come from?" or, "Where does the air go to?" Since we are used to studying flow patterns at synoptic hours, our forecasting experience and forecasting rules have come to be based on the succession of these synoptic charts. In other words, we think in terms of change of flow patterns rather than in terms of change of position of the air parcels composing the flow. Hence, construction of trajectories requires special techniques.

The first large-scale attempt at computing atmospheric trajectories was done by Shaw and Lempfert [27] who studied trajectories of the surface currents over England and northwest France. In the United States, Meisinger [21] was a pioneer. He made several "constant"-altitude balloon flights from 5000 to 10,000 feet and compared the trajectories with the sea-level ("surface") pressure chart (the only chart available at that time). In one flight from Fort Omaha to Arkansas, he found that the actual average speed of the balloon (5000 feet) and the average speed computed from the gradient wind, coincidentally, agreed within 1 knot.

Interest in constant-level balloons was revived during and after World War II, when their potentialities for meteorological research again became apparent.

1.2. Constant-Pressure Balloons.

The balloons currently in use ascend at a rate of 700-1000 feet per minute, and can be controlled to float at a predetermined pressure. Balloons have been flown in the past at a wide variety of pressures, mostly ranging from 300 mb to 50 mb, or even higher.

When the balloon approaches the intended floating pressure, gas is let out to decrease buoyancy and stop the ascending motion. If the balloon for some reason should start sinking below this pressure level, ballast is expended to increase the buoyancy. The flows of gas and ballast are controlled barometrically. To keep the expenditure of gas and ballast at a minimum and to keep the oscillations about the stable pressure value small, the baroswitch flow-controls are quite complex devices to provide some kind of damping on the oscillations.

Disturbances that may upset the equilibrium after it is once established, may stem from various sources: vertical currents, diffusion of gas through the balloon, changes of temperature of the ambient air,

changes in temperature of the gas in the balloon due to change in the insolation and long-wave radiation. The changes in insolation are particularly large at sunrise and sunset and would cause large changes in the altitude of the balloon if not compensated for by release of gas or ballast. Hence, expenditure of gas and ballast is greatest at sunset and sunrise and largely determines the practical limit of the flight duration of present constant-pressure balloon systems.

The duration may be several days. Balloons released from points in the western and mid-western United States have been recovered from as far as Norway and Algeria after about 3 days flight. During World War II the Japanese released their "balloon bombs" from Japan. About 10% of these were found on the West Coast of the North American Continent and many more probably reached land without being discovered. This represents a distance of 5000 miles or more.

The balloons are usually able to stay within 10-15 mb of the intended floating pressure.

The balloons may carry a radio transmitter and a power supply for tracking purposes and for sending other pertinent information such as pressure altitude, ballast expenditure, etc. A parachute may be attached to recover instruments after flight termination.

Constant-pressure ballons are valuable tools in meteorological research. They provide measurements of winds and accelerations, to an accuracy not obtained before. Indirectly, they can provide estimates of derived quantities such as pressure gradients, vertical motions, eddy spectra, etc.

It has been suggested that constant-pressure balloons released at regular intervals from favorable sites be used to supply upper-air data for routine synoptic charts (Navy transosondes).

1.3. Weather Requirements for Balloon Launching.

Strong surface winds and precipitation adversely affect the launching of the balloons.

Launching in winds of more than 25 knots is usually not attempted with present launching techniques. The wind direction also has to be considered locally with regards to clearing ground obstructions.

Rain or snow increases the load on the balloon and upsets the planned ascent rates or even prevents it from rising.

Launching in strong convective storms must be avoided for obvious

reasons (turbulence, icing, and precipitation of rain, snow, or hail).

Similarly, the balloon must not rise through cloud layers that contain supercooled droplets. Even light icing is likely to terminate the flight.

1.4. Kinematic and Dynamic Methods.

A constant-pressure balloon will drift with the air that surrounds it at any time. Hence, if the wind in the pressure surface is known at all points and at all times during the flight, the trajectory can be constructed as follows: starting at the initial point and time, move the balloon with the wind for a short time interval, determine the wind at the new position and time, and then move it on for another time interval with this new wind, etc. Methods of constructing the trajectory in this manner from knowledge of the wind field are called kinematic methods.

In practice the wind field is analyzed or prognosticated only at certain synoptic times, usually 12 or 24 hours apart, and the kinematic methods to be used in practice must be based on these synoptic charts. Some assumption as to how the flow on Chart h gets transformed into the flow on Chart h + 12 hours or h + 24 hours has to be made. It is mainly as to how this transformation occurs that the various kinematic methods differ. For instance, the Central Tendency Method assumes that the flow remains stationary for a period from 6 hours before to 6 hours after map time and that the transition to the flow of the next chart occurs discontinuously. Another example: the Linear Interpolation Method assumes that the wind at a point changes linearly with time in the period between two charts.

The kinematic methods that are described in Section I of this Manual are: 1) Petterssen's Method, 2) the Central Tendency Method, 3) Consecutive Streamline Methods, 4) the Linear Interpolation Method, 5) the Relative Trajectory Method, and 6) General Mill's Method.

These methods all have their particular advantages and it cannot be stated that any one of them is superior to the others under all conditions. This fairly complete list of standard kinematic methods has, therefore, been included in the Manual. The selection of the optimum method under certain conditions depends on many factors. Among these factors are: accuracy of the chart representation of the flow, length of period between synoptic charts, the flow patterns themselves and

their behavior, the time available for trajectory construction, and the desired accuracy of the trajectory. (See 1.15 for choice of method.)

There is another avenue open for constructing constant-pressure trajectories. This is the dynamic approach. The horizontal motion (acceleration) of an air parcel is determined by the magnitude and direction of the horizontal pressure force acting on it and by the Coriolis force. In addition, the vertical motion of the air through the pressure surface turns up as an influencing term when we pass from considering the horizontal motion of an air parcel to considering the horizontal motion of a constant-pressure balloon. This vertical motion influence has to be neglected since we as yet have no means of charting the vertical motions; furthermore, it can be neglected with a fair approximation. The magnitude of the errors which may result from this is discussed in paragraph 2.1.2.

The Coriolis force depends on the instantaneous velocity of the air and latitude. The pressure force can be measured from contour charts. Hence, if the initial position and velocity of the balloon is known, the future path and velocity can be determined from the contour gradient through which it moves.

The only two practical dynamic methods which have been proposed to date are the Franceschini-Freeman Method and the AWS Method described in sub-sections 1.12 and 1.13, respectively. Dynamic methods in general are discussed in sub-sections 2.1.1 through 2.1.9.

1.5. Special Requirements Imposed on Analysis and Forecasting.

When analytical and prognostic charts are being prepared for use in trajectory computations, they must be prepared with this special purpose in mind. Errors of analysis and prognostication will affect the trajectory forecast differently than they will affect, for instance, the forecast winds for an aircraft flight. When forecasting for an aircraft flight, the main concern is to make the mean vector error of the forecast along the track as small as possible. In light winds the wind direction may well be 180 degrees off without materially affecting the planned flight. This is not the case for air trajectories. If the balloon floats in an area of light winds and the computed direction is wrong by a large amount, the balloon will gradually drift off in a direction opposite to the one expected and may get into a stronger air current of a direction entirely different from that of the forecast

trajectory.

This example illustrates the need for all possible care to get an accurate analysis and prognosis of the wind field (when kinematic methods are used) or of the contour field (when dynamic methods are used) at each individual point in the general region of the expected trajectory.

1.5.1. Kinematic Methods. When kinematic construction methods are used, the primary concern is to obtain a correct representation of the wind field. To get a correct contour field is only a secondary object. The contour field is important only insofar as it may serve to give estimates of the wind field through approximations such as the geostrophic wind, gradient wind, or other wind-contour relationships. Such estimates are necessary wherever the wind observations alone are not dense enough to define the wind field. Only over limited regions of the chart are the wind observations dense enough to permit a direct wind analysis; and even in these regions, height values have to supplement the analysis at levels above 200 mb where wind observations become sparse.

In ordinary analysis work both winds and pressure heights are used in a complementary way to draw the topography of constant-pressure surfaces. Increasing reliance is placed on wind reports and less on height reports with higher levels, since the errors in the pressure heights increase about linearly with height. In addition to contour analysis, isotachs are often entered on the charts to give a better definition of the wind-speed field when the data warrants such a specific definition.

Over a fairly dense network as in the United States and Western Europe, isotach analysis should definitely be added to the analysis to help define the wind field as well as possible. On prognostic maps the contours may be used as streamlines since in prognoses it is usually not possible to distinguish between the directions of streamlines and contours. Streamlines should be drawn for the purpose of hindcasting trajectories, preferably by the Sandstrøm technique.

To permit an accurate streamline and isotach analysis the winds must be plotted with a protractor and the direction and speed entered in numbers. This is a requirement for trajectory work in sparse-data regions also.

The isotachs should also be carried on the prognostic charts for

up to 24 hours. Beyond 24 hours it is doubtful if anything be achieved by carrying isotachs on the prognostic charts.

In a somewhat less-dense data region, e.g., the North Atlantic Ocean, isotachs may also be entered on the constant-pressure analysis from 300 to 150 mb. Since wind reports at these levels are far apart, the analyst has to rely on his experience of associating the isotach patterns with the lower, better documented levels. Above 150 mb the speeds again decrease so that they can be represented with the accuracy of which we are capable by means of contours.

In regions of limited data coverage the flow analysis hinges on height reports to a large extent. The question here arises as to what relationship between height field and wind field should be used.

Hughes et al [16] investigated empirically various methods for computing upper-level winds from constant pressure charts.

The authors recommend that Lambert conformal projections be used in such computations since the curvature of a line on the map will then closely approximate the geodesic curvature of the line on the earth. Using for instance a polar stereographic projection the difference between the real and the measured curvature can theoretically result in errors of 20-25% in the computed wind in the jet region.

The authors found that the gradient speed is a better approximation to the observed speed than the geostrophic speed in areas of cyclonic curvature of the contours; in anticlyclonic curvature the gradient speed is not an improvement on the geostrophic speed; in fact, the geostrophic speed was somewhat better.

It was further attempted to reduce the differences between computed and observed wind speed by taking into account the speed of the pressure system. The results of this attempt, however, were inconclusive. Hence, until it has been shown that a significant improvement on the simple gradient wind computation is effected by correcting for the speed of the pressure system, it is recommended that the straight gradient wind be used in cyclonic curvature of the contours.

In anticyclonic curvature of the contours the geostrophic wind should be used if it is less than 40 knots. If the speed is greater than 40 knots, add 20% to it. This is entirely an empirical correction, but by applying it to their sample the authors found that the accuracy of the computations in the anticyclonic cases became comparable to that of the cyclonic cases. The errors were less than 10% of the observed wind speed one-third of the time and less than 30% two-thirds of the time.

Several authors have attempted to find a more accurate wind-contour relationship than the gradient wind, including factors such as speed of the pressure system, spreading or tightening of contours, confluence or diffluence of contours, etc. Perkins' [24] Central Wind Solution is from a theoretical point of view probably the most satisfactory formula that has been proposed. It appears, however, that the difficulties involved in measuring the quantities involved from upper air maps are so great that only the crudest effects such as that of the cyclostrophic correction are worth including in practical computations. This was the conclusion arrived at by Gustafson [14] in a study on wind-contour relationships.

To sum up: In cyclonic curvature of the contours the gradient wind should be used. In anticyclonic curvature the geostrophic speed should be used when it is less than 40 knots. When it is more than 40 knots, add 20% to the speed.

For computation of the gradient wind see AWS Manual 105-32. Gradient wind scales for various projections and map scales have been issued as AWS Form 32 (A-F). They are to be used with the tables in AWS Manual 105-32.

1.5.2. Dynamic Methods. When trajectories are to be constructed by dynamic methods, for instance by the Air Weather Service Method, the analysis (or prognosis) should aim at an accurate representation of the contour field. Wind and height reports both have to be used in a complementary way in the analysis, particularly at high levels where the height reports become unreliable. The primary object is now the contour field; the wind field is a secondary object and it serves to help determine the contour field. In this determination the wind-contour relationships recommended in the previous paragraph are used in reverse. In cyclonic flow, space the contours so that the observed wind becomes the gradient wind determined from the contour spacing and curvature. In anticyclonic flow, space and contours geostrophically if the observed wind is less than 40 knots. If the observed wind is more than 40 knots, reduce it by 20% and space the contours to agree geostrophically with this reduced speed. (The reduction should be 1/6 or about 17% to get full consistency with sub-section 1.5.1, but the difference between 17 and 20% is here immaterial.)

1.6. Petterssen's Method.

Petterssen [25] (see footnote to sub-section 2.2.2) has suggested a procedure of successive approximations whereby we can construct the trajectory during a period T from flow charts at t = 0 and t = T.

The method is based on the assumption that the particle has a constant vector acceleration during the period. In this respect Petterssen's method differs from the other kinematic methods described below; these are essentially based on some simple assumption of how the flow field at time t = 0 is transformed into the flow field at time t = T. For a further discussion of Petterssen's method see sub-section 2.2.2.

In Figure 1, P_o is the initial point at time t = 0. We measure the velocity at this point on Chart 0 and denote this velocity by $\vec{v}(0, 0)$ which is the velocity at point 0 and time 0. This velocity times the period to the next chart, Chart T, is $T\,\vec{v}(0, 0)$. This vector is set off from P_o equal to $\overrightarrow{P_oA} = \vec{r}_o$. Next, we measure the velocity at point A on Chart T, $\vec{v}(\vec{r}_o, T)$ which is the velocity at point $\vec{r}_o$ at time T and set off a vector $\overrightarrow{P_oB_o} = T\,\vec{v}(\vec{r}_o, T)$. The midpoint of AB_o is P_1 and represents the first approximation to the trajectory terminal. If the velocity at P_1 on Chart T is equal to the velocity $\vec{v}(\vec{r}_o, T)$ within the chart accuracy, the computation can stop here, and P_1 is the desired terminal. If not, the velocity at P_1 on Chart T, $\vec{v}(\vec{r}_1, T)$, multiplied by T, is set off as a vector, $\overrightarrow{P_oB_1} = T\,\vec{v}(\vec{r}_1, T)$. The midpoint of AB_1 is P_2 and is the second approximation. The velocity at P_2 is compared with the velocity at P_1, both on Chart T. If this time the velocities agree within the chart accuracy, P_2 is the desired terminal; if not, the process can be continued and the points P_1, P_2, ... will usually converge upon a point P_n so that the velocities at P_n and P_{n-1} finally become identical when "n" is chosen sufficiently large. Usually the second approximation P_2 will come so close to P_1 that we cannot determine any difference in the velocities at the two points on Chart T. and P_2 will be the terminal of the trajectory.

Once the terminal of the trajectory is located, the trajectory can be drawn in by making it tangential to the velocity at P_o on Chart 0, and tangential to the velocity at the terminal on Chart T.

1.7. The Central Tendency Method.

In this method it is assumed that the instantaneous flow depicted by a synoptic flow chart is valid for a period of 12 hours, i.e., from 6 hours before until 6 hours after map time.

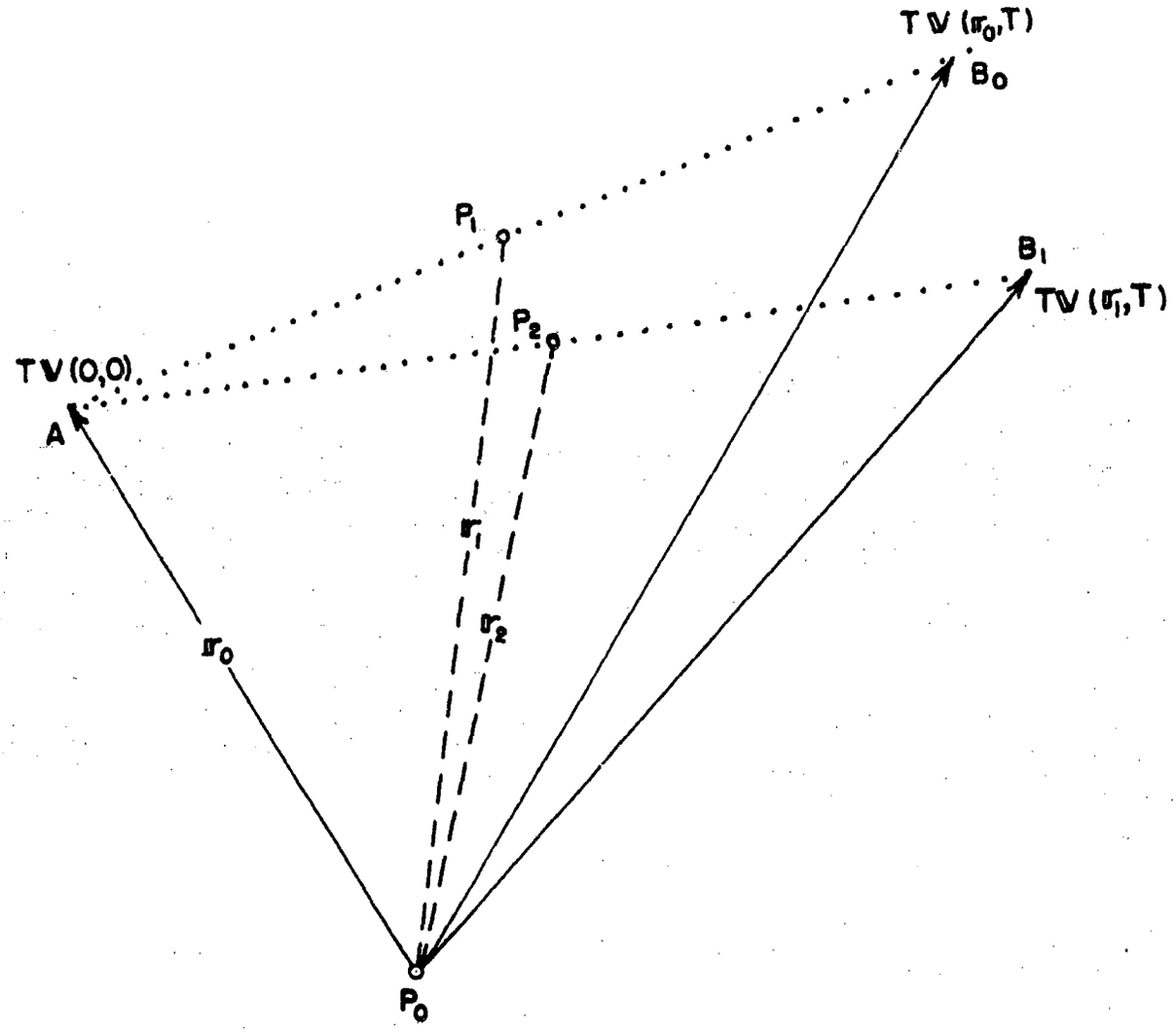

Figure 1.* Petterssen's Method of Successive Approximations. Object starts at P_o at time = 0. T is the period between two consecutive synoptic charts. $\vec{r}_o$, $\vec{r}_1$, $\vec{r}_2$ .... are position vectors from P_o. $\vec{v}(0, 0)$ is the wind at point 0 (P_o) on Chart 0, $\vec{v}(\vec{r}_1, T)$ is the wind at $\vec{r}_1$ on Chart T, etc. P_1 and P_2 are the first and second approximations of the trajectory terminal at time = T.

*NOTE: Double-lined (bold-faced) letters are used in the figures to designate vectors, e.g., $\vec{v}$ in the text is the same as $\mathbb{V}$ in the figures.

The flow chart may be a contour chart, an isotach and streamline chart, or a combination of the two methods of flow representation where the contours are taken as streamlines and isotachs are added to give a better definition of the speed field.

Figure 2 shows a trajectory constructed for a period of 24 hours by the Central Tendency Method. The balloon, supposed to float at 300 mb, starts out at point A at 21Z, 11 February 1953. The 300-mb chart for 03Z, 12 February gives the trajectory from A to B. In this construction the contours were taken as streamlines, and the speeds were estimated from the contours by applying the curvature correction as outlined in sub-section 1.5. The subsequent chart at 15Z gives the trajectory from B to C. Kinks in the trajectory where the maps join, as at B, will usually occur when the flow patterns have moving waves. The kinks should be smoothed out as indicated by the dashed line.

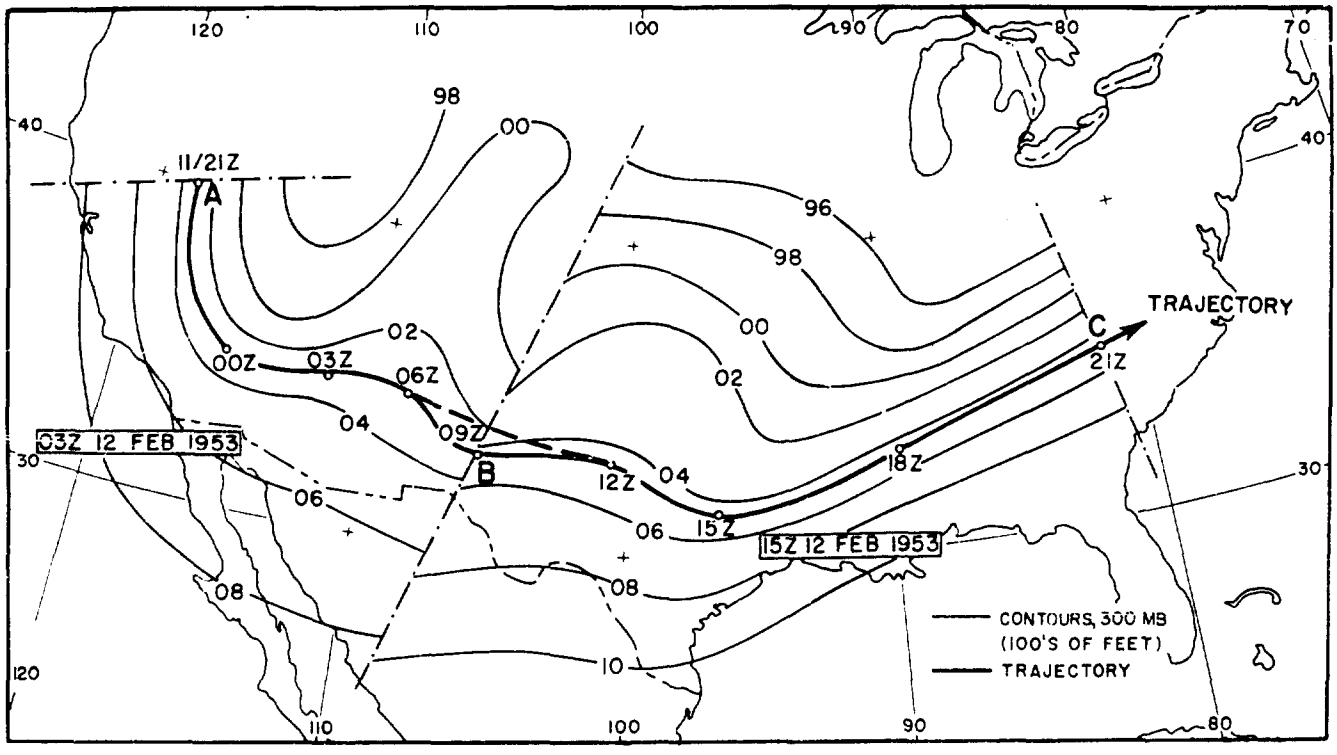

Figure 2. The Central Tendency Method.

The Central Tendency Method is probably the most commonly used method. It is rapid and gives an over-all accuracy that compares favorably with other methods.

The flow field to be used with the Central Tendency Method for

forecasting or hindcasting individual trajectories should, of course, be the best one available. In this respect the considerations in sub-section 1.5 apply. The method will for obvious reasons work best when the flow patterns are fairly stationary. When rapidly moving closed circulations, troughs, or ridges occur near the trajectory, the method may give seriously erroneous trajectories. This difficulty can be overcome by interpolating intermediate maps of the area where the trajectory encounters such flow patterns. One interpolation between the 12-hourly maps (each map valid for 6 hours) will reduce this error considerably.

For climatological studies on trajectories the Central Tendency Method used with the geostrophic flow will give sufficiently accurate answers. For most climatological estimates the Central Tendency Method may be extended to 24 hours and thus reduce somewhat the time required for the study.

1.8. Consecutive Streamline Methods.

These methods, as the name implies, utilize streamlines on consecutive charts. There are several variants of them. Two of them which were described by Macnta [18] are illustrated below.

In Figure 3a, P_o is the initial point on the trajectory at time h, the map time. Follow the streamline through P_o on Map h for 12 hours. The speed will usually be variable so it is advisable to proceed in 3-hourly steps by means of a displacement scale. If the speed is given by contours, the Geostrophic Displacement Scale described in sub-section 1.10 may be used. If the speed field is determined by isotachs, the special 3-hourly displacement scale for various speeds should be used. (It is recommended that this be entered on the Geostrophic Displacement Scale.) We thus arrive at point Q_1. Similarly, we follow the streamline through P_o on the following chart, Chart h + 12, and arrive at point Q_2. The midpoint P of Q_1Q_2 is the terminal of the trajectory. The trajectory is drawn by starting out from P_o tangential to the streamline at P_o on the Chart h and ending up tangential to the streamline through P on Chart h + 12. The process is continued for as long as desired. In Figure 3b another variant is illustrated. Q_1 is obtained as in Figure 3a. The streamline through Q_1 on Map h + 12 is then followed backwards for a distance of 12 hours to arrive at point B. Vector $\overrightarrow{BQ_1}$ is next set off from P_o equal to $\overrightarrow{P_oQ_2'}$. Midpoint P' of

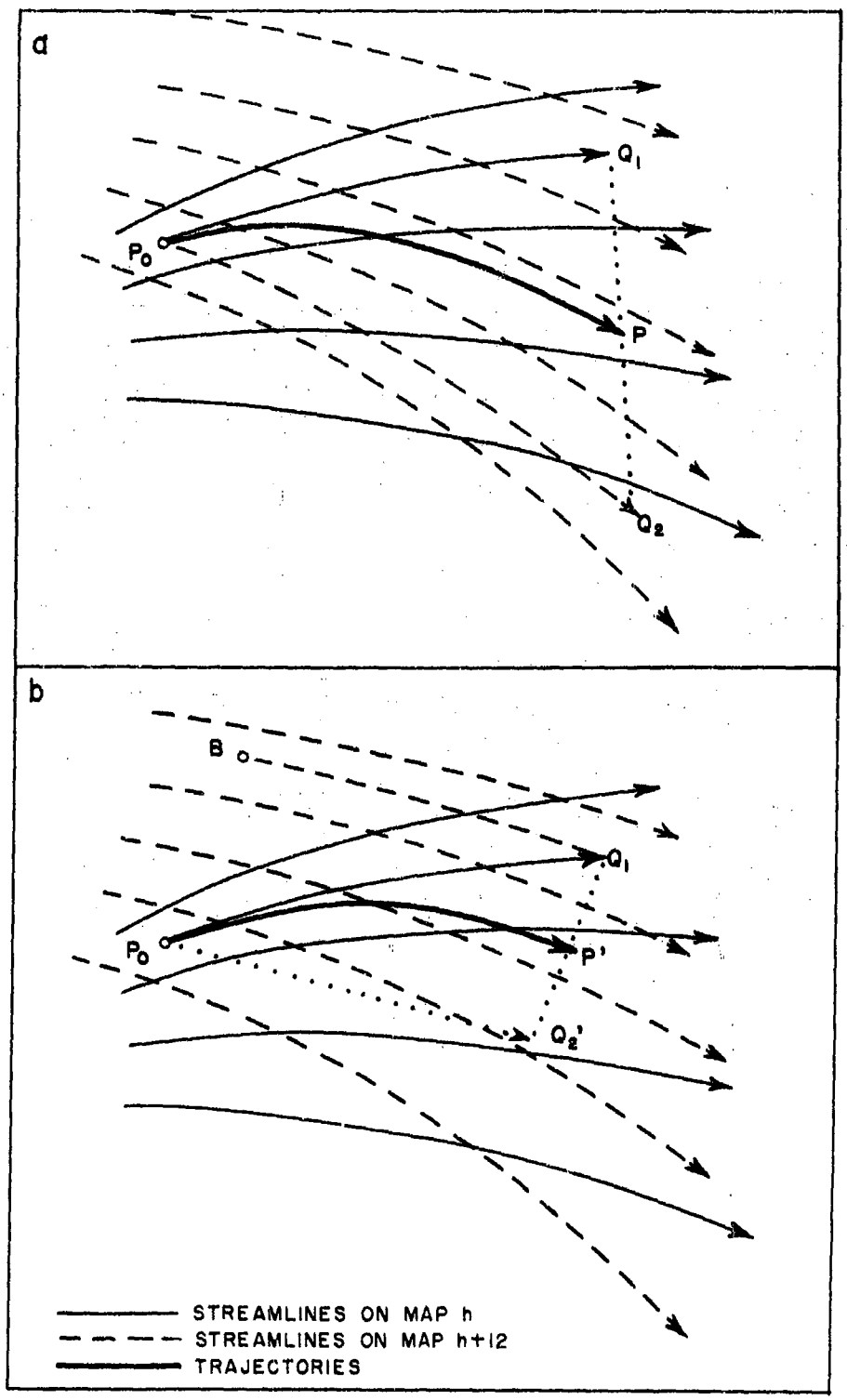

Figure 3. Consecutive Streamline Methods

a. Foreward tracking
b. Backward tracking

Q_1Q_2' is the terminal of the trajectory. The trajectory is drawn as in Figure 3a.

A third method is described in AWS Technical Report 105-62, June 1950. The various consecutive streamline methods will usually give slightly different results, but from principle there are no reasons to prefer one to another.

1.9. The Linear Interpolation Method.

This method is based on the assumption that the wind at a point changes linearly with time.

The trajectory is constructed in 3-hour steps, as illustrated in Figure 4. The construction is explained in the legend.

For the theory of this construction, see sub-section 2.2.4. The proportionate parts to be used for intervals other than 3 hours can be found from a formula in that sub-section.

1.10. The Relative Trajectory Method.

If the flow pattern maintains its shape and intensity but moves across the map, trajectories can be obtained by the Relative Trajectory Method.

The method is based on the fact that if we observe the flow from a coordinate system that follows the motion of the pattern, the flow will appear non-changing with time, and the relative trajectories (i.e., paths of air parcels described in this system) and relative streamlines (i.e., streamlines in this system) will coincide. The relative velocity which would be measured is $\vec{v} - \vec{c}$. Here, $\vec{v}$ is the motion relative to the earth and is, of course, the one plotted and analyzed on the map; $\vec{c}$ is the velocity of the pattern.

If the $\vec{v}$ field is represented by contours, the relative velocity field, $\vec{v} - \vec{c}$, is found by adding a fictitious contour field representing $-\vec{c}$ to the basic contour field. The $-\vec{c}$ contour field consists of a set of straight and parallel lines whose equidistance and labeling is determined such that the field represents a geostrophic wind equal to $-\vec{c}$.

Next, the motion of the balloon is followed in this relative-contour field by proceeding from the initial point parallel to the relative contours with a speed which is determined by a geostrophic wind scale from the distance between adjacent relative contours. In this

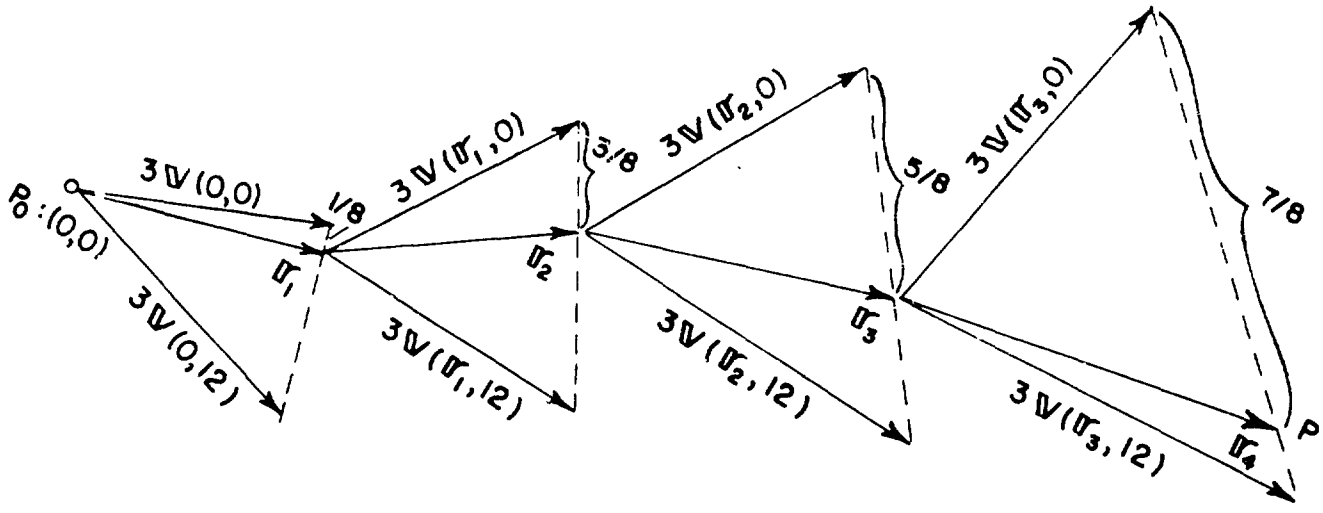

Figure 4. Construction by the Linear Interpolation Method of the Trajectory from P_o to P During a 12-hour Period. The period is divided into four 3-hour periods. The vectors (set off from P_o), $\vec{r}_1$, $\vec{r}_2$, $\vec{r}_3$, and $\vec{r}_4$, indicate the positions of the balloon after 3, 6, 9, and 12 hours. The vectors $\vec{r}_2$, $\vec{r}_3$, and $\vec{r}_4$ have not been entered in the Figure, but the symbols $\vec{r}_2$, $\vec{r}_3$, and $\vec{r}_4$ are entered at the position of the head of these vectors. $\vec{v}(0, 0)$ indicates the wind at P_o on Chart 0, $\vec{v}(0, 12)$ is the wind at P_o on Chart 12 (12 hours after Chart 0), $\vec{v}(\vec{r}_1, 0)$ is the wind at point $\vec{r}_1$, on Chart 0, etc. $3\vec{v}(0, 0)$ is the 3-hour wind travel with the wind $\vec{v}(0, 0)$ set off as a vector on the chart, etc. First, the vectors $3\vec{v}(0, 0)$ and $3\vec{v}(0, 12)$ are set off from P_o, the starting point of the trajectory. The end points of these vectors are connected with a straight line. This line is dissected in the ratio 1/8 to 7/8, thus locating the end point of vector $\vec{r}_1$ as indicated in the Figure. Next, the velocity at this point is measured on Chart 0 and on Chart 12, and the 3-hour wind travel with these velocities are set off as vectors. These vectors are $3\vec{v}(\vec{r}_1, 0)$ and $3\vec{v}(\vec{r}_1, 12)$ respectively. The connecting line between the end points of these vectors are dissected in the ratio 3/8 to 5/8, thus locating the end point of $\vec{r}_2$. The winds at this point on Charts 0 and 12 are measured, the 3-hour wind travels set off, and the procedure is repeated. The ratio is this time 5/8 to 3/8, and the last time the ratio is 7/8 to 1/8, computed from the end point of the wind travel on Chart 0.

manner we can determine the relative position of the balloon at any time we desire.

The position relative to the earth, or the chart position, is found by adding the displacement of the system during the elapsed time to the relative displacement.

The construction is illustrated by some examples. In Figure 5 the velocity field, $\vec{v}$, has concentric circular streamlines (contours) and the speed is constant, determined by the geostrophic spacing between the contours. This rotating field moves from left to right across the map with a velocity $\vec{c}$. This translational speed is here chosen equal to the wind speed, but that is not essential. The contour field given by the dashed lines represents $-\vec{c}$. By graphically adding the two contour fields the relative velocity field, $\vec{v} - \vec{c}$, is obtained. The chart trajectory of a particle starting out at point A and time

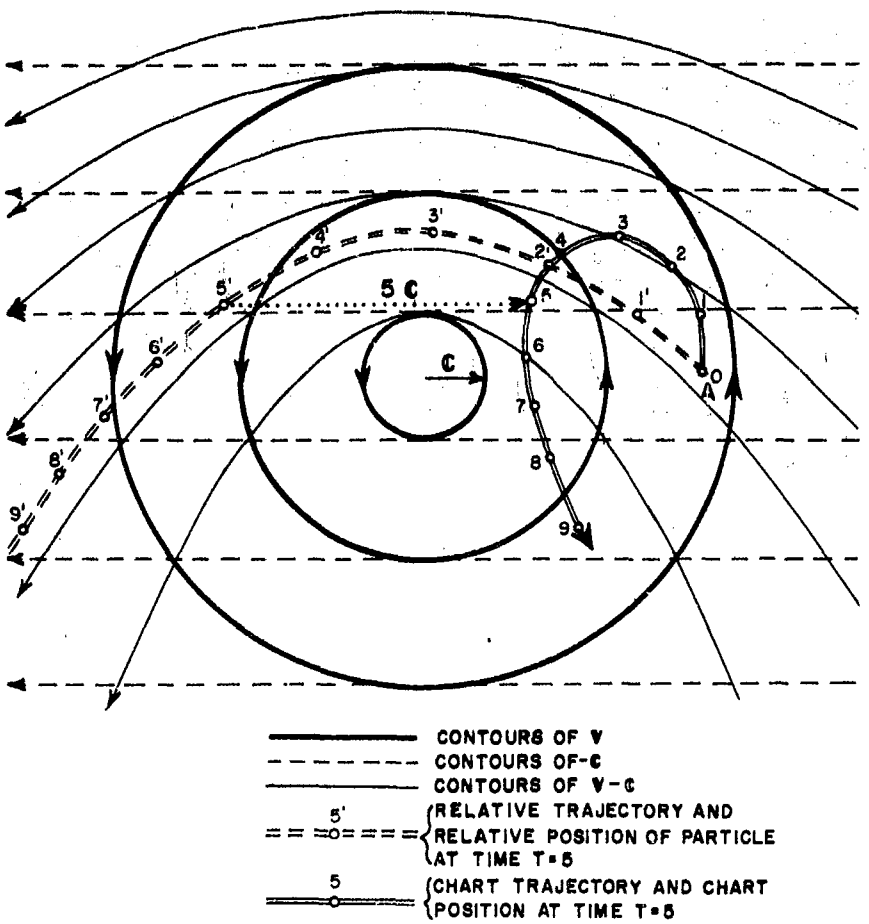

Figure 5. Trajectory by the Relative Trajectory Method. A circular vortex of uniform speed moves to the right with constant speed $\vec{c}$. The relative trajectory and the chart trajectory, starting from a point A, are indicated.

t = 0 is computed. The double-dashed line is the relative trajectory and the relative positions, marked 0, 1', 2' ... , are computed in steps at time t = 1, 2, ... by measuring the varying speed with a geostrophic wind scale from the relative contours. Next, the succession of points which form the chart trajectory is obtained by setting off vectors $\vec{c}$, $2\vec{c}$, $3\vec{c}$ ... from the points 1', 2', 3', ... In Figure 5 this is shown for time = 5. In this manner we arrive at points 1, 2, 3 ... , and the line joining them is the chart trajectory.

A second example resembles more the patterns on actual weather maps. In Figure 6 the contours represent a detail of a 300-mb map. Let us assume that the best prognosis possible is a simple translation of this contour field with a velocity $\vec{c}$ indicated on the map. This velocity $\vec{c}$ might have been obtained from comparison with an earlier map.

Two trajectories have been computed, one which starts from a point in the center of the low (point A) at the time of the map (t = 0) and one which starts from point B in the westerly flow north of the low. The top diagram shows the construction of the relative flow field, $\vec{v} - \vec{c}$, and the computed chart trajectories. In the bottom diagram the relative flow field is repeated, and the construction of the relative trajectories and the chart trajectories is shown in detail.

In the bottom left-hand corner is a diagram of a Geostrophic Displacement Scale which is convenient to use for trajectory computations. The ordinate is the displacement per time unit. A convenient time unit to use for high-level trajectories is t = 3 hours. The abscissa is the contour spacing. By transferring the contour spacing from the chart to the displacement scale by means of a pair of dividers, the 3-hour travel of the object is set in the dividers and in turn spaced off on the map. In the diagram the isoline for only one latitude has been shown. The isolines are all equilateral hyperbolas. The scale is analogous to a geostrophic wind scale. Instead of showing the speed as a number it gives the 3-hour geostrophic travel as a distance. It is recommended that the scale be constructed locally for the map projection and map scale used.

The auxiliary contour field representing $-\vec{c}$ may be prepared permanently as a set of templates containing straight parallel lines with the spacing varying from template to template. For a given system motion $\vec{c}$ and a given latitude the template giving the best spacing can be selected. The spacing on the template may be identified by a number which is entered on the Geostrophic Displacement Scale. Enter the

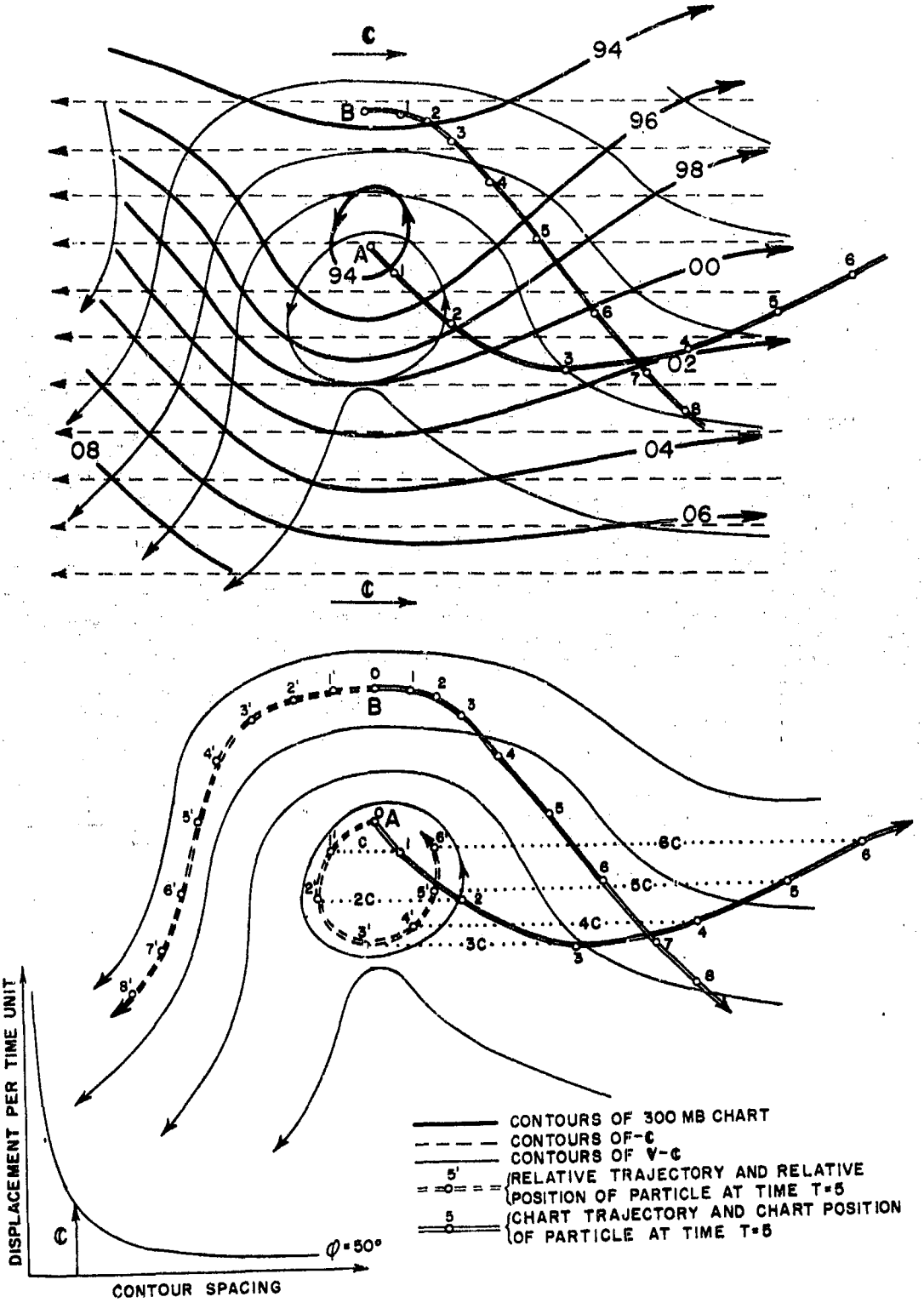

Figure 6. Trajectories in the 300-mb Surface Computed by the Relative Trajectory Method.

numbers along the abscissa such that — when we enter the Geostrophic Displacement Scale with the 3-hour travel of the system as ordinate, go right to intersection with proper latitude, and down to intersection with the abscissa — the nearest number will select the correct template. A set of 8 templates with spacings for 5, 10, 15, 20, 25, 30, 40, and 50 knots at 40°N will suffice.

The Geostrophic Displacement Scale should be standard equipment for trajectory work. On it may also be marked 3-hour travel for various speeds to be used in conjunction with isotach charts. It will then be useful for all kinematic methods.

1.11. General Mills' Standard Objective Method.

This method may be considered as a version of the Relative Trajectory Method. The assumptions underlying the two methods are the same: The flow pattern does not change shape or intensity but is merely translated with constant speed across the map.

Instead of getting a continuous trajectory, as by the Relative Trajectory Method, this method constructs the trajectory in 6-hour steps, the flow being assumed stationary during each 6-hour interval.

Figure 7 illustrates the method. The flow pattern, given by the streamlines and isotachs, moves toward the right. The 6-hour travel of the pattern is indicated by the arrow above the pattern. The balloon starts out at A_o at the time of the map. The balloon displacement during the first 6 hours is the line segment, A_oA_1, found by going first left from A_o a distance equal to the 3-hour travel of the pattern to a point B_1 and proceeding from there for 6 hours along the streamline through B_1 with a speed given by the isotachs to arrive at point C_1. The line segment B_1C_1 is then transferred parallel to itself to A_o and set off as A_oA_1; A_1 is the position of the balloon after 6 hours. Next, we go left from A_1 for 9 hours (or what is the same, left from C_1 for 6 hours), construct the new line segment B_2C_2, transfer this segment back to A_1, and arrive at A_2 which is the location of the balloon after 12 hours. In this manner we can proceed for as long as we desire. The construction, of course, will only be valid for as long as the basic assumptions hold, i.e., the pattern is permanent and moves with constant speed. A variable speed of the pattern may be introduced in the system by altering the 6-hour displacements to the left as we see fit.

Instead of transferring the line segments B_1C_1, B_2C_2, etc. to the

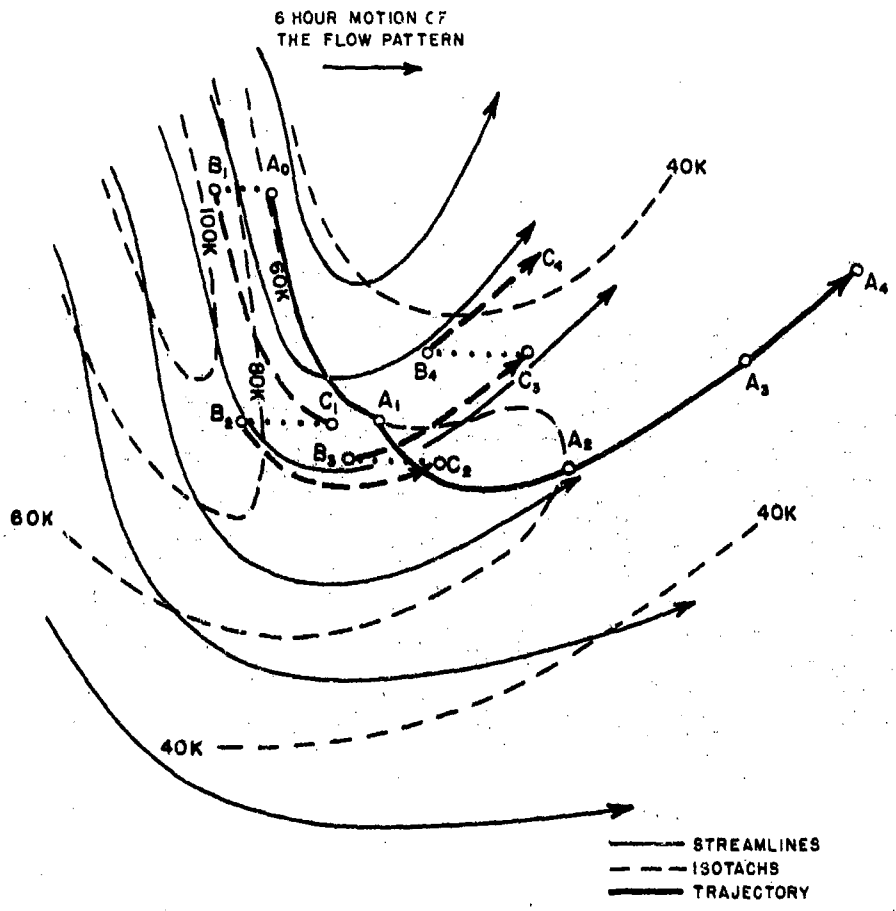

Figure 7. A Trajectory Computed by the General Mills' Standard Objective Method.

right, it is more convenient to construct the trajectory on a transparent overlay and move the overlay in the opposite direction to the motion of the system, (i.e., to the left in the case above) a 3-hour displacement for the first 6-hour trajectory interval and an additional 6-hour displacement to the left for each of the subsequent 6-hour intervals.

When the patterns have strong streamline curvatures or strong wind shears, it may be advisable to shorten the steps to 3 hours. In fact, the shorter the steps the more will the trajectory resemble the continuous trajectory obtained by the Relative Trajectory Method.

The advantage of the General Mills' Method over the Relative Trajectory Method is that it is independent of the manner in which the flow is represented. It works equally well with a contour as with a streamline and isotach representation. Construction of the relative

flow field needed for the Relative Trajectory Method is a tedious procedure when the flow is determined by streamlines and isotachs, as the relative flow field has to be analyzed from vectors obtained by adding vectorially two vectors point by point. Only when the flow is given by contours (stream functions to be exact) is the Relative Trajectory Method more rapid and probably also more accurate than the General Mills' Method. It is emphasized here again that when the Relative Trajectory Method is used, the contours should be drawn to fit the winds (geostrophically) rather than the height reports. This is the usual practice anyway when analyzing high-level contour charts, since the height reports become increasingly more inaccurate as we proceed upward in the atmosphere. (Sub-section 1.5).

The General Mills' Method and also the Relative Trajectory Method are preferable to the Central Tendency Method or the Consecutive Streamlines Method when the trajectory passes near fast or moderately fast-moving features of the flow that possess marked streamline curvature or shear, e.g., highs, lows, ridges or troughs, and jet streams. Very often the best estimate that can be made of the future behavior of such systems is an extrapolated (on prognostic maps) or interpolated (when hindcasting) translation of the pattern without altering its shape and intensity. For these cases the Relative Trajectory Method or the General Mills' Method will give the best trajectories.

1.12. The Francescbini-Freeman Method [9].

This is a dynamic method. Required for the computation are the initial wind and position when the balloon reaches the intended floating pressure, and contour charts of this pressure surface at 12-hour intervals for as long as the trajectory is desired.

The Coriolis force, which is given by the balloon velocity, and the pressure force, which is obtained from the contour charts, will each try to deflect the path of the balloon, the Coriolis force to the right (in the Northern Hemisphere) and the pressure force toward lower contours. The resulting motion of the balloon is computed in 2-hourly steps by means of a "Displacement Nomogram." This Nomogram, shown in Figure 8, is valid for all map scales and projections. The time interval of 2 hours cannot be changed.

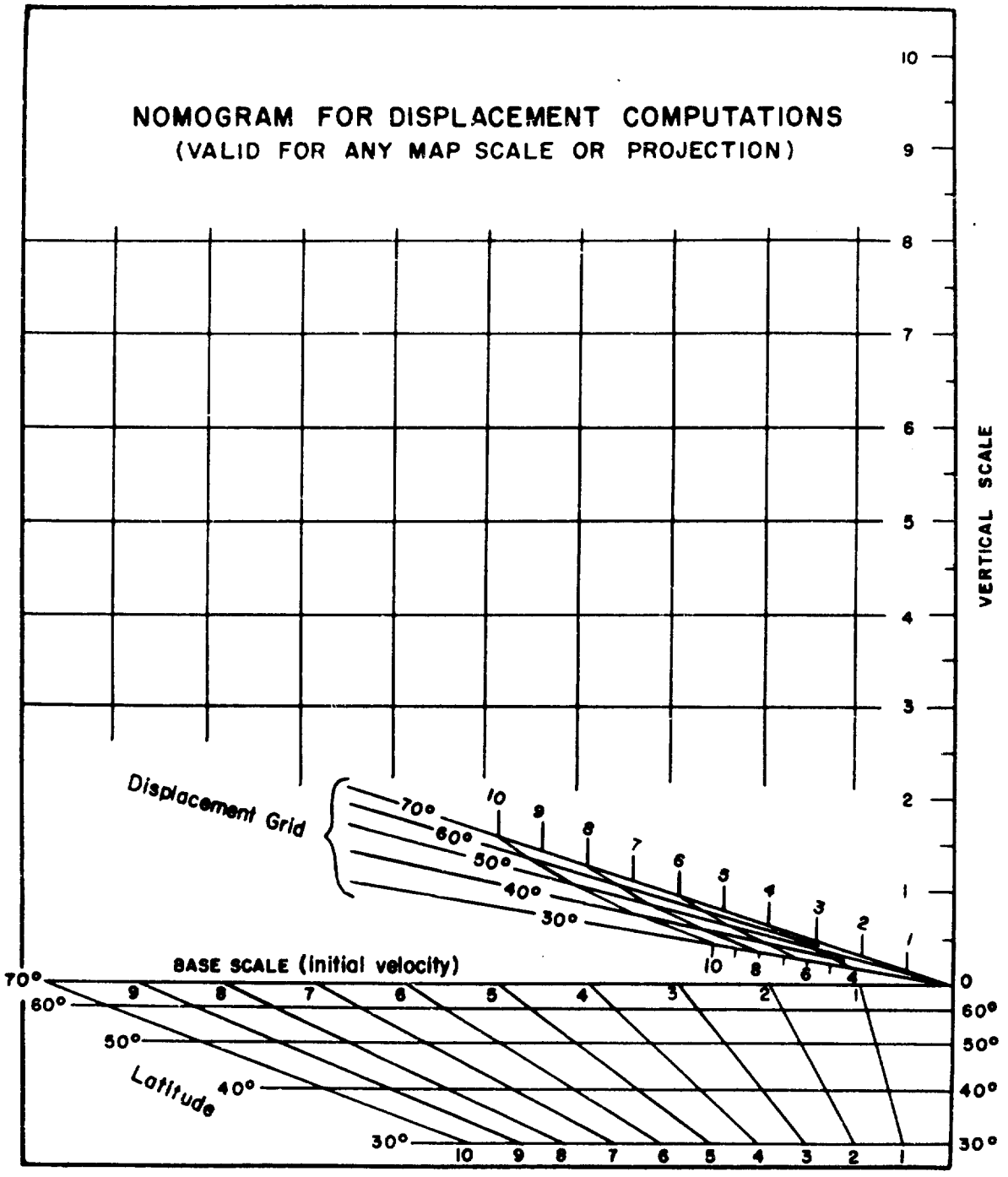

Figure 8. Nomogram for Computing the Displacement and Final Velocity of an Air Parcel After a 2-hour Interval. (After Franceschini and Freeman.) 0 is the origin. See text for instruction on use.

1.12.1. Stepwise Procedure for Constructing the Trajectory.

a. First Time Interval.

(1) Find the climb displacement as explained in paragraph c below and adjust this to the nearest multiple of 2 hours as explained in paragraph d below. The point obtained is the adjusted initial position.

(2) Determine the initial velocity $\vec{v}_o$ as explained in e below. Set off a vector 2 hours $\times \vec{v}_o$ to scale on the base map or on a transparent overlay from the adjusted initial position.

(3) Determine the average geostrophic velocity $\vec{v}_g$ over the interval as explained in f below. Set off a vector 2 hours $\times \vec{v}_g$ to scale from the same origin as in (2) above. Only the terminals of $2\vec{v}_o$ and $2\vec{v}_g$ need be indicated.

(4) Place the Displacement Nomogram as follows: the origin at the terminal of $2\vec{v}_o$ and the Vertical Scale passing through the terminal of $2\vec{v}_g$. The Nomogram now remains fixed for steps (5) and (6).

(5) Note the value of the terminal of $2\vec{v}_g$ on the Vertical Scale. This is $|2(\vec{v}_o - \vec{v}_g)|$ on an arbitrary scale.

(6) Enter with the value of (5) and the proper latitude (at midpoint of $2\vec{v}_o$) the Displacement Grid of the Nomogram. The intersection of the isolines locates a point. This point is the terminal of the computed trajectory for the first interval. Mark this point on the map or a transparent overlay.

b. Second and Subsequent Intervals.

(1) Determine a new initial velocity displacement for the second interval by using the points from the first interval as follows:

(a) Using the Vertical Scale measure the distance from the point determined in step (6) above to terminal of $2\vec{v}_g$.

(b) Place the Nomogram as follows: the origin at terminal of $2\vec{v}_o$ and the Vertical Scale parallel to the distance measured in step (a) above. In the grid below the Base Scale locate the intersection

of the proper latitude line and the sloping isopleth of the value in (a) above. Mark on the Base Scale the projection of this intersection point on the Base Scale.

(c) The line from the initial point of the preceding time interval to the point marked in (b) above represents the initial-velocity displacement for the second interval. Set off this vector from the end point of the first trajectory segment as in a(6).

(2) Determine the average geostrophic-velocity displacement for the second interval as explained in paragraph f below. Set off this vector from the same origin as in b(1)(c) above.

(3) The following steps are now identical to steps a(5) and a(6).

(4) For subsequent intervals proceed as for the second interval using the points of the previous interval to compute a new initial velocity displacement for the interval. The trajectory terminals are marked on the base map with proper time indications as we go along.

c. Climb Displacement and Time at Altitude. The climb displacement can be computed when the time of release and the climb rate of the balloon are known.

(1) We first compute the climb vector. It will be sufficiently accurate to use the winds at 10,000-ft intervals. For example, if $\vec{v}_2$, $\vec{v}_{10}$, etc., denote winds at 2000, 10,000 feet, etc., we have the following for the climb vector to 300 mb:

$$\vec{v} = \frac{1}{3}\left[\frac{\vec{v}_2 + \vec{v}_{10}}{2} + \frac{\vec{v}_{10} + \vec{v}_{20}}{2} + \frac{\vec{v}_{20} + \vec{v}_{30}}{2}\right]$$

$$= \frac{2}{3} \times \frac{1}{2}\left[\frac{\vec{v}_2 + 2\vec{v}_{10}}{2} + \frac{2\vec{v}_{20} + \vec{v}_{30}}{2}\right]$$

(2) From this expression for the climb wind, an easy construction on AWS-WPC-10-4 follows. The construction is illustrated by the following example. $\vec{v}_2$ = 320° 20 knots, $\vec{v}_{10}$ = 300° 35, $\vec{v}_{20}$ = 270° 50, $\vec{v}_{30}$ = 250° 60. The points A, B, C, and D of Figure 9 represent $\vec{v}_2$, $2\vec{v}_{10}$, $2\vec{v}_{20}$, and $\vec{v}_{30}$, respectively, plotted on AWS-WPC-

10-4. Midpoints of AB and CD are E and F and represent $\frac{1}{2}(\vec{v}_2 + 2\vec{v}_{10})$ and $\frac{1}{2}(2\vec{v}_{20} + \vec{v}_{30})$, respectively. Midpoint of $\vec{EF}$ is G and represents half the sum of these vectors; the climb vector $\vec{v}$ is 2/3 of $\vec{OG}$.

(3) Similar constructions can be found to 200 mb and other surfaces.

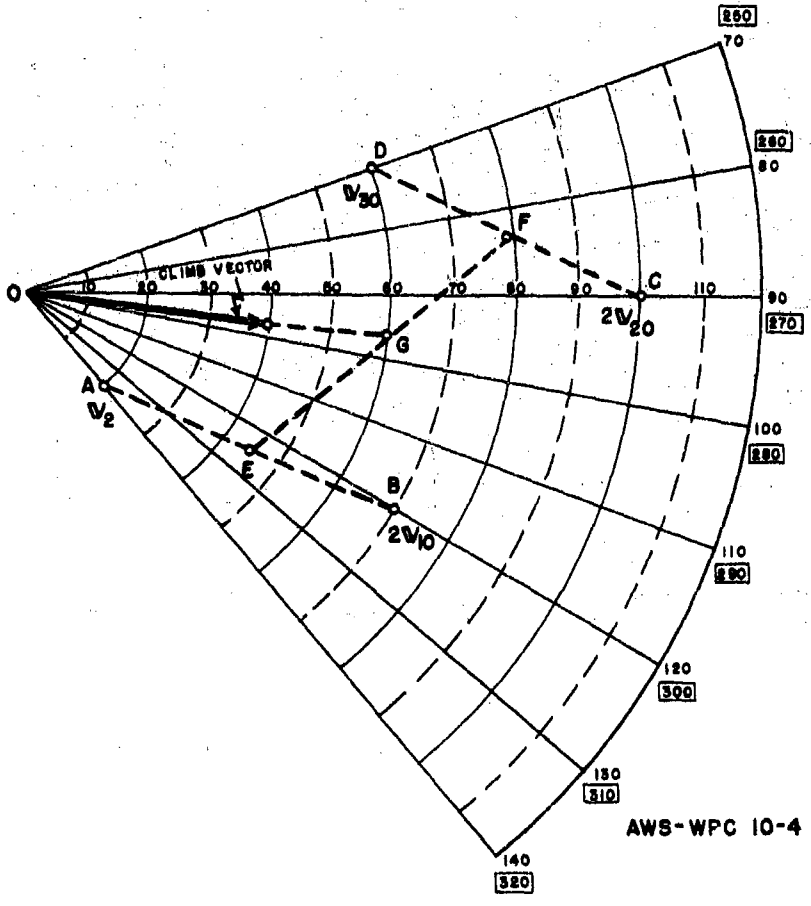

Figure 9. Construction of the Climb Vector to 300 mb on AWS-WPC-10-4.

(4) The displacement of the balloon during climb is then $\vec{r}_c$ when S is the climb rate in feet per minute, z the pressure altitude of floating pressure in feet, and $\vec{v}$ in knots:

$$\vec{r}_c = \frac{\vec{v}\, z}{60\, S} \text{ nautical miles}$$

(5) The time when the balloon first reaches altitude is, of course, release time plus the climb time, z/S minutes.

d. Adjustment to Nearest 2-hourly Interval. Since the computations are carried out in 2-hourly steps, it is convenient to start from the position of the balloon at a time which is a multiple of 2 hours, i.e., 00Z, 02Z, 04Z, etc. If, for example, the balloon is computed to be at altitude at 0130Z, move it on with the wind at altitude (see e below) for another 30 minutes and obtain the position at 0200Z. This is the adjusted initial position.

e. The Initial Velocity. It is important to determine the wind accurately.

(1) If rawins from the release point taken a few hours prior to release are available (up to 6 hours before), these should be used.

(2) If no rawin observations are taken from the release point or if these are more than 6 hours old, the initial wind should be obtained from an extrapolated streamline and isotach analysis in the area of the release point. If no winds or very few wind reports appear on this analysis, winds have to be estimated from the contours. The correction for curvature of the contours should then be used in accordance with sub-section 1.5.

(3) If the trajectory forecast is not needed prior to release and the balloon is tracked for the first few hours, the initial wind may be obtained from the first part of the trajectory.

f. The Average Geostrophic Velocity for an Interval. This should properly be the time-space average over the appropriate trajectory segment; but since the trajectory is not known at the outset, use as an approximation the average geostrophic wind over the initial velocity displacement, $2\vec{v}_o$.

(1) The geostrophic wind field for intervals between the map times 03Z and 15Z may be obtained by a time-linear interpolation between the two successive charts bracketing the interval. The intervals may be numbered as indicated:

Zero Interval	02Z-04Z
1st "	04Z-06Z

2nd	Interval	06Z-08Z	(determined from the
3rd	"	08Z-10Z	03Z and the following
4th	"	10Z-12Z	15Z charts)
5th	"	12Z-14Z	
Zero	"	14Z-16Z	(determined from the
1st	"	16Z-18Z	15Z and the following
	etc.		03Z charts).

The change of the geostrophic wind is given by the 12-hour height-change chart. Since the gradients of this chart vary less than the gradients of the contour chart, it will generally be a good enough approximation to use a constant geostrophic wind-change over an interval. If we denote the 12-hour geostrophic wind-change, measured at the midpoint of $2\vec{v}_o$, by $\Delta\vec{v}_g$, the geostrophic wind-change for the interval will be zero for a zero interval, 1/6 $\Delta\vec{v}_g$ for a 1st interval, 2/6 $\Delta\vec{v}_g$ for a 2nd interval, etc. This change vector is then added vectorially to the average geostrophic wind over $2\vec{v}_o$ measured from the basic contour chart. As an example, Figure 10 illustrates how to find the average geostrophic wind for the interval 08Z-10Z (3rd interval), 3 August.

In the Figure the initial velocity displacement, $2\vec{v}_o$, is set off to scale from the initial point A. This is $\overrightarrow{AB}$. We measure the geostrophic wind at A, $\vec{v}_{g(A)} = \overrightarrow{AC}$ and at B, $\vec{v}_{g(B)} = \overrightarrow{BF}$. $\vec{v}_{g(B)}$ is set off from C equal to $\overrightarrow{CD}$. At midpoint M of $\overrightarrow{AB}$ the 12-hour geostrophic wind change $\Delta\vec{v}_g$ is measured from the height change contours.

The average geostrophic wind change over $\overrightarrow{AB}$ during the period from the basic chart at 03Z and the mid-time of the interval, 09Z, is then 3/6 $\Delta\vec{v}_g$. However, we want the 2-hour displacement with the average geostrophic velocity; therefore, set off 2 × 3/6 $\Delta\vec{v}_g$ from D, equal to $\overrightarrow{DE}$. $\overrightarrow{AE}$ is now the desired 2-hour displacement $2\vec{v}_g$, computed from the formula $\overrightarrow{AE} = 2 \times [\frac{1}{2}(\vec{v}_{g(A)} + \vec{v}_{g(B)} + 3/6\ \Delta\vec{v}_g]$. This vector addition is best performed on AWS-WPC-10-4 or a similar hodograph.

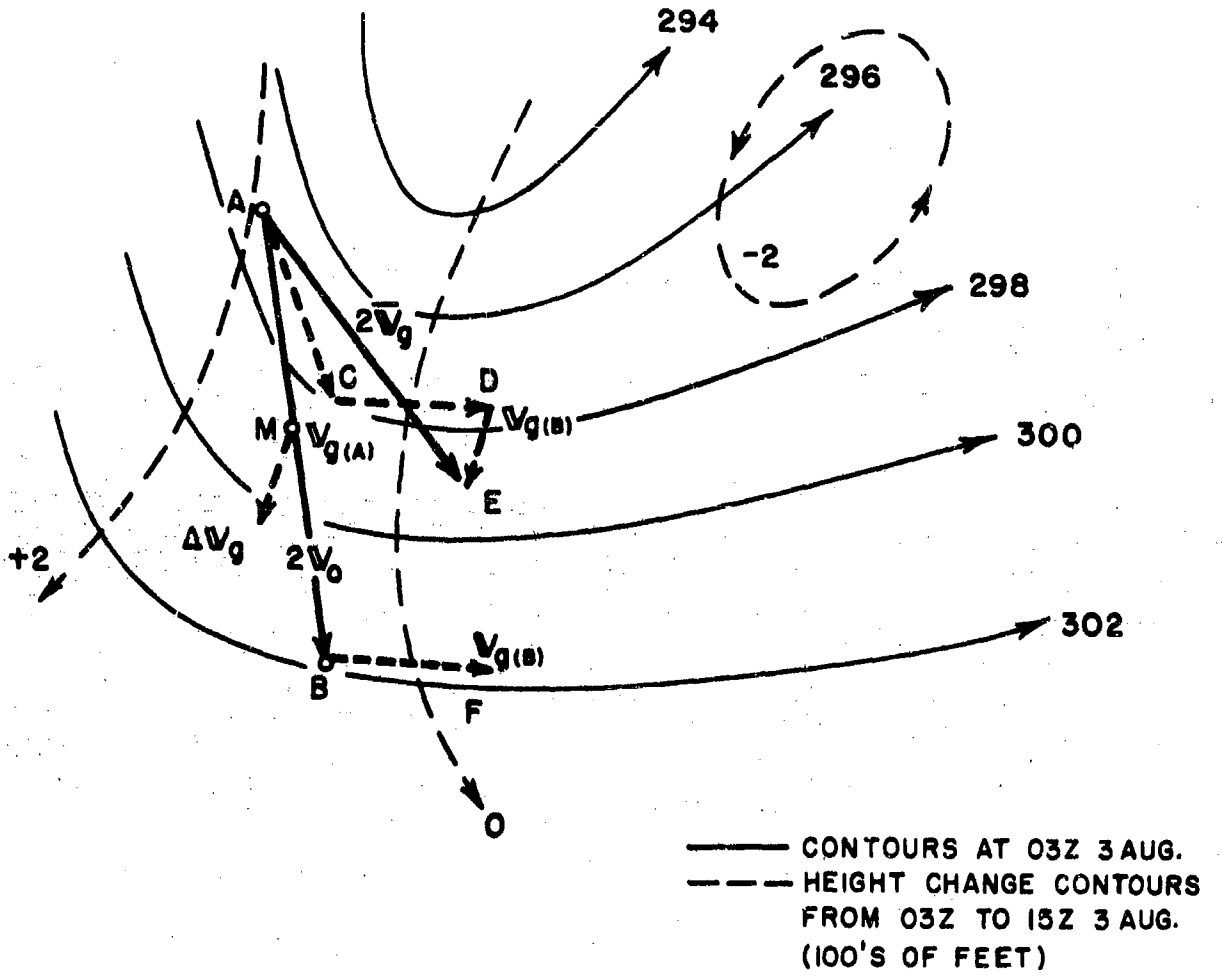

Figure 10. The Mean Geostrophic Displacement Velocity for a 2-hour Interval.

(2) An alternate method which requires less time is to use a separate linear time interpolation for the direction and the speed of the geostrophic wind at point M.

Example: Geostrophic Wind at point M at 03Z: 260° 40 knots

Geostrophic Wind at point M at 15Z: 290° 60 knots

Geostrophic Wind to be used for a 3rd interval (08Z-10Z) will then be 275° 50 knots since the 3rd interval is midway between 03Z and 15Z.

1.13. The Air Weather Service Method.

1.13.1. Introduction. The AWS Method is a dynamic method. Needed for construction of a trajectory are:

a. The initial velocity
b. Contour charts at 12-hour intervals
c. The AWS Trajectory Graph
d. A transparent Polar Diagram (similar to AWS-WPC-10-4).

The AWS Method and the Franceschini-Freeman Method, both being dynamic methods, have several points in common. They both require an initial velocity of the object at the beginning of the computation period and the pressure distribution during the period. In the Franceschini-Freeman Method the computation period is 2 hours. In the AWS Method, it is 12 hours or, occasionally, 6 hours. The advantage of the latter method is that it is quicker since the computation period is much longer; also, it is believed to be somewhat more accurate and less tedious to apply since it avoids working with small displacement increments.

A basic assumption underlying the AWS Method is that the geostrophic wind vector, which follows the object, changes linearly with time during the computation period. The period is 12 hours in regions of the map where the space variations of the geostrophic wind are moderate or small (about 9 knots or less per latitude degree of progression) and 6 hours where this variation is large such as it will be near marked troughs or ridges surrounded by strong contour gradients. The trajectory terminal is found by a procedure of successive approximations reminiscent of that used by Petterssen (see sub-section 1.6). For the theory of the AWS Method see sub-sections 2.1.7 and 2.1.8.

Sooner or later, the future will see trajectories traced by electronic computers. When it becomes possible to simulate the behavior of upper-air pressure patterns (300 mb, 200 mb, etc.) through numerical prediction, the programming of the computer for obtaining dynamic constant-pressure trajectories as a by-product is a relatively simple matter.

1.13.2. The Polar Diagram. The Polar Diagram (Figure 11) is used as an overlay on the AWS Trajectory Graph to compute the displacement during the computation period and the object velocity at the end of the computation period. These computations are made from the known geostrophic velocities at the beginning and at the end of the trajectory

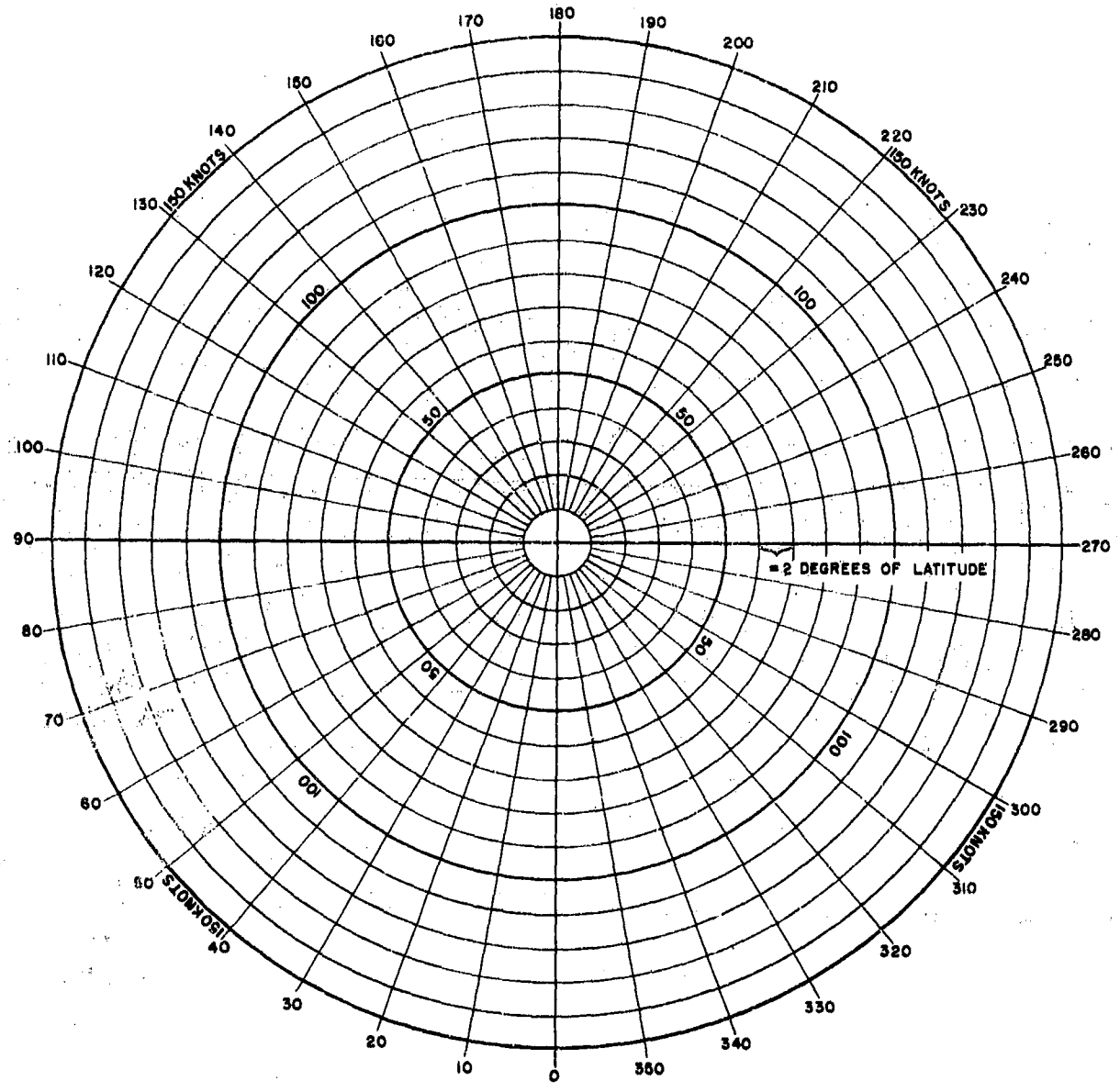

Figure 11. The Polar Diagram.

segment of this period. It is recommended that the Polar Diagram be prepared locally on transparent material.

If a Lambert conformal projection is used for the contour maps, the distance between consecutive concentric circles corresponding to a 10-knot speed increment should be made equal to 2 latitude degrees at the standard latitude of the maps used. Thus, displacements and velocities can be treated interchangeably for a computation period of 12 hours since the displacement during a 12 hour period of an object moving at 10 knots is 2 latitude degrees. If the computation period is reduced to 6 hours, the displacements are halved. This is possible because the scale of the Lambert conformal projection (true at 30°N and

60°N) varies only insignificantly between 65°N and 25°N.

If a polar stereographic projection is used in chart work, velocities and distances can no longer be treated as equivalents because the length of a latitude degree varies by about 40% between 65°N and 25°N, our main area of interest. The Polar Diagram will, however, still give true displacements in latitude degrees, 2 degrees for every 10 knots of speed on the diagram for a 12-hour period and 1 degree for every 10 knots for a 6-hour period. The correct length of the displacement to be set-off on the map is then the length of the number of latitude degrees indicated by the speed, measured at the mean latitude of the trajectory segment. When the polar stereographic projection is used, there is no longer any specific advantage in constructing the Polar Diagram by the formula: 2 latitude degrees = 10 knots. Any reasonable distance between the circles can be used. Since the AWS-WPC-10-4 is available, this may be used.

1.13.3. The AWS Trajectory Graph. This graph (Figures 12a and b) contains 2 diagrams. The left one computes displacements during a 12-hour (or 6-hour) period, and the right one computes the velocity at the end of the 12-hour (or 6-hour) period. This final velocity becomes, of course, the initial velocity for the next computation period.

The scale of the graph is arbitrary as only the configuration is of consequence. It may be reproduced on any scale. The scale reproduced in this Manual is too small for practical use with ordinary weather charts (scales equal to or larger than 1:20,000,000). A separate print of the Graph on a larger scale (large enough for scales up to 1:10,000,000) is available for field use as a separate item (AWSM 105-47A).

1.13.4. Choice of Computation Period. The computation period is either 12 hours or 6 hours. Which period to use depends on the space variation of the geostrophic wind on the contour map at the end of the period. If this variation is less than about 9 knots per latitude degree of progression (60 nautical miles in any direction) in the region of the trajectory segment, use 12 hours. Otherwise, use 6 hours. In the Trajectory Graph the continuous radial lines labelled for latitude (unbracketed) are to be used for 12 hours; the dashed radial lines with bracketed labelling of latitude are for 6 hours.

Incidentally, choice of too long of a computation period will automatically be signalled by the failure of the computed trajectory

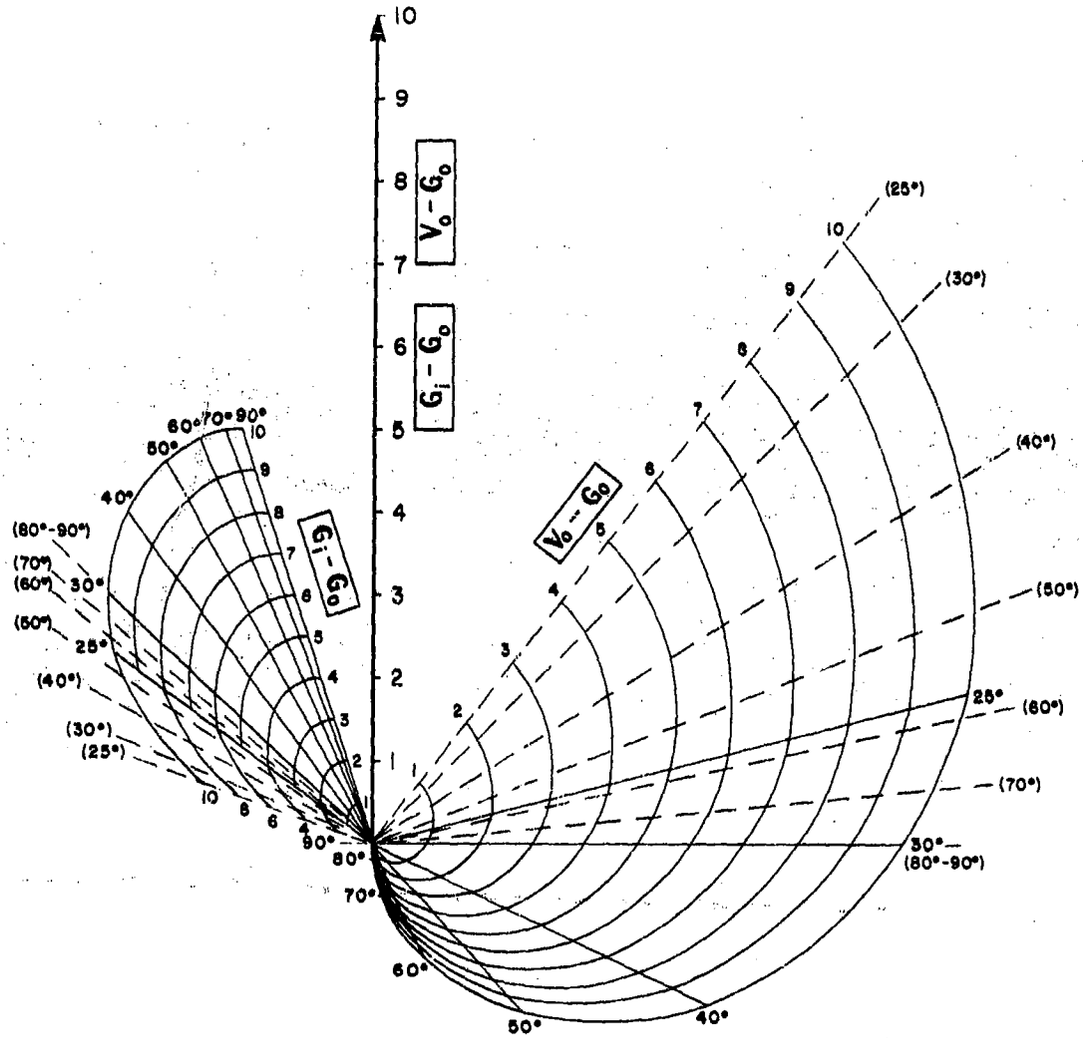

Figure 12a. The AWS Trajectory Graph — Displacement. Dashed radial lines and bracketed latitude values refer to 6-hour trajectories. Solid radial lines and non-bracketed latitude values refer to 12-hour trajectories.

terminals to converge upon a stable solution; 6 hours must then be used.

When a 6-hour computation period is used, a contour map intermediate between the 03Z and the 15Z maps must be sketched in the area of the trajectory segment; i.e., if the beginning of the period is 15Z, an intermediate map valid at 21Z must be interpolated between the 15Z and the following 03Z map.

1.13.5. Stepwise Procedure for Constructing the Trajectory.

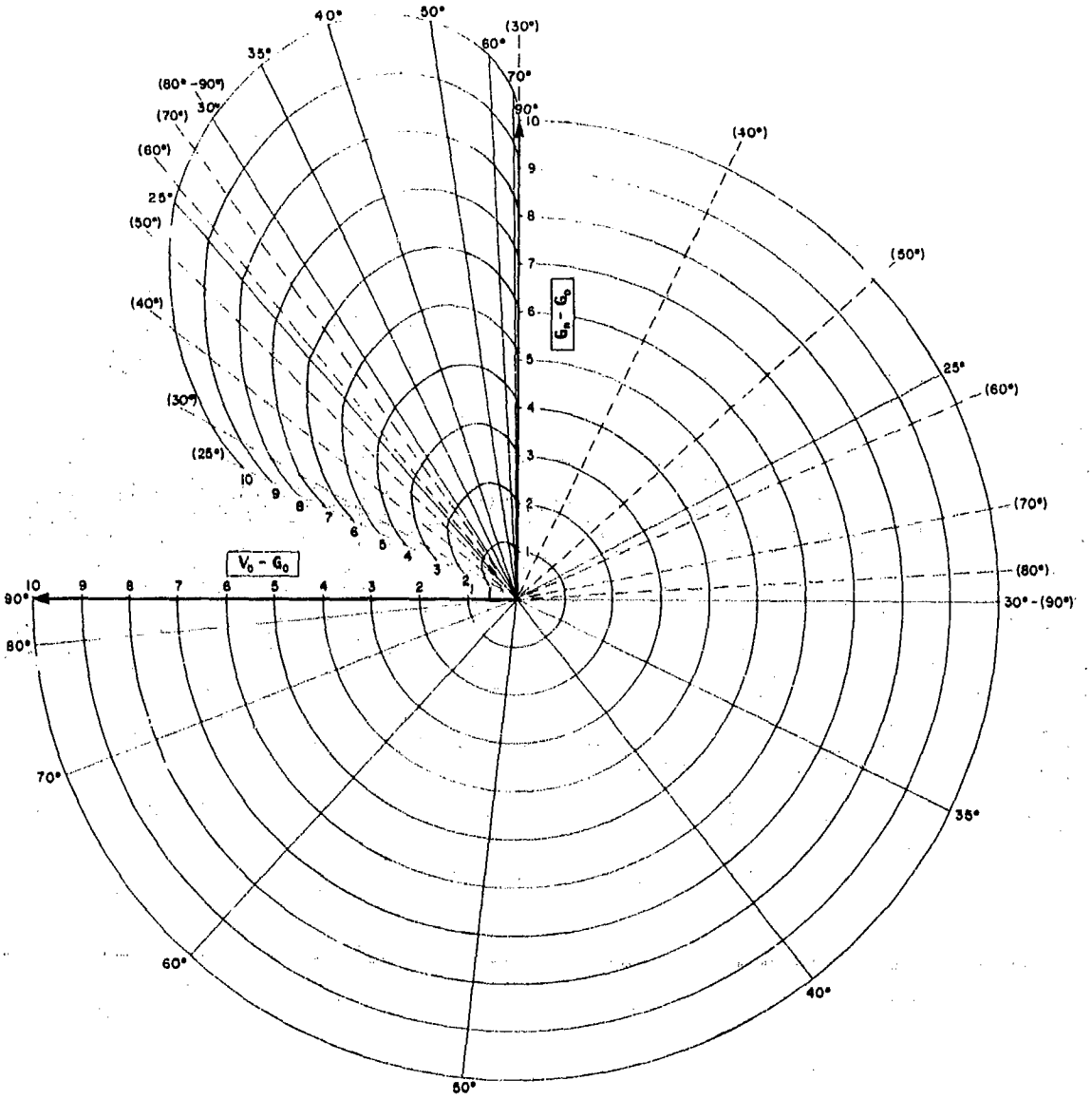

Figure 12b. The AWS Trajectory Graph — Final Velocity. (See legend in Figure 12a.)

a. First Computation Period.

(1) Find the climb displacement and the time at altitude as explained in paragraph 1.12.1.c and adjust to the nearest 6-hourly upper-air synoptic hour (03Z, 09Z, 15Z, and 21Z) kinematically. This is the adjusted initial position. If the position is at 09Z or 21Z, the first computation period is 6 hours to bring the computation scheme in phase with the available maps at 03Z and 15Z. If it is at 03Z or 15Z, the period is 12 hours or 6 hours, according to sub-section 1.13.4.

(2) Determine the initial velocity $\vec{v}_o$ as outlined in paragraph 1.12.1.e and enter $\vec{v}_o$ as a point v_o on the Polar Diagram.

(3) Determine the geostrophic velocity $\vec{G}_o$ at the adjusted initial position on the chart valid at this time. If the adjusted initial position is at 03Z or 15Z, this is done directly; if it is at 09Z or 21Z, it is interpolated from the values on the two bracketing 03Z and 15Z maps. Enter $\vec{G}_o$ as a point G_o on the Polar Diagram.

(4) Make an estimate of the end point of the trajectory for the period in question and mark this point Z_1 on the contour map valid at the end of the period. Henceforth, this map will be referred to simply as "the contour map." This estimate may conveniently be the end point of the C. T. M. trajectory (Central Tendency Method, see subsection 1.7). Measure the geostrophic velocity at Z_1 and mark this velocity $\vec{G}_1$ as a point G_1 on the Polar Diagram.

(5) Place the Polar Diagram on the left diagram (marked Displacement) of the AWS Trajectory Graph such that point G_o coincides with the underlying center (where the radial lines meet) and the point v_o falls on the vertical axis (thick line with arrow). Read the value under v_o on the axis scale. Without moving the diagrams enter the grid (marked $\vec{v}_o - \vec{G}_o$) to the right of the axis with this value for the spirals and the appropriate latitude for the radial lines and determine an intersection point. Mark this as point A on the Polar Diagram and draw the vector $\overrightarrow{G_oA}$. This vector remains on the Polar Diagram throughout the period. The latitude to be used is the mean latitude of the initial point and Z_1. (Bracketed values of latitude are for 6-hour periods and unbracketed values for 12-hour periods.)

(6) Rotate the Polar Diagram, with G_o remaining on the center, until G_1 falls on the axis. Read the value under G_1. With this value enter the spirals of the grid (marked $\vec{G}_1 - \vec{G}_o$) to the left of the axis and find the intersection with the appropriate latitude line. Mark this point on the Polar Diagram.

(7) From the point determined under (6), set off the vector $\overrightarrow{G_0A}$ on the Polar Diagram. Only the end point of the resultant need be marked. Label this point Z_2.

If Lambert conformal maps are used and the Polar Diagram is constructed on the formula: 2 latitude degrees = 10 knots speed increment, proceed to (8) and skip (8'). If not, skip (8) and proceed to (8').

(8) With its center on the initial point and 180° pointing north, place the Polar Diagram on the contour map. Mark on the contour map the point under Z_2 and also label this point as Z_2. Z_2 is the second approximation to the trajectory terminal for a 12-hour period. For a 6-hour period the displacement is half of this, and the corresponding terminal on the contour map is labelled Z_2.

(8') With its center on the initial point and 180° pointing north, place the Polar Diagram on the contour map. Z_2 obtained under (7) indicates the azimuth of the second approximation to the trajectory terminal. The radial distance to the terminal is set off with dividers as the distance of the number of latitude degrees indicated by Z_2, measured on the contour chart at the appropriate latitude. Mark this terminal Z_2 on the contour chart also. (For example, if Z_2 is 273° 80 knots and the mean latitude of the trajectory segment is 35°N, the displacement is set off on the contour chart as 273° azimuth and $\frac{80}{10} \times 2 = 16$ degrees of latitude measured on the map as the length of 16 latitude degrees at the latitude of 35°N. This is for a 12-hour period. For a 6-hour period the displacement will be 273° azimuth and 8 degrees of latitude. A scale which allows setting off the distance directly by entering the scale with the speed of Z_2 and the appropriate latitude should be constructed locally.)

(9) Measure the geostrophic velocity $\vec{G}_2$ at Z_2 and mark it as a point G_2 on the Polar Diagram. If $\vec{G}_1$ and $\vec{G}_2$ agree within the accuracy with which we can estimate geostrophic velocities on our maps, the construction can stop here, and Z_2 is the desired terminal. For practical purposes this accuracy may be taken as 5 knots or 10% of $\vec{G}_2$,

whichever is highest. If $\vec{G}_2$ differs from $\vec{G}_1$ by more than this value, proceed to (10).

(10) Proceed as under (6) and (7) with G_2 now replacing G_1 in the instructions, thereby determine Z_3, and set it off on the contour map as done for Z_2 under (8) or (8'), as appropriate.

(11) Measure the geostrophic velocity $\vec{G}_3$ at Z_3. If $\vec{G}_3$ and $\vec{G}_2$ agree within the stated limits, Z_3 is the desired terminal and the computation can stop here. If not, proceed again as under (6) and (7), G_3 now replacing G_1 in the instructions, and thereby determine Z_4. Set Z_4 off on the contour chart, $\vec{G}_4$ at Z_4 is measured, etc. The process is repeated until a point Z_n is reached on the contour chart such that the geostrophic velocity $\vec{G}_n$ at this point agrees with $\vec{G}_{n-1}$ within the desired limits. Usually 2 or 3 approximations will suffice.

The final velocity at the end of the first period, which will be the new initial velocity for the next period, is now determined by using the points v_o, G_o, and G_n on the Polar Diagram as follows:

(12) Place the Polar Diagram on the right diagram (marked Final Velocity) of the AWS Trajectory Graph, such that G_o falls on the underlying center and v_o falls on the horizontal axis (marked $\vec{v}_o - \vec{G}_o$). Proceed along the circle under v_o to intersection with the appropriate latitude line (brackets for 6-hour intervals). Mark this intersection point v_1 on the Polar Diagram.

(13) Rotate the Polar Diagram with G_o remaining on the center until G_n falls on the vertical axis (marked $\vec{G}_n - \vec{G}_o$). Proceed along the spiral under G_n to the intersection with the appropriate latitude line. Mark the intersection point as v_2 on the Polar Diagram.

(12) Add v_1 from (12) and v_2 from (13) vectorially on the Polar Diagram. The point arrived at represents the final velocity of the first period and the new initial velocity of the second period. Plot this velocity as an arrow on the contour chart at Z_n. This aids in drawing the trajectory, which is tangent to it.

b. Second and Subsequent Computation Periods. The determination of the displacement and final velocity during the second period is quite analogous to the procedure outlined under paragraph a, above, except for (1), (2), and (3) which now do not apply. The new $\vec{v}_o$ has already been found under (14), and the new $\vec{G}_o$ is $\vec{G}_n$ of the first period. v_o and G_o of the second period are again marked as points on the Polar Diagram, and the procedure from there on is as from sub-paragraphs a(4) through (14), above. The new $\vec{G}_1$, $\vec{G}_2$, etc., are determined from the contour chart valid at the end of the second period at the points Z_1, Z_2, etc.

For subsequent periods the process is again analogous to the second period. The final velocity and $\vec{G}_n$ of the previous period are used each time as $\vec{v}_o$ and $\vec{G}_o$ for the present period, and the velocities $\vec{G}_1$, $\vec{G}_2$, etc., are read at the points Z_1, Z_2, etc., on the contour map valid at the end of the present period.

Finally, if desired, the total trajectory may be traced (using a light table) on a separate chart by transferring the terminals and velocities already entered on the individual contour charts. The trajectory is drawn tangent to the velocities at the terminals of each period.

1.13.6. Limitations of Dynamic Methods. Theoretically, we may carry on a dynamic trajectory for as long as contour charts are available (analytic or prognostic). However, when the chain of constructions depends on only one actual condition at the beginning of the first period and since this condition is only approximately known, the longer the chain the more will the trajectory depart from reality. This is particularly true in complex contour patterns. With large ageostrophic components $(\vec{v}_o - \vec{G}_o)$ the trajectory takes the form of cycloids of large amplitude which cut drastically across the contour patterns. This is a sign that departure from reality has been reached. An example of this is Figure 15b of sub-section 1.14.2.

When this occurs, it is a sign that errors have accumulated to the point that the flow pattern indicated by the trajectory is out of phase with the contour pattern to a degree that is not realized in nature. In nature a mutual adjustment of pressure pattern and flow pattern occurs continuously at the pressure level in question as well as at all other levels. This adjustment is complex since all levels are linked together hydrostatically. At present only our experience in comparing the pressure and flow patterns on synoptic charts can tell us how far

they can get out of phase with each other. It must, therefore, be left to our experience to decide at which point in the chain the constructed dynamic trajectory is no longer valid.

If we are using prognostic contours it may, of course, be the contour charts which are in error. It has, in fact, been suggested that the trajectory may be used to test whether or not the prognosis is "dynamically" correct.

If the trajectory is being hindcast and winds are available on the analytic contour charts, a new initial velocity can be estimated from the wind field for each period. In this manner it is ascertained that the dynamic trajectory will be reasonably in accord with the pressure pattern.

From the preceding remarks, the impression must not be gathered that dynamic trajectories are erroneous when they cut across contours. Actual trajectories do, in fact, cut appreciably across contours more often than not, particularly in curved flow. Data gathered from actual balloon trajectories indicate that the geostrophic departures at 300 mb are on the average of the order of 30-40% of the wind speed (see subsection 2.1.9).

When forecasting a dynamic trajectory, it will usually not get unreasonably out of phase with the contour pattern until some time after 36-48 hours. Should unreasonable ageostrophic wind components arise, it is best to relax the initial velocity toward the geostrophic wind, for example, by halving the geostrophic departure or by making the new initial velocity entirely geostrophic.

In spite of these difficulties to which protracted dynamic trajectories are subject, it is felt that when the task is hindcasting trajectories in regions where upper-wind reports are much more sparse than height reports, or when forecasting trajectories from prognostic charts for up to 2 days, such methods as the Franceschini-Freeman Method and the AWS Method have definite advantages over other methods.

1.14. Accuracy of Constant Pressure Trajectories.

1.14.1. Statistics on Forecast and Hindcast Accuracies. Machta [18] computed the trajectories for eleven balloon flights at 200 mb, released from Ellsworth AFB, South Dakota, and Holloman AFB, New Mexico, during the period August 1949 to March 1950. The trajectories were constructed by three different methods, i.e., the Consecutive Streamline Method (C.S.M.), the Central Tendency Method (C.T.M.), and the Linear Interpolation Method (L.I.M.).

In Table I the distance between the end points of the computed and actual trajectory is listed as the error. The percentage error is the error as a percent of the actual distance travelled by the balloon.

TABLE I

Trajectory Hindcast Errors, 200 mb, 11 cases (after Machta)

Mean length of the trajectories: 865 naut. miles Mean duration of the flights: 15½ hours				
Method used	Error — naut. mi.		Error — percent	
	Mean	Range	Mean	Range
C. S. M.	196	39 - 660	28	4 - 125
C. T. M.	237	42 - 780	35	5 - 147
L. I. M.	225	65 - 696	33	7 - 131
All 3 methods	219	39 - 780	32	4 - 147

According to this Table the Consecutive Streamline Method turned out to give slightly better results than the other two methods, but judging from the wide range of the errors and the small sample, this small difference is not significant. The errors for an individual flight computed by the various methods showed very small differences.

Machta [19] also tested various kinematic methods in mathematically defined flow patterns; the differences were found to be small, the patterns chosen were such that they gave very small errors for the trajectories, far smaller than those incurred in actual practice; hence, we cannot safely draw any conclusions for the case of actual trajectories.

Table I gives a realistic picture of the accuracy of trajectory

hindcasts that can be attained with a network of observations similar to the one that existed over the United States at 200 mb in 1949-50. Since then, wind coverage and accuracy has increased considerably.

The Air Weather Service Bulletin for November 1952, pp. 16-19 [2], gives the result of an AWS trajectory forecast project. Purpose of the project was to determine the accuracy with which trajectories could be forecast. The duration of the forecasts is not stated. The level was 300 mb. The error summary, which is reproduced below, refers to the "deviation of the forecast from the observed end point of the trajectory expressed as a percentage of the radial distance from the launching site to the observed terminal position. The error is expressed as an error along and at right angles to the trajectory." Table II below summarizes the results. The 76 cases presumably refer to several AWS detachments forecasting for the same trajectories.

TABLE II

Frequency of Trajectory-Forecast Errors Within Percentages Indicated

Percent	Case of Error Across Trajectory	Cases of Error Along Trajectory
0 to 9.9	27	15
10 to 19.9	24	19
20 to 29.9	8	17
30 to 39.9	4	10
40 to 49.9	6	8
50 to 59.9	3	1
60 to 69.9	1	4
70 to 79.9	1	1
80 to 89.9	2	1
90 to 99.9	0	0
Totals	76	76
Avg. % error	19.5	25.9

Assuming the distribution of component errors is such that we can find the percentage absolute error as $\sqrt{(19.5)^2 + (25.9)^2} = 32.5\%$, we may compare this value with the value of 32% from Machta's evaluation of hindcasts. We note that there is surprisingly little difference between the accuracy of hindcast and forecast.

The similarity of the average accuracies of hindcast and forecast

trajectories has also been remarked upon by Moore et al [22]. Their experience relates to 300-mb flights: "Attempts were made to forecast the impact points of the balloons at the end of their flights. Multiple forecasters and procedures were used to minimize subjectivity. Although it was found that better forecasts could be made in certain selected flow patterns and that experience improved the forecasts, the accuracy which could be obtained was limited. Average errors in the prediction of the impact point amounted to about 23% of the total range under all weather situations for which balloons were flown. Under conditions selected by the forecaster as optimum, this error could not be reduced below 18% of the distance travelled.

"It was recognized that operational degradation would reduce the effectiveness of the forecasts whenever the time of launching, rate of rise, floating altitude, or flight duration were different from those assumed by the forecaster. In addition, errors in the basic forecast of the pressure and wind fields to be encountered during flight would affect the accuracy of the trajectory forecast."

A study was made of 20 flights selected for good mechanical behavior, i.e., adherence to the 300-mb level and extension to an average length of 1,000 miles. Hindcasts for these 20 flights had an average error of 20% of the total flight length. This large hindcast error amounted to 80% of the original forecast error for the same flights.

1.14.2. Influence of Flow Patterns on Accuracy of Computed Trajectories. In broad zonal currents of fairly uniform speed the computed trajectories will usually have smaller percentage errors than in flows characterized by large horizontal shears and streamline curvatures, such as usually occur in a low-index situation with closed circulations and generally complex flow patterns.

Figure 13 shows a case of the former type. The trajectory has been computed using the Central Tendency Method with geostrophic winds. It can be seen from the consecutive sections of the contour charts that the situation is fairly stationary. Although the percentage error at first is fairly large (see, for example, at 17/15Z) the percentage error decreases with time, since there is little tendency for the absolute error to accumulate. The data for the observed trajectory, Transosonde #994, is taken from Mastenbrook and Anderson [20].

Figures 15a, b, and c illustrate a case of the latter type. All three Figures refer to Transosonde #993; the hindcast trajectory has

been constructed by three different methods to illustrate their relative merits for this case. In Figure 15a the Central Tendency Method with geostrophic winds has been used, in Figure 15c the Central Tendency Method with streamline and isotach analysis, and in Figure 15b the Franceschini-Freeman Method. Figures 14a-c show the contour patterns during three days of the trajectory.

The balloon kept floating for more than 3 days. On the last day the trajectory completed a loop around the low. Only the Central Tendency Method used with streamline and isotach analysis imitated this loop. The errors of the three constructions are listed in Table III.

TABLE III

Errors in Computed Trajectories of Transosonde #993
(in Degrees Latitude)

Period (hours)	Central Tendency Method (Geostrophic)	Central Tendency Method (Streamline and Isotach)	Franceschini-Freeman Method
6	0.5	0.4	0.5
12	0.3	1.6	0.1
18	3.2	3.0	0.2
24	6.1	4.0	1.2
30	7.4	3.7	2.2
36	11.7	5.3	2.4
42	17.7	9.6	5.8
48	22.0	13.0	3.5
54	23.2	8.8	5.0
60	24.3	5.4	5.9
66	29.4	10.3	3.0
72	41.3	5.6	10.8
78	49.5	5.6	23.3
84	49.3	6.1	24.5
Average	20.4	5.9	6.3

There is a marked increase in error with time. For the C.T.M.-geostrophic this occurs already after 18 hours, for the F.F.M. after 66 hours. The C.T.M.-isotach and streamline analysis starts going off twice but recovers after making the loop.

Such a gradual edging off into a part of the pattern which then rapidly takes the computed trajectory away from the actual trajectory, is typical of such complex patterns as illustrated above. "Getting off

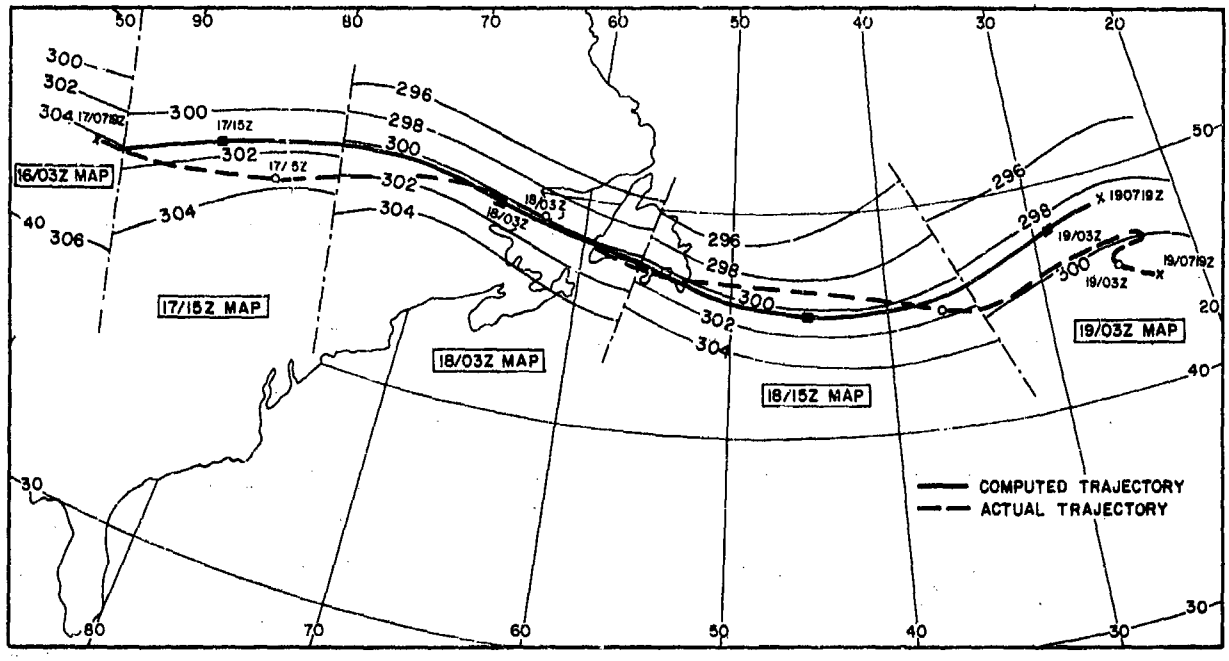

Figure 13. A Trajectory in a Broad Zonal Current. Trajectory is of Transosonde #994, May 1953, at 300 mb; a hindcast of the trajectory is computed by the Central Tendency Method using geostrophic winds. Thin lines are contours of the 300-mb surface in 100's of feet.

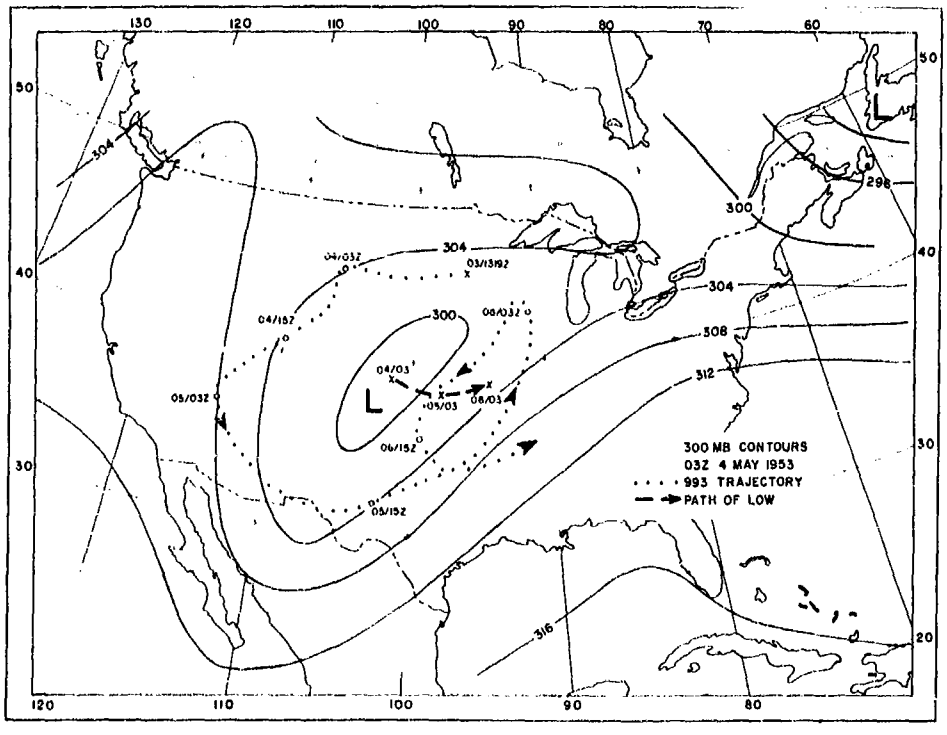

Figures 14a-c. A Trajectory in a Complex Pattern. Shown are 300-mb contours for 0300Z on 4, 5, and 6 May 1953. Path of low center is indicated. Trajectory of Transosonde #993 is entered. (See page 44 for Figures 14b and c.)

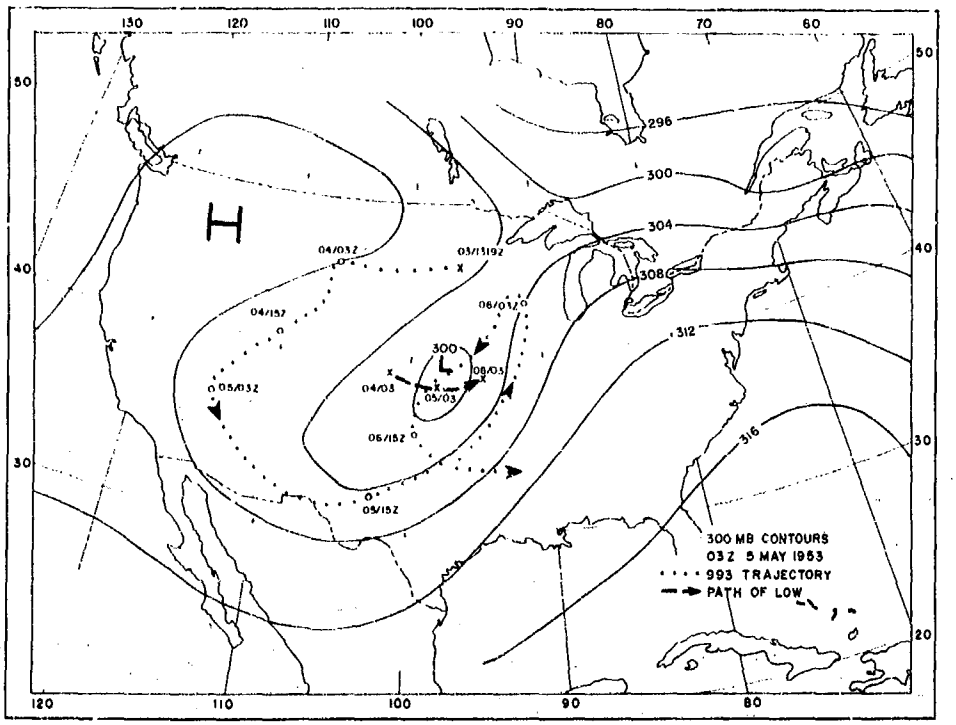

Figure 14b. (See Figure 14a, page 43 for legend.)

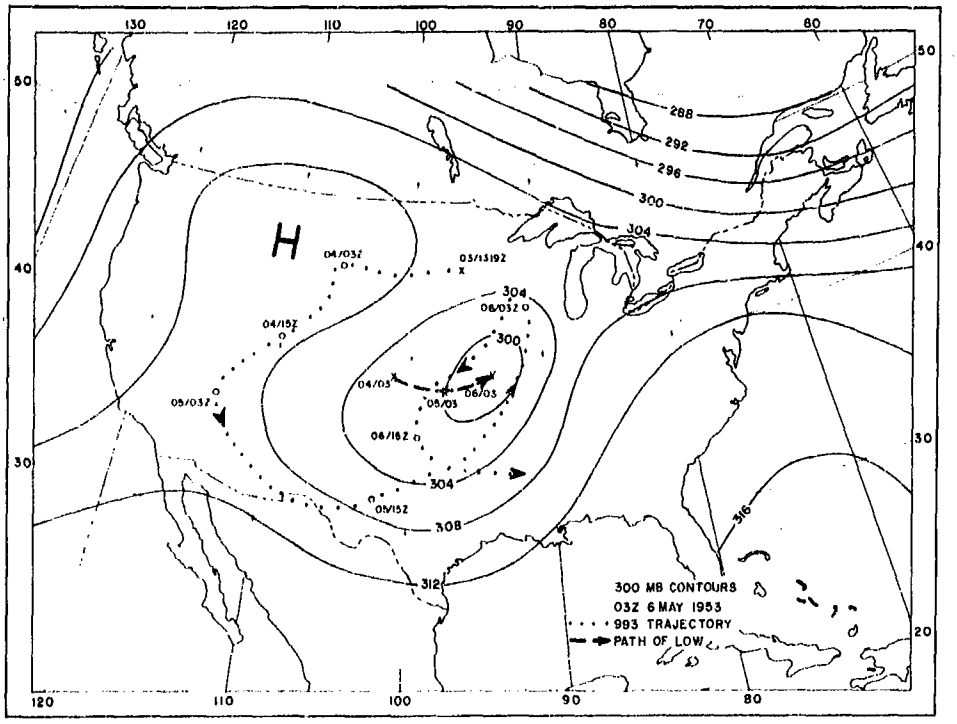

Figure 14c. (See Figure 14a, page 43 for legend.)

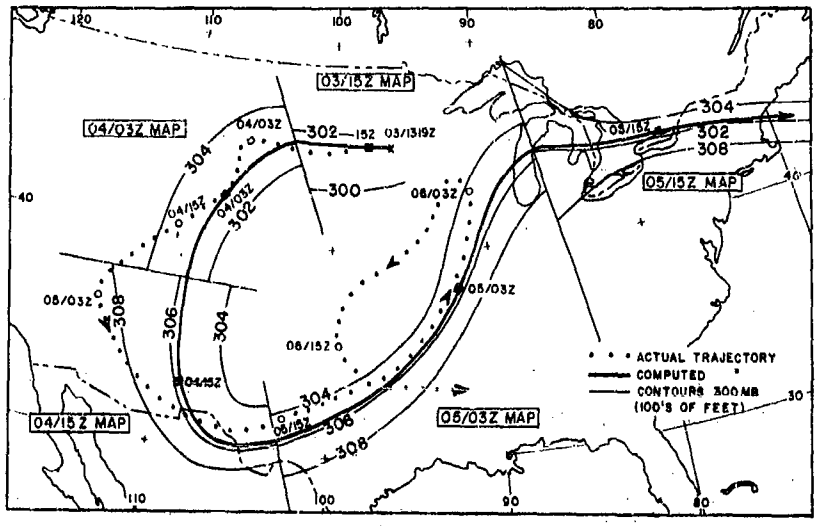

Figure 15a. Hindcast of the Trajectory of Transosonde #993, May 1953, Computed by the Central Tendency Method, Geostrophic Winds. Actual trajectory is entered. The official WBAN 300-mb analyses were used. Sections of the contour analysis in the neighborhood of 12-hour legs of the computed trajectory are shown. The division lines between these sections go through the computed balloon positions at 09Z and 21Z.

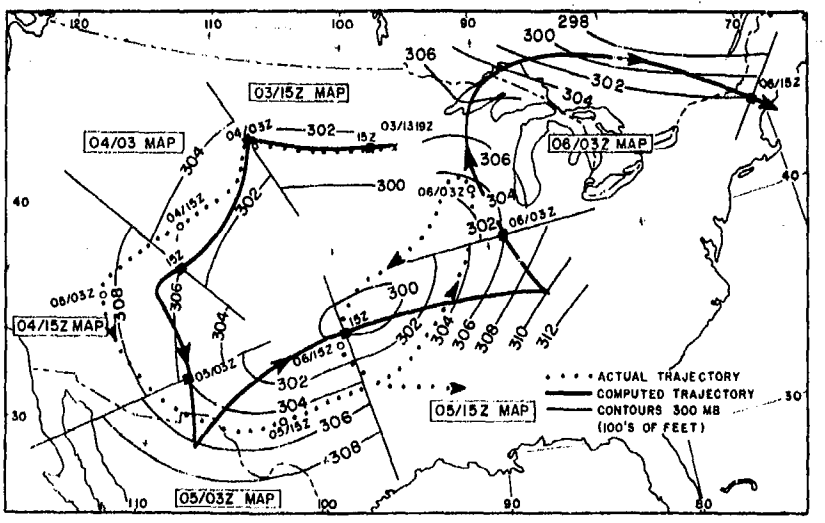

Figure 15b. Hindcast of the Trajectory of Transosonde #993, May 1953, Computed by the Franceschini-Freeman Method. Sections of the contour analyses (official WBAN analyses) in the neighborhood of 12-hour legs of the computed trajectory are shown. The division lines between these sections go through the computed balloon positions at 03Z and 15Z.

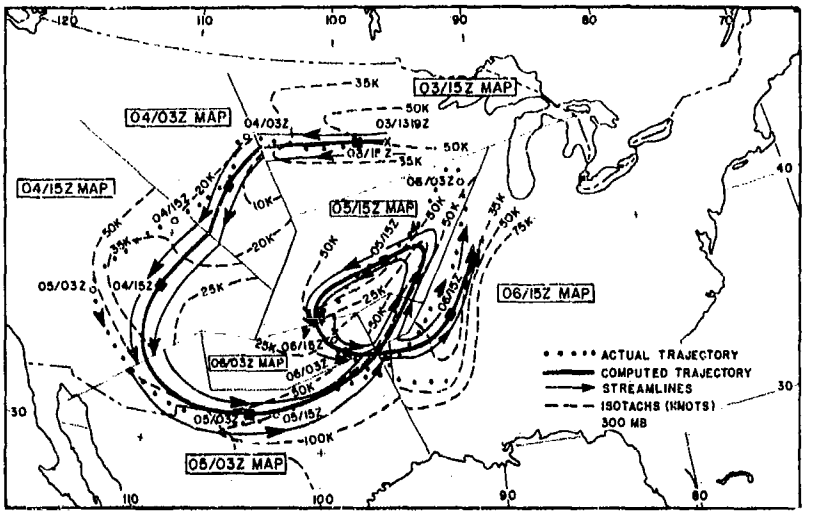

Figure 15c. Hindcast of the Trajectory of Transosonde #993, May 1953, Computed by the Central Tendency Method Using Streamline and Isotach Analyses (analyses by AWS Scientific Services). Sections of the streamline and isotach analyses in the neighborhood of 12-hour legs of the computed trajectory are shown. The division lines between these sections go through the computed balloon positions at 09Z and 21Z. Near the loop the divisions become more complex. The little pentagon in the loop belongs to the 05/03Z map, and the little triangle to the right of the trajectory crossing belongs to the 06/03Z map.

the rails" in this manner may occur early in the trajectory and make the whole trajectory poor, as was the ease with the C.T.M.-geostrophic in this example.

Furthermore, large errors in the trajectory forecast may occur if the balloon is released near or comes near an axis of diffluence so that uncertainty exists as to which side of the axis the balloon will float; also, near neutral points (cols, centers of highs and lows) the trajectories are often erratic.

If the forecaster has any control over the release time and it is imperative to forecast with accuracy, he should wait for a pattern such that confidence in the forecast exists.

1.14.3. Comparison of Methods. Headquarters Air Weather Service recently evaluated the relative merits of some of the most well-known trajectory constructions. The methods involved were:

Method (1) - Central Tendency Method with geostrophic winds.

Method (2) - Central Tencendy Method with winds from streamline

and isotach analysis.

Method (3) - Consecutive Streamline Method, backtracking (see Figure 3b), with geostrophic winds.

Method (4) - Consecutive Streamline Method, backtracking, with winds from streamline and isotach analysis.

Method (5) - The Franceschini-Freeman Method.

Streamline and isotach analysis was attempted only over the U.S. where data were adequate to warrant such an analysis. This eliminated comparison with methods (2) and (4) for the part of the trajectories that passed outside this area.

The trajectories used for verification were Transosondes #990, 991, 993, 994, 995, 996, 998, and 999 at 300 mb [20] and the balloon flights F30, F31, F35, F37, and XF41 at 200 mb from, "Constant Altitude Balloon Flights at 39,000 feet from October through December 1954," Appendix I, Atmospheric Devices Laboratory, Geophysics Research Directorate, Air Force Cambridge Research Center, May 1955.

The tables below show some of the comparisons.

In Table IV the averages in parentheses cannot be compared directly with the other values, since they are based on a smaller number of trajectories.

It is apparent from Tables IV and V that the success of a trajectory computation depends more on the flow pattern than on the particular method used.

1.15. Choice of Method.

From the evaluation reported on in the preceding paragraph, a preference for any particular one of the tested methods could not be established. Comparative evaluations by other authors also show that the various constructions accomplish about the same statistically.

We should not draw the conclusion from this that the method used in any individual case is irrelevant. The statistics only show that if a method is used consistently in all sorts of flow patterns, the average accuracy is about the same for all methods.

Some of the methods have their peculiar advantages and disadvantages depending on the flow pattern. For example, in rapidly changing flow patterns any method that freezes the flow pattern for the period between two consecutive charts, such as the Central Tendency Method,

TABLE IV

Errors (degrees latitude) of 300-mb Trajectory Hindcasts by Various Constructions, as a Function of Flight Time. (Balloons released from Minneapolis, April to August 1953.)

	Flight Time of Transosonde												
	6 hours				12 hours				18 hours			24 hours	
Method No.	1	2	3	4	1	2	3	4	1	2	3	1	3
Flight No.													
990	1.3	0.8	1.2	0.8	3.4	2.3	2.8	2.7	5.4	7.4	5.2	6.3	6.7
991	1.2	2.4	1.3	---	2.8	5.4	2.5	---	3.9	10.1	4.7	5.8	7.9
993	0.5	0.4	0.5	0.4	0.3	1.6	1.7	1.5	3.2	3.0	1.2	6.1	2.0
994	0.9	---	0.8	---	0.4	---	0.5	---	0.4	---	0.5	1.3	1.4
995	1.1	---	1.1	---	6.1	---	5.8	---	9.6	---	11.2	16.0	18.9
996	3.0	---	3.0	---	5.2	---	2.5	---	3.4	---	1.5	---	---
998	0.4	---	0.4	---	0.9	---	1.6	---	0.9	---	2.3	2.6	2.7
999	0.4	---	0.4	---	1.6	---	1.6	---	4.1	---	4.6	7.3	8.5
Average	1.1	(1.2)	1.1	(0.6)	2.6	(3.9)	2.4	(2.1)	3.9	(6.8)	3.9	6.5	6.9

	30 hours		36 hours		42 hours		48 hours		54 hours		60 hours	
Method No.	1	3	1	3	1	3	1	3	1	3	1	3
Flight No.												
990	5.2	7.8	7.7	9.4	10.3	10.8	13.0	11.5	---	---	---	---
991	6.2	7.6	6.2	7.6	4.7	7.2	3.7	7.4	9.2	4.0	10.4	3.4
993	7.4	2.2	11.7	4.5	17.7	8.0	22.0	12.8	14.4	23.2	6.3	24.3
994	0.9	1.7	2.5	3.3	1.8	4.0	2.4	0.6	---	---	---	---
995	23.5	27.1	28.4	31.4	30.3	32.0	30.9	33.6	34.0	30.0	37.2	33.2
996	---	---	---	---	---	---	---	---	---	---	---	---
998	4.1	1.6	7.3	4.5	12.9	10.0	16.7	11.1	13.4	16.7	16.2	17.0
999	10.8	10.3	8.5	6.5	4.5	3.9	3.3	3.2	4.7	3.0	---	---
Average	8.5	8.4	10.3	9.6	11.7	10.8	13.1	11.4	15.4	15.1	19.5	17.5

TABLE V

Average Errors (degrees latitude) of 200-mb Trajectory Hindcasts by Methods No. 1 and No. 5. (Flights launched from Vernalis, California, December 1954.)

	AACS Fixes			CAA Fixes		
Flight No.	Method No.1	Method No.5	Number of Fixes	Method No.1	Method No.5	Number of Fixes
F30	2.6	2.4	62	2.2	1.2	4
F31	2.2	2.0	43	1.8	1.9	3
F35	2.5	2.5	20	4.4	3.4	3
F37	3.4	2.1	65	5.2	3.5	6
XF41	2.0	2.6	55	2.1	2.1	17
Average	2.5	2.3	—	3.1	2.4	—

will usually give poor trajectories. In patterns that change slowly or little the Central Tendency Method is a fine method because of its ease of application.

In rapidly changing flow patterns where the change can be described fairly well as a translation of the flow patterns, the Relative Trajectory Method or the General Mills' Method will give good results. In practice, however, the change of the flow pattern can be described as a constant translation only over a limited region of the chart. Outside this region the patterns may move with a different speed or remain stationary; consequently, here a different system displacement or some method other than the Relative Trajectory Method must be used.

When the flow patterns change rapidly and the change cannot be described well as a translation of the type assumed in the Relative Trajectory Method, some other method should be used. An example of such a type of pattern is a circulation that intensifies as it moves along. Petterssen's Method, the Linear Interpolation Method, and the dynamic methods are designed to take such changes into account.

From the aforesaid it is apparent that the flow pattern should influence the selection of the method. The broad principles for this selection are outlined above.

In complex flow patterns with pronounced shears, curvatures, branch points, and singularities there will, at times, be regions where dual possibilities exist for two diverging trajectories. The forecaster who prepares the trajectory forecast will then be faced with a dilemma: he has to choose between two possible but widely different trajectories. The dilemma may occur right at the start of the trajectory or sometimes later in the trajectory. It happens whenever the balloon comes into the vicinity of a line of diffluence or of a singular point in the flow (cyclonic or anticyclonic circulation center or a col). The scientific approach to resolve this dilemma is to indicate two trajectories and point out to the using agency that equal probabilities exist for each of them. The using agency can then incorporate this facet in their operational decision.

1.16. Climatological Trajectory Studies.

In planning constant-level balloon operations many problems of a climatological nature arise. Climatology deals with the probabilities of certain incidents as determined by the historical behavior of the

atmosphere. The frequencies of these incidents are established on the basis of past weather records, and it is assumed that the future probabilities can be estimated from these frequencies.

Some examples of the questions which may be asked can serve to illustrate the object and method of such climatological trajectory studies:

a. Given a certain Area A and a number of potential release points, what are the most "favorable" release points in a certain month for balloons floating at 300 mb? When balloons are released from all potential release points according to some prearranged schedule, the "favorable" release points are the ones which have the highest number of trajectories crossing Area A.

b. What percentage of the balloons released from a point according to a prearranged schedule can be expected to hit A? (A hit is a crossing of Area A by a trajectory.)

c. What is the probable percentage of hits if a forecaster were to select the release time? This percentage should be expected to be higher than in "b" on the basis that a forecaster is able to forecast the trajectories with some skill. This will be the case if the scatter of the forecast error is smaller than the scatter of balloons released according to a prearranged schedule, irrespective of flow pattern. Thus, it is seen that the forecasting ability enters as a factor in this question.

d. What is the probable distribution of flight time among the trajectories from a point to Area A?

These are just a few of the questions which might have to be answered in the planning of constant-level balloon operations.

One way of providing the answers to these questions is to operate with "paper" flights. For instance, to answer question "a" a series of historical 300-mb maps for the pertinent month can be used for construction of a series of trajectories from the potential points. The number of trajectories that intersect Area A from the various points are tabulated and will yield the required information. It is to be noted that several years of data have to be used since the flow patterns during a certain month may vary considerably from one year to the next. The table will also answer question "b".

Gathering the data needed for climatological trajectory studies by the "paper"-flight method is a laborious task since a large number of trajectories have to be constructed to obtain representative samples.

At the present this must be done by hand. At some future date it is visualized that analyses for machine processing will be available and the task will be considerably lessened.

There is another avenue of approach offered by the statistical theory of turbulence. If the statistical properties of the "large-scale" turbulence could be established by analogy with those of the small-scale turbulence, these properties could be used directly. However, the necessary statistical properties of the "large-scale" turbulence are not sufficiently known at the present time if, indeed, they do exist.

S. B. Solot has developed a semi-empirical method of solving climatological problems in connection with trajectories. The method is much less time consuming than the "paper-flight" method and gives, it is claimed, results of comparable accuracy. For information on the method, reference is made to Air Force Surveys in Geophysics No. 61, "Meteorological Aspects of Constant Level Balloon Operations," Air Force Cambridge Research Center, December 1954.

Section II

SOME THEORETICAL ASPECTS OF CONSTANT-PRESSURE TRAJECTORIES

2.1. Trajectories by Particle Mechanics.

2.1.1. Trajectories and the Contour Field. With a few minor simplifications which amount to less than 1/10 of a knot per hour, the acceleration of the horizontal motion of the atmosphere may be written:

$$(1) \qquad \vec{v} = -f\vec{k} \times (\vec{v} - \vec{v}_g)$$

where $\vec{v}$ is the horizontal velocity, $\vec{v}_g$ is the geostrophic wind, f is the Coriolis parameter, and $\vec{k}$ is a vertical unit vector.

Turbulent stresses have here been neglected, but even so the equation probably has a high degree of fidelity for the scales of motion dealt with on synoptic charts — except for the motion in the lowest few thousands of feet. Here $\vec{v}_g$, the geostrophic wind, is an expression for the horizontal pressure force $-\alpha \nabla_H p = -g \nabla_p z$; ∇_p is the horizontal del-operator applied to a quantity in an isobaric surface, and z the height of this surface.

$$(2) \qquad \vec{v}_g = \frac{g}{f} \vec{k} \times \nabla_p z$$

Thinking of the wind $\vec{v}$ as a function of horizontal position, for instance x and y, pressure p, and time t:

$$\vec{v} = \vec{v}(x, y, p, t),$$

we can write:

$$(3) \qquad \dot{\vec{v}} = \left(\frac{\partial \vec{v}}{\partial t}\right)_p + \vec{v} \cdot \nabla_p \vec{v} + \frac{dp}{dt} \frac{\partial \vec{v}}{\partial p}$$

Defining

$$(4) \qquad \dot{\vec{v}}_p = \left(\frac{\partial \vec{v}}{\partial t}\right)_p + \vec{v} \cdot \nabla_p \vec{v},$$

$\dot{\vec{v}}_p$ may be interpreted as the horizontal acceleration of an object that is constrained to remain in the pressure surface p and that undergoes a horizontal displacement identical to that of the air that surrounds it at any time.

This motion is well approximated by a constant-pressure balloon. By means of a control device a high-level constant-pressure balloon is usually kept within ±10-15 mb of the intended floating pressure. The large horizontal drag coefficient of the balloon makes it respond to accelerations in the wind almost instantaneously, so that the trajectory of the balloon will closely be determined by the equation.

$$(5) \qquad \vec{v}_p = -f\vec{k} \times (\vec{v} - \vec{v}_g) - \frac{dp}{dt}\frac{\partial \vec{v}}{\partial p}$$

The trajectory of such an object that stays in the pressure surface and moves with the winds in this surface will be referred to as a constant-pressure trajectory.* We see from Equation (5) that the horizontal acceleration of this object is determined by:

a. The Coriolis acceleration of the geostrophic departure $\vec{v} - \vec{v}_g$ in the surface and

b. A term $-\frac{dp}{dt}\frac{\partial \vec{v}}{\partial p}$ composed of the individual pressure change dp/dt of the air in the pressure surface and the vertical wind shear $\partial\vec{v}/\partial p$. Since dp/dt is mainly given by the vertical motion, the second term will be referred to as the vertical motion term.

2.1.2. Effect of the Vertical Motion Term on Constant-Pressure Trajectories. The vertical motion term can also be written:

$$-\frac{dp}{dt}\frac{\partial \vec{v}}{\partial p} = \frac{\partial \vec{v}}{\partial z}[\vec{v}\cdot\nabla_p z - (w - w_p)]$$

where w is the vertical velocity component of the air and w_p is the vertical motion of the pressure surface. Since the motion is mainly geostrophic $\vec{v}\cdot\nabla_p z$ is small compared to $w - w_p$ if the latter is appreciable at all. This can be seen by an example:

$$\vec{v}\cdot\nabla_p z = \frac{f}{g}\vec{v} \times \vec{v}_g \cdot \vec{k}$$

Choosing $\vec{v}_g$ = 50 m sec^{-1} with a geostrophic departure normal to $\vec{v}_g$ of 10 m sec^{-1} magnitude, $(\vec{v}\cdot\nabla_p z) = 10^{-4}$ $sec^{-1} \times 10^{-1}$ sec^2 $m^{-1} \times$ 10 m $sec^{-1} \times$ 50 m sec^{-1} = 0.5 cm/sec. at 40°N.

*Since the main concern is this Manual is the construction of constant-pressure trajectories, they will often be referred merely as trajectories, meaning constant-pressure trajectories if nothing else is stated.

Even this fairly large ageostrophic motion is equivalent to the very modest vertical motion of 0.5 cm/sec. Hence, the term $\vec{v}\cdot\nabla_p z$ can be neglected when compared to $(w - w_p)$ which measures the vertical motion through the pressure surface. We obtain for the vertical motion term:

$$-\frac{dp}{dt}\frac{\partial\vec{v}}{\partial p} = -\frac{\partial\vec{v}}{\partial z}(w - w_p)$$

We will assess the magnitude of this term by a numerical example. Choosing $w - w_p = 3$ cm/sec and $\partial\vec{v}/\partial z = 5$ knots/1000 feet, we get

$$-\frac{dp}{dt}\frac{\partial\vec{v}}{\partial p} = -1.8 \text{ knots/hour.}$$

If these conditions, $(w - w_p) = 3$ cm/sec and $\partial\vec{v}/\partial z = 5$ knots/1000 feet, were sustained over 10 hours of the trajectory we would make an error in the computation of the position of the object of approximately $+\frac{1}{2} \times 1.8$ knots/hour $\times 10^2$ hour^2 = 90 nautical miles by neglecting the vertical motion term and computing the trajectory according to the equation:

$$(6) \qquad \vec{v}_p = -f\vec{k} \times (\vec{v} - \vec{v}_g)$$

The trajectory will be too long by 90 miles in the example.

The conditions in the example chosen cannot be said to be unusual. Maximum-wind and shear charts [32] show that $\partial\vec{v}/\partial z \geq 5$ knots/1000 feet may occur in long elongated bands in pressure surfaces underneath the maximum-wind level, and similarly $-\partial\vec{v}/\partial z \geq 5$ knots/ 1000 feet above the level of maximum winds. 3 cm/sec appears to be a moderate rate of vertical motion. Various studies show that vertical motions of this magnitude may occur over large areas for extended periods of time.

Neiburger and Angell [23] evaluated the vertical motion term along constant-pressure-balloon trajectories using the adiabatic method for obtaining dp/dt and obtaining $\partial\vec{v}/\partial p$ from rawins in the vicinity. They found that the magnitude of the vertical motion term was on the average 20-25% of that of $-f\vec{k} \times (\vec{v} - \vec{v}_g)$; omission of the term as done in Equation (6) leads to a fair approximation of the trajectory.

Since vertical motions are mostly unknown, there is at present no method whereby we can make allowance for the vertical motion term when computing constant-pressure trajectories. All we can state is that cumulative errors up to 100 nautical miles may be made over a period of 10 hours when computing trajectories according to Equation (6) because of omitting the vertical motion term. However, other sources of error, such as insufficient knowledge of the contour field, $\vec{v}_g$, at

all times, usually lead to more serious errors. Therefore, we may state that in the present state of the art of constructing constant-pressure trajectories by means of dynamic methods, omission of the vertical motion term in most patterns does not lead to any gross errors.

When the wind shear is large, it is usually directed along the trajectory. The large-scale vertical motions in the upper atmosphere are in the mean distributed according to the formula: subsidence downstream from ridges and upstream from troughs, upward motion downstream from troughs and upstream from ridges.

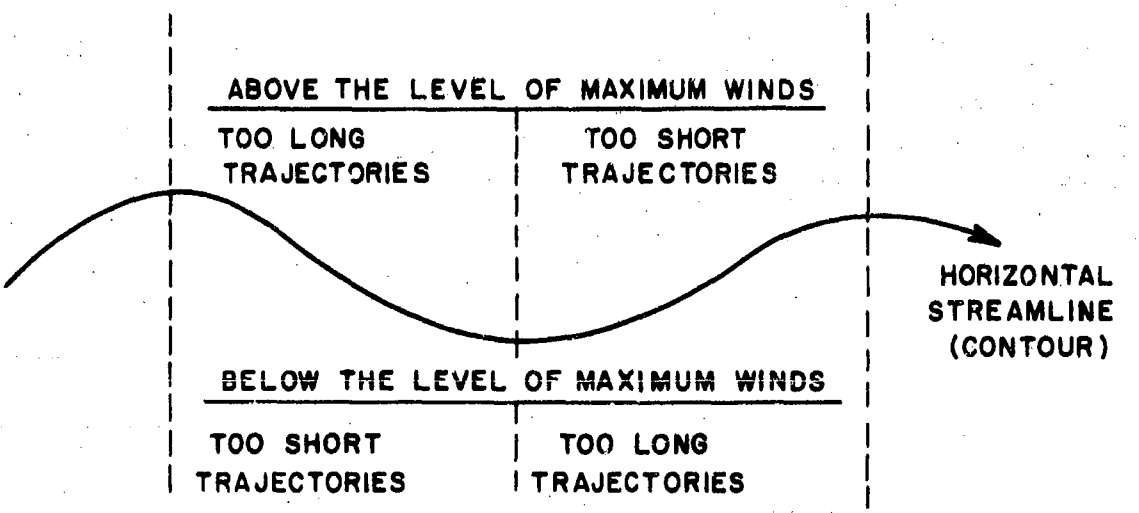

Figure 16. Schematic Diagram of the Effect of Neglecting the Vertical Motion Term when Computing Dynamic Trajectories.

Hence, neglect of the vertical motion term will lead to the type of errors illustrated in Figure 16, when the trajectories are computed by dynamic methods.

2.1.3. Dynamic Methods of Trajectory Computations. Referring again to Equation (6), we see that if the contour field of the pressure surface is known as a function of x, y, and t, the trajectory of an object is uniquely determined if its initial position and velocity at a time, t = 0, is known.

Methods utilizing Equation (6) for constructing trajectories will be referred to as dynamic methods, and the trajectories computed by them as dynamic trajectories.

The efforts that have been made in the past on dynamic trajectories can be grouped in two classes according to how $\vec{v}_g$ is prescribed:

a. The contour field is prescribed by mathematical functions.

b. The contour field is prescribed graphically.

The work carried out in the first class is not directly applicable in practical trajectory computations since the contour fields occurring in practice only poorly resemble mathematical models, both stationary and moving ones. Nevertheless, the contributions in this field have great theoretical interest. They illustrate the air flow in the various pressure patterns. Also, they have been particularly interesting through demonstrating that large ageostrophic motions may occur; this has later been verified by study of actual trajectories, computing $\vec{v} - \vec{v}_g$ from the accelerations obtained from the trajectories (Durst and Davis [4], Emmons [6], Neiburger and Angell[23], and Godson [11]).

The graphical methods are directly applicable to the practical meteorological situation; i.e., $\vec{v}_g$ is given by contour charts at intervals of 12 hours or 24 hours.

In between standard synoptic hours, intermediate charts may be drawn by interpolation for sufficiently small intervals to satisfy the convergence criteria of the graphical integration method, or some transition from one chart to the next (such as a time-linear transition in the local $\vec{v}_g$) may be assumed. Two of the graphical methods will, therefore, be described in detail further on.

2.1.4. Mathematical Trajectories. These are trajectories in Class a, above.

2.1.4.1. $\vec{v}_g$ = constant.

The simplest of all geostrophic-wind fields is a stationary uniform one, $\vec{v}_g$ is constant in space and time. Equation (6) is directly integrable. Since $\vec{v}$, $\vec{v}_g$, and $\dot{\vec{v}}$ are all coplanar vectors, it is convenient to replace the vector symbols by their complex equivalents:

$$\vec{v} = \epsilon = u + iv$$
$$\vec{v}_g = \gamma = u_g + iv_g \qquad i = \sqrt{-1}$$

Equation (6) may then be written:

$$(6') \qquad \dot{\epsilon} = -fi(\epsilon - \gamma)$$

or for the position vector $z = x + iy$:

$$\ddot{z} + fi\dot{z} - fi\gamma = 0$$

with the solution $\epsilon = \gamma + (\epsilon_o - \gamma)e^{-ift}$

$$(7) \qquad z = \gamma t - \frac{i}{f}(\epsilon_o - \gamma)(1 - e^{-ift})$$

for the initial conditions $z = 0$, $\epsilon = \epsilon_o$ when $t = 0$.
f has been treated as a constant.

This motion plays a fundamental part in the theory of atmospheric trajectories and will be discussed here in some detail.

In vector notation:

$$(8) \quad \vec{r} = \vec{v}_g t + \frac{\sin(ft)}{f}(\vec{v}_o - \vec{v}_g) - \frac{[1 - \cos(ft)]}{f}\vec{k} \times (\vec{v}_o - \vec{v}_g)$$

where $\vec{r}$ is the position vector of the object. Equation (7) or (8) gives the trajectory of the object. Its displacement has two components: a steady progression, $(\vec{v}_g t)$, and an oscillatory displacement with a period

$$T = \frac{2\pi}{f} = \frac{12 \text{ hours}}{\sin\Phi} = \text{half a pendulum day.}$$

Figure 17 illustrates a graphical construction of the displacements. The object starts out at A at $t = 0$. With the geostrophic velocity it would be at B at time t; with the initial velocity it would be at C; actually it arrives at D. D is located thus: From A, a right normal to $\vec{v}_o - \vec{v}_g$ is drawn; centered on this normal a circle with a radius $\frac{1}{f}|\vec{v}_o - \vec{v}_g|$ is drawn through A. From OA an angle $\theta = ft$ intersects the circle at E. $\overrightarrow{AE}$ is the oscillatory component. When $\overrightarrow{AE}$ is added to $\overrightarrow{AB}$, $\overrightarrow{AD} = \vec{r}$ is obtained. When t varies from 0 to T, point E runs around the entire circle anticyclonically (inertial circle).

It will be seen from Figure 17 that the trajectory is described by the point A rigidly fastened to a wheel, radius $\frac{1}{f}|\vec{v}_g|$, concentric with the first circle, and rolling on line L_1L_1. The point runs through the trajectory at the proper speed when the wheel rolls with an angular speed of f. When $|\vec{v}_o - \vec{v}_g| \lessgtr |\vec{v}_g|$ the trajectory will be a curtate, common, and prolate cycloid respectively. The prolate cycloids have loops.

Figure 18 shows the trajectory at 43°N corresponding to conditions

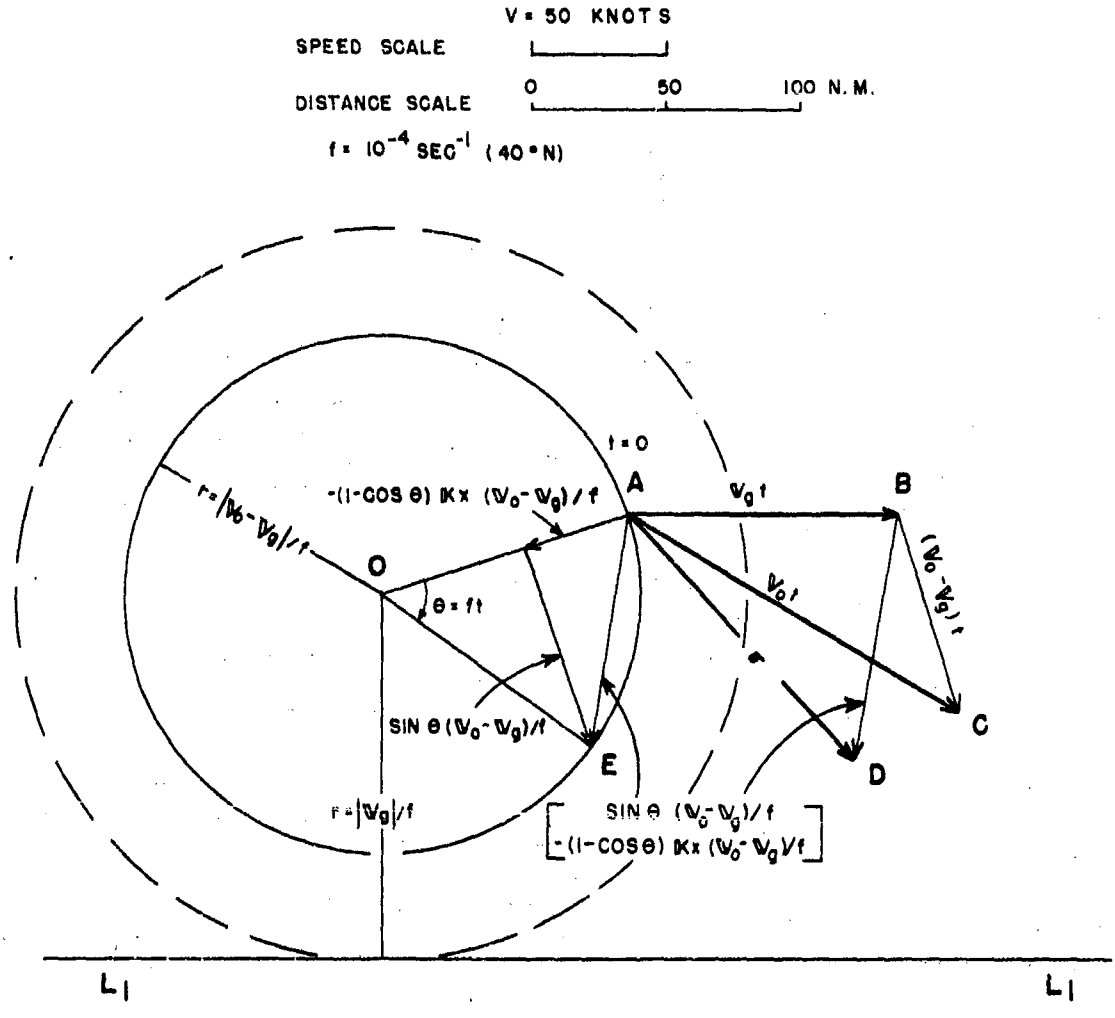

Figure 17. Construction of Trajectory of a Uniform Geostrophic Wind Field.

$\vec{v}_g$ = 50 knots, $\vec{v}_o$ = 70 knots 30 degrees to the right of $\vec{v}_g$. The distance scale gives an idea of the deviations from the geostrophic trajectory that arise. The period at 40°N is 17.8 hours. The trajectory is a curtate cycloid.

In this connection it is interesting to note that Neiburger and Angell [23] in their study of Navy transosonde flights (at 300 mb) found an average period of about 18 hours in the sign of the cross-contour motion of the balloons. The mean latitude of the trajectories was 35-40°N; release point was Minneapolis. It appears that this oscillatory motion around the geostrophic trajectory as a mean position line with a period near half a pendulum day may be a common occurrence

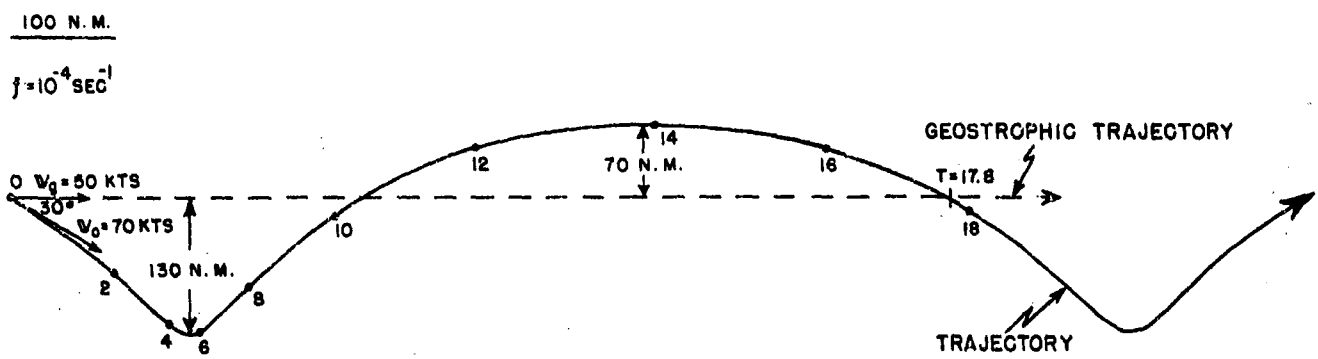

Figure 18. A Trajectory in a Uniform Geostrophic Wind Field at 43°N. With the initial conditions stated in the diagram the trajectory is a curtate cycloid with a period of 17.8 hours (half of a pendulum day).

in actual trajectories, although the period of the oscillation will be more complex in the actual contour patterns of the synoptic charts.

Referring again to Equation (8) and defining a dimensionless operator $X\cdot(\ )$ (applied to a vector quantity) as

$$X\cdot(\ ) = \frac{\sin(ft)}{ft}(\ ) - \frac{1-\cos(ft)}{ft}\vec{k}\times(\ )$$

where X depends on latitude and time only, we can write

$$\vec{r} = \vec{v}_g t + X\cdot(\vec{v}_o - \vec{v}_g)t.$$

For angles of $ft \ll 1$ Equation (8) may be approximated by

$$(9) \qquad \vec{r}^* = \vec{v}_g t + X^*\cdot(\vec{v}_o - \vec{v}_g)t$$

where

$$X^*\cdot(\ ) = -\frac{ft}{2}\vec{k}\times(\ ) - \frac{(ft)^2}{6}(\ )$$

For $t = 2$ hours, $f = 10^{-4}$ sec^{-1} (40°N), $\vec{r} - \vec{r}^* \approx 0.16\,\vec{k}\times(\vec{v}_o - \vec{v}_g)$. For $|\vec{v}_o - \vec{v}_g| = 20$ knots, $|\vec{r} - \vec{r}^*| = 3.2$ nautical miles. This small difference is negligible in ordinary map work.

For the velocity at the end of the trajectory we obtain with the same approximations from Equation (7):

$$(10) \qquad \vec{v}^* = \vec{v}_o - f\vec{k}\times(\vec{r}^* - \vec{v}_g t)$$

Formulae (9) and (10) are of interest since they are the formulae used by Franceschini and Freeman [9] in their graphical trajectory construction. In their procedure $\vec{v}_g$ is identified with the time-space mean of the geostrophic wind over the trajectory, and only a short bit

of the trajectory to t = 2 hours is used.

2.1.4.2. $\vec{v}_g = \vec{v}_g(t)$ or $\gamma = \gamma(t)$.

This case, where $\vec{v}_g$ is independent of x and y but changes with t, was first studied by Hesselberg [15] and later by Stewart [28] and Forsythe [8].

The general solution is

$$\epsilon = \epsilon_o e^{-ift} + ife^{-ift} \int_o^t e^{ift}\, \gamma(t)dt.$$

Choosing a simple function

$$\gamma(t) = \gamma_o + \alpha t$$

where α is the constant rate of the local geostrophic wind change, we obtain

$$(11) \quad \epsilon = \gamma_o + \alpha t + \frac{i\alpha}{f} + (\epsilon_o - \gamma_o - \frac{i\alpha}{f})e^{-ift}$$

Brunt and Douglas [3] called the quantity $\frac{i\alpha}{f}$ the isallobaric wind.

For the trajectory we get

$$(12) \quad z = \gamma_o t + \frac{i\alpha t}{f} + \frac{1}{2}\alpha t^2 - \frac{i}{f}(\epsilon_o - \gamma_o - \frac{i\alpha}{f})\,(1 - e^{-ift})$$

The magnitude of the local variation of the geostrophic wind may be approximated by that of the wind itself. Sutcliffe and Sawyer [29] give the 24-hour root-mean-square vector change of the wind at 300 mb as 48 knots. This gives a smoothed root-mean-square value for α of 2 knots/hour. This case is further discussed in sub-section 2.1.6.

2.1.4.3. Other Mathematical Functions for $\vec{v}_g$. Forsythe [8] studied trajectories in the field, $\vec{v}_g = (ax + by + c)\vec{i} + (dx + ey + h)\vec{j}$ (stationary linear vector field), and also the general case of stationary circular contours.

Gustafson [12] used various mathematical models for the contour field, among them a propagating geostrophic jet-stream wave. He was also able to take the variation of the Coriolis parameter into account. A differential analyzer was used since the models were defined by equations that could not be integrated by tabulated functions.

2.1.5. Graphical Construction of Dynamic Trajectories. In practice the $\vec{v}_g$ field is given by synoptic contour charts at 12- or 24-hour intervals. These charts may be analytic or prognostic. The characterization of the contour field is now much less precise than when it is presented mathematically.

The chart may be divided up in sections such that the "character" of the contour field may be said to be fairly uniform within one and the same section, but varies from section to section. The size of a section may, for instance, be 100 × 100 (nautical miles)^2. Within a section, $\partial\vec{v}_g/\partial t$ may be assumed to be constant during a time interval, for instance, 2 hours. By having "uniform character" is meant that the contour field within the section is sufficiently accurately described by constant values of certain parameters. The whole chart is then built up of these mosaic sections with the characteristic parameters constant within one and the same section and time interval, but generally different from one section to the next and from one time interval to the next.

As far as characteristic parameters are concerned, the choice is to a certain extent open. The parameters must be easily measurable and graphically presentable. Furthermore, only parameters can be used which determine such a contour field within the section so that the trajectory through it may readily be obtained. The degree of complexity of the parameters we may choose is also greatly limited by the uncertainty with which the contour field is known. On analytical contour charts this uncertainty is imposed by insufficient data coverage, observational errors, and indeterminacy of the contour field between the synoptic hours. On prognostic contour charts the uncertainty is enhanced by errors of prognosis.

The sections and intervals do not have to be of the same size. Where the parameters vary slowly in space and time, longer sections and intervals may be chosen than when the variations are pronounced.

As parameters we may think of: $\vec{v}_g$ itself, $\partial\vec{v}_g/\partial t$, geostrophic shear, contour diffluence, contour curvature, the constants of the best linear fit to the $\vec{v}_g$ field, etc. Even if trajectories through fields characterized by constancy of $\vec{v}_g$, $\partial\vec{v}_g/\partial t$, $\partial\vec{v}_g/\partial n$, etc., or combinations thereof may be obtained by graphical means, measurement of the parameters and the ensuing graphical trajectory construction is so time consuming that the process for any but the simplest parameters is not justified in view of the uncertainty already mentioned.

One of the graphical methods for construction by dynamical trajectories is the method of Franceschini and Freeman [9].

2.1.6. The Franceschini-Freeman Method. This method assumes a constant $\vec{v}_g$ over a section and no change of $\vec{v}_g$ during a time interval.

The time interval is chosen equal to 2 hours. The section is chosen as a strip along a vector 2 hours times $\vec{v}_o$ where $\vec{v}_o$ is the initial velocity, which must be known. The width of the strip is chosen so that it takes in the trajectory. At the outset the trajectory is unknown, of course, but a sufficiently good approximation of it can be made to determine the width of the strip. The average geostrophic wind over this strip is measured. We will denote it with $\vec{v}_g$. Usually the space-time average $\vec{v}_g$ over 2 hours times $\vec{v}_o = \overrightarrow{AB}$ is good enough (see Figure 10). This quantity $\vec{v}_g$ is an approximation of the space-time average geostrophic wind over the trajectory.

With $\vec{v}_g$ as a constant field, Equation (9) gives the displacement with sufficient accuracy for t = 2 hours. For t = 2 hours, operator X* becomes

$$X^* \cdot (\ ) = -0.52 \sin \phi \, \vec{k} \times (\ ) - 0.18 \sin^2 \phi \, (\ ).$$

X* is dimensionless and only dependent on latitude ϕ.

The authors have constructed a scale for performing the operation X*( ) on the vector 2 hours times $(\vec{v}_o - \vec{v}_g)$. The graph is reproduced in Figure 8. The use of it is explained in sub-section 1.12.

The velocity at the end of the 2-hour period, which will be the initial velocity for the next period, is found from Equation (10). The initial-velocity displacement to be used for the next interval will then be

$$\vec{v}^* t = \vec{v}_o t - ft\vec{k} \times (\vec{r}^* - \vec{v}_g t)$$

For t = 2 hours we get

$$2\vec{v}^* = 2\vec{v}_o - 1.05 \sin \phi \, (\vec{r}^* - 2\vec{v}_g)$$

Figure 19 shows diagrammatically how the Nomogram of Figure 8 determines the trajectory terminal $\vec{r}^*$ and the next initial-velocity displacement $2\vec{v}^*$.

To get $\vec{v}_g$ for the 2-hour intervals between synoptic hours, the assumption can be made that the local $\vec{v}_g$ varies linearly with time:

$$(\vec{v}_g)_k = (\vec{v}_g)_h + \frac{k}{6} [(\vec{v}_g)_{h+12} - (\vec{v}_g)_h]$$

where $(\vec{v}_g)_h$ and $(\vec{v}_g)_{h+12}$ are the geostrophic winds at the synoptic hours h and h + 12, respectively. $(\vec{v}_g)_k$ is the geostrophic wind during the kth interval after h-hour. For choice of intervals see paragraph 1.12.1.f.

It will be noted that the changing geostrophic wind field is taken into account when it comes to determining the constant $\vec{v}_g$ during an interval, but the effect of geostrophic wind change during this interval

is neglected. The effect during this interval is that of the isallobaric wind, as exemplified in the case of Equation (12).

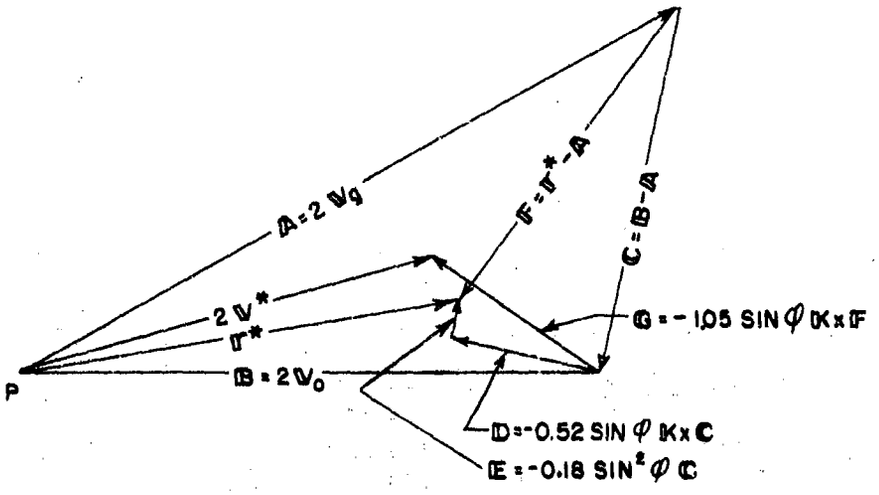

Figure 19. Franceschini and Freeman's construction of the trajectory for 2 hours starting from point P. $\vec{A}$ is the 2-hour displacement with the mean geostrophic velocity $\vec{v}_g$ and $\vec{B}$ the 2-hour displacement with the initial velocity $\vec{v}_o$. From these basic vectors the terminal of the trajectory, $\vec{r}^*$, and the velocity at this point, $\vec{v}^*$, are determined as shown in the diagram. The initial-velocity displacement for the next 2-hour period is $2\vec{v}^*$ and is set off from the end point of $\vec{r}^*$; a new mean geostrophic-velocity displacement $\vec{A}$ is determined, and the process is repeated for as many periods as is desired.

If we denote the displacement computed with the isallobaric effect from Equation (12) by z_α and the displacement computed without this effect after Equation (7) by z, their difference is

$$z_\alpha - z = \frac{i\alpha t}{f} + \frac{1}{2}\alpha t^2 - \frac{\alpha}{f^2}(1 - e^{-ift});$$

for ft <1 this approximates

$$z_\alpha - z = \frac{i\alpha f t^3}{6}.$$

Using the smoothed root-mean-square value of α from sub-section 2.1.4, α = 2 knots/hour and t = 2 hours, $|z_\alpha - z|$ is less than 1 nautical mile at 40°N. Hence, the effect of local changes of the contour field may

generally be ignored during a short period of 2 hours, and the formula (9) of Franceschini and Freeman is valid for an interval of 2 hours even with large local changes.

2.1.7. Extension of Dynamic Methods to Longer Intervals. A dynamic method may be constructed for periods longer than 2 hours. Because of the slow convergence of the series e^{-ift} for values of $ft > 1$, the power series for the exponential cannot be used.

In addition it is no longer feasible to approximate the $\vec{v}_g$ field by the mean over the trajectory since new effects arise through the varying $\vec{v}_g$ field and these effects assume considerable proportions for $t > 2$ hours. One approach is to assume some simple type of transition in the field either tied to fixed coordinates or to coordinates following the motion of the air.

The graph and the operations do not become more complicated by using the exponential instead of the power series. The power series used by Franceschini and Freeman is a convenience when computing the trajectory by numerical methods for short periods but is an unnecessary approximation in graphical computations. However, the form of transition of the $\vec{v}_g$ field will have to be determined by the values of $\vec{v}_g$ at the initial and terminal points of the trajectory. The location of the terminal point is not known at the outset; so $\vec{v}_g$ at this point cannot be evaluated either. This difficulty can be overcome by resorting to a series of successive approximations.

The result is that some time is saved by extending the method to periods > 2 hours. Greater accuracy probably is achieved also by working with larger increments since accumulative scaling errors, which arise through working with small increments, can be eliminated.

A dynamic method of this type will be described in the next section under the name of the Air Weather Service Method.

2.1.8. The Air Weather Service Method. In sub-section 2.1.4.2. the trajectory was computed through a geostrophic field that is constant in space but changes linearly with time, $\gamma = \gamma_o + \alpha t$ where α is the local acceleration. The trajectory is determined by (11) and (12) for the initial conditions: $z = 0$ and $\epsilon = \epsilon_o$ for $t = 0$.

We may also interpret this solution differently. We may assume that the geostrophic wind affecting the particle in its trajectory changes linearly with time or, in other words, that the individual acceleration of the geostrophic wind is constant:

$$\frac{d\vec{v}_g}{dt} = \dot{\gamma} = \beta = \text{constant}$$

where β is a constant vector.

$$\gamma = \gamma_o + \beta t$$

$$\beta = \frac{\gamma - \gamma_o}{t} \tag{13}$$

$$0 \leqq t \leqq T$$

where T is the period of validity. We need not be concerned about how this linear change of γ along the trajectory arises. It may be through local changes of the contour gradient, through curvature or spreading of the contours, or through lateral shear of the geostrophic wind. These all have to be balanced such that

$$\frac{d\vec{v}_g}{dt} = \frac{\partial \vec{v}_g}{\partial t} + \vec{v}\cdot\nabla_p\vec{v}_g = \beta = \text{constant}$$

during the period in question.

The success of the method will, of course, partly depend on how well condition (13) is met in nature. Since upper-air charts are available at 12 hour intervals, it is natural to choose 12 hours as the period. For a period of 12 hours, Equation (13) is usually a good description of the pressure forces acting on a parcel. Whenever this is not the case, T = 6 hours will be used. The choice of the period is discussed at the end of this sub-section.

A priori, there is no reason to believe that a transition of type (13) is inferior to the assumption that the local geostrophic wind, changes linearly with time.

With assumption (13) the dynamic equation (6') is again integrable and has the solution, formally identical with (11) and (12):

$$z = \gamma_o t + \frac{i\beta t}{f} + \frac{1}{2}\beta t^2 - \frac{i}{f}\left(\epsilon_o - \gamma_o - \frac{i\beta}{f}\right)\left(1 - e^{-ift}\right) \tag{14}$$

$$\epsilon = \gamma_o + \frac{i\beta}{f} + \beta t + \left(\epsilon_o - \gamma_o - \frac{i\beta}{f}\right) e^{-ift} \tag{15}$$

for the same initial conditions: z = 0, and $\epsilon = \epsilon_o$ for t = 0.

Inserting the value of β from (13) and writing $\theta = ft$, we obtain after some rearranging:

$$\frac{z}{t} = \gamma_o + (\gamma - \gamma_o)\left[\frac{1}{2} + \frac{i}{\theta} - \frac{1}{\theta^2}\left(1 - e^{-i\theta}\right)\right] - (\epsilon_o - \gamma_o)\frac{i}{\theta}\left(1 - e^{-i\theta}\right) \tag{14'}$$

$$\epsilon = \gamma_o + (\gamma - \gamma_o)\left[1 + \frac{i}{\theta}\left(1 - e^{-i\theta}\right)\right] + (\epsilon_o - \gamma_o)\, e^{-i\theta} \tag{15'}$$

This form is convenient for graphical evaluation.

Once the period "t" is chosen, we notice that the trajectory is determined by three quantities: 1) the initial geostrophic wind, γ_o; 2) the vector change of the geostrophic wind over the period, $\gamma - \gamma_o$; and 3) the initial geostrophic departure, $\epsilon_o - \gamma_o$. Each of these quantities are multiplied by operators that depend on latitude only. If the velocity vectors γ_o, $(\gamma - \gamma_o)$, and $(\epsilon_o - \gamma_o)$ are represented on a scale of 10 knots corresponding to 2 degrees of latitude on the map-scale and projection used, z/t will directly be the map displacement after 12 hours since a velocity of 10 knots corresponds to a displacement of 120 nautical miles = 2 degrees of latitude.

The length of a latitude degree varies somewhat with latitude for the map projections used by the Air Weather Service. Least variation is found on the Lambert conformal projections. For example, on the Lambert conformal projection true at 30° and 60° the length of a latitude degree deviates from the standard (at 30° and 60°) by less than 3½% between 25° and 65°.

On a polar-stereographic projection the length of a latitude degree varies between 25° and 65° by as much as 18% from the mean length at about 38°. Hence, when the Lambert conformal projection is used, it will be accurate enough to use a constant scale for the latitude degree in the latitude band from 25° to 65°. For a polar-sterographic projection the varying scale of the map must be used, i.e., when the answer comes out as a displacement of so and so many latitude degrees, the corresponding map displacement must be set off by using the length of a latitude degree at the appropriate latitude. This illustrates the advantage of using Lambert conformal projections in trajectory work.

In equations (14') and (15') γ, the geostrophic wind at the end point of the trajectory, is not known at the outset since it is the end point we seek. However, we may use a procedure of successive approximations whereby we can find an end point satisfying equation (14'). This procedure is reminiscent of the procedure used by Petterssen in his kinematic method (see sub-sections 1.6 and 2.2.2).

The procedure is schematically illustrated in Figure 20a. We can rewrite equation (14'):

$$(14'') \qquad \frac{z}{t} = A + B \cdot [\gamma - \gamma_o]$$

where the vector A and the non-dimensional operator B· are determined by the conditions at the initial point only (latitude, initial velocity,

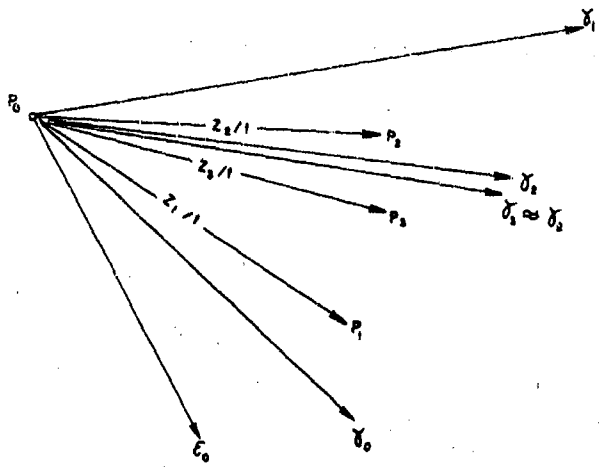

Figure 20a. AWS Method — Successive Approximations for End Point of Trajectory.

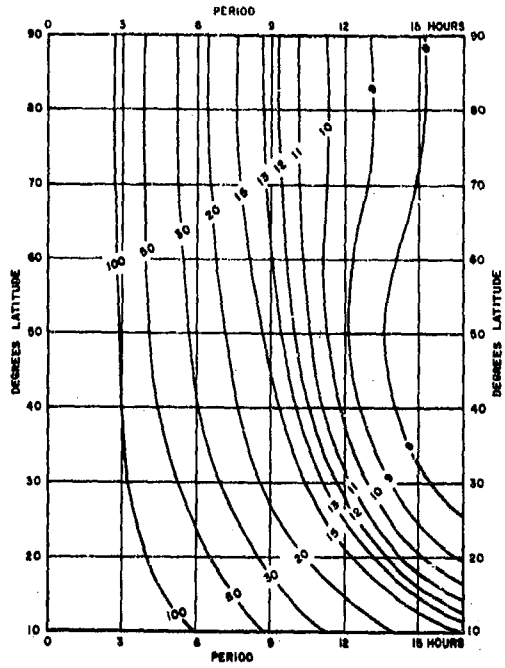

Figure 20b. Convergence Diagram for the AWS Method. Spatial variation of geostrophic wind $(|d\gamma|/|dz|) = 1/|B|t$ is given in knots per latitude degree as a condition for absolute convergence of terminal point of trajectory during a specified period.

and initial geostrophic wind).

$$(15a) \qquad A = \gamma_o - (\epsilon_o - \gamma_o)\,\frac{i}{\theta}\,(1 - e^{-i\theta})$$

$$(15b) \qquad B' = \left[\frac{1}{2} + \frac{i}{\theta} - \frac{1}{\theta^2}\,(1 - e^{-i\theta})\right].$$

First, an approximate location of the terminal is determined. This may conveniently be the terminal of the trajectory through the initial point in the stationary geostrophic flow of the Chart h (beginning of 12-hour period). This first approximation we may denote by z_1. The geostrophic wind at this point on Chart h + 12 (end of 12-hour period) is γ_1. In Figure 20a, P_o is the initial point and P_1 is the first approximation of the terminal. Next, γ_1 is inserted in equation (14")

and a new terminal, z_2, is computed (P_2 in Figure 20a):

$$\frac{z_2}{t} = A + B\cdot[\gamma_1 - \gamma_o]$$

Usually, the geostrophic wind at P_2, γ_2, is different from γ_1. If γ_2 and γ_1 agree within the accuracy of measuring geostrophic winds on the map, P_2 is the terminal sought. Otherwise, the step is repeated and we arrive at a series of approximations:

$$\frac{z_3}{t} = A + B\cdot(\gamma_2 - \gamma_o)$$

$$\frac{z_4}{t} = A + B\cdot(\gamma_3 - \gamma_o)$$

$$\vdots$$

$$\frac{z_{n+1}}{t} = A + B\cdot(\gamma_n - \gamma_o)$$

where the geostrophic velocities $\gamma_2, \gamma_3, \ldots, \gamma_n$ are read off the Chart h + 12 at points $z_2, z_3, \ldots, z_n$ respectively. This series is extended until the difference $\gamma_n - \gamma_{n-1}$ no longer exceeds the accuracy of the chart evaluation of geostrophic winds. This accuracy is about 5 knots or 10% of the wind speed, whichever is greater. This stage will be reached usually at the second or third approximation.

A graphical method for solving (14') and (15') by the series above is described in sub-section 1.13.

This series above may be represented by:

$$\frac{z_{n+1}}{t} = A + \sum_{k=1}^{k=n} B\cdot(\gamma_k - \gamma_{k-1})$$

$$n = 1, 2, \ldots .$$

z_1 is an initial guess of the terminal and γ_1 the geostrophic wind at this point. The series $z_1, z_2, \ldots . z_n$ is absolutely convergent when

$$\frac{|B\cdot(\gamma_{n+1} - \gamma_n)|}{|B\cdot(\gamma_n - \gamma_{n-1})|} < 1.$$

Since $B\cdot(\gamma_n - \gamma_{n-1}) = (z_{n+1} - z_n)\frac{1}{t}$, we obtain as the condition for absolute convergence:

$$(16) \qquad \frac{|d\gamma|}{|dz|} < \frac{1}{|B|t}$$

In the limit we have written $\gamma_{n+1} - \gamma_n = d\gamma$ and $z_{n+1} - z_n = dz$.

It should be noted that γ is generally not an analytical function of z so that the value of the differential quotient $\left|\frac{d\gamma}{dz}\right|$ depends on the azimuth of dz. The factor |B| is determined from (15b):

$$|B| = \left(\left[\frac{1}{2} - \frac{1}{\theta^2}(1 - \cos\theta)\right]^2 + \left[\frac{1}{\theta} - \frac{1}{\theta^2}\sin\theta\right]^2\right)^{\frac{1}{2}}$$

The condition for convergence may be expressed in graphical form as the limiting value for the vector change of the geostrophic wind over a horizontal distance of one degree latitude (60 nautical miles). This is done in Figure 20b.

Since this is the condition for <u>absolute</u> convergence, convergence in actual cases may be obtained in fields of greater space variation than indicated by these limits if the azimuths of space progression are favorable.

2.1.9. <u>Practical Difficulties of Obtaining Accurate Trajectories by Dynamic Methods</u>. In the methods described in 2.1.6 – 2.1.8 we have procedures for constructing fairly accurate trajectories when the contour fields are accurately known. The vertical motion term which is about 25% of the effect of the geostrophic departure is, of course, neglected. This is, however, a minor source of errors as will be pointed out later in this section and as also is apparent from sub-section 1.14.

Is the upper-level contour field known so accurately that the "dynamic" trajectories constructed from them are improvements on trajectories constructed from more simple assumptions, for example, geostrophic trajectories?

Studies of actual constant-pressure-balloon trajectories may throw some light on this question. The accelerations of a constant-pressure balloon may be computed from the observed trajectory. The root-mean-square (RMS) error of the acceleration is given by:

$$\sigma(\Delta A) = \frac{\sqrt{2}\sigma(\Delta r)}{tT}$$

where $\sigma(\Delta r)$ is the RMS-fixing error; t and T are the time intervals over which velocities and accelerations respectively are averaged (e.g., see Anderson [1]). For t = 2 hours, T = 4 hours, $\sigma(\Delta r)$ = 2.5 nautical miles, $\sigma(\Delta A)$ = 0.45 knots/hour. The figure $\sigma(\Delta r)$ = 2.5 nautical miles is applicable when the balloon fixes are given by following aircraft. When fixes have been obtained from time-lapse photos by cameras suspended from the balloon, still greater accuracy is possible. Fixes obtained by radio direction finding (RDF) are far less accurate. For a certain

sample of balloon flights at 300 mbs, Neiburger and Angell [23] found $\sigma(\Delta r)$ = 8.2 nautical miles for positioning by RDF.

Emmons [6] calculated accelerations from constant-pressure balloon data at 200 mb. The fixes were determined by trailing aircraft. Hence, the value $\sigma(\Delta A)$ = 0.5 knot/hour is applicable to this sample. From Equation (6) he computed the associated geostrophic departures, $\vec{D} = \vec{v} - \vec{v}_g$. We will denote the departure computed from the trajectory in this manner by $\vec{D}_t$. He also computed $\vec{D}$ directly: $\vec{v}$ was obtained from the trajectory, and $\vec{v}_g$ was obtained by 2 different methods as follow:

a. From the usually smoothed 200-mb contour charts analyzed from height data alone (no pibals or rawins used). The departure computed by this method will be denoted by $\vec{D}_z$.

b. Objectively from the constant contour field fixed by 3 stations in a triangle bracketing the trajectory segment. Sometimes 2 different triangles were tried for the same segment. We denote this departure by $\vec{D}_3$ or $(\vec{D}_3)_1 - (\vec{D}_3)_2$ when two triangles were used.

Table VI gives a comparison of the departures $\vec{D}_t$, $\vec{D}_z$, and $\vec{D}_3$ over nine different segments meeting the accuracy requirements stated above.

Emmons checked the vertical motion term and found that it did not exceed 0.5 knot/hour in any of the cases. Therefore, the values in the first line of the Table must be taken to be very near the true values. Even using Neiburger and Angell's mean value for the vertical motion term, the first line should give the departures with an average error of 25%.

We notice that the departures obtained by the methods discussed in sub-paragraphs "a" and "b" above are generally too large; the departures obtained by triangulation are in the mean more than twice the true ones.

Lines 4 and 5 show that the errors of the departures obtained from charts are larger than the departures themselves. From this it does not appear feasible to determine the "correct" geostrophic departures from contour analysis at 200 mb. By "correct" geostrophic departures is meant the departures which would give the correct behavior of the balloon when computed from Equation (6). From line 6, the discrepancy between the methods in "a" and "b" above is in the mean 24 knots, which is larger than the quantity we want to measure. Line 7 shows that the choice of triangle influences the result by 23 knots in the mean.

TABLE VI

Comparison of 200-mb Geostrophic Departures (knots) from Contour Charts ($\vec{D}_z$ and $\vec{D}_3$) with Those from Constant-Pressure-Balloon Trajectories ($\vec{D}_t$). (Where two values appear in a square, two triangles were used.)

	Case Number									
	1	2	3	4	5	6	7	8	9	Mean
$\lvert\vec{D}_t\rvert$	5	5	11	11	18	3	15	20	40	14
$\lvert\vec{D}_z\rvert$	4	39	32	8	10	12	22	49	22	22
$\lvert\vec{D}_3\rvert$	9	63 60	43 36	21	14 23	19 4	37 24	76 54	12 15	32
$\lvert\vec{D}_t - \vec{D}_z\rvert$	5	37	36	15	9	9	13	32	54	23
$\lvert\vec{D}_t - \vec{D}_3\rvert$	12	51 62	51 45	18	6 8	20 5	17 6	37 64	40 25	30
$\lvert\vec{D}_z - \vec{D}_3\rvert$	13	22 25	67 23	14	4 13	27 12	21 28	6 37	34 31	24
$\lvert(\vec{D}_3)_1 - (\vec{D}_3)_2\rvert$	--	3	54	--	9	16	20	36	20	23
$\lvert\vec{v}\rvert$	24	63	66	61	53	40	64	50	104	59
$\lvert\vec{D}_t\rvert/\lvert\vec{v}\rvert$	0.21	0.08	0.17	0.18	0.33	0.08	0.23	0.40	0.39	0.23

These discrepancies are mainly due to the errors in the heights at 200 mb. The smoothed analysis removes part of these errors so that Method "a" is generally a better method than "b", but the residual error is still so large that the departures cannot be assessed.

Note that $\lvert\vec{D}_t - \vec{D}_z\rvert = \lvert\vec{v} - (\vec{v}_g)_t - \vec{v} + (\vec{v}_g)_z\rvert = \lvert(\vec{v}_g)_t - (\vec{v}_g)_z\rvert$. Consequently, the mean vector errors in determining the geostrophic wind by Methods "a" and "b" were also 23 and 30 knots, respectively. The last two lines give the wind and the relative geostrophic departure. The average ratio $\lvert\vec{D}_t\rvert/\lvert\vec{v}\rvert$ was found to be 0.23. Neiburger and Angell found 0.394 at 300 mb for a much larger sample. I appears from this study that the error in determining $\vec{v}_g$ in middle latitudes is 20-25 knots at 200 mb over a well-observed area such as the United States (1949-50). Admittedly, this is only a tentative value because of the smallness of the sample. Sutcliffe and Sawyer [29] arrive at a somewhat smaller value, 14 knots at 200 mb; however, their value was

based on a quite different approach.

Using the mean of 14 and 23 knots, i.e., 19 knots, a Franceschini-Freeman trajectory for 2 hours at 40°N would result in a mean error of displacement of about 13 nautical miles due to inaccuracies in determining $\vec{v}_g$. This estimate, applicable to middle latitudes, is found by averaging Equation (9) and is, of course, applicable only to any individual 2-hour leg of the trajectory. The extent to which this error is cumulative is unknown.

The difficulties implied above increase with decreasing latitude. The errors in the height reports are very much the same at all latitudes but lead to larger errors in $\vec{v}_g$ and $\vec{D}$ in low latitudes than in high latitudes. South of 20-25°N the errors in $\vec{v}_g$ approach the magnitude of $\vec{v}_g$ itself, and any dynamic method will be useless here.

2.2. Kinematic Methods.

2.2.1. Introduction. In practice the flow fields in the atmosphere are given by synoptic charts at regular intervals. The problem then is to construct a trajectory starting from a known point P_o, at time $t = 0$, during the time interval T which is the period between synoptic charts.

At this stage we need not be concerned about how the flow is represented. It may be by streamlines and isotachs, by contours, or by other means.

In order to construct the trajectory some assumption has to be made about how the flow on Chart 0 changes into the flow on Chart T.

Generally, the velocity varies both in time and space. $(\vec{R}, t)$ is defined as a space-time point where $\vec{R}$ is the position vector from some chosen origin and t is the time of the point. $\vec{v}(\vec{R}, t)$ is the velocity at point $(\vec{R}, t)$; $\dot{\vec{v}}(\vec{R}, t)$ is the acceleration, and $\frac{\partial \vec{v}}{\partial t}(\vec{R}, t)$ is the local acceleration at point $(\vec{R}, t)$, etc.

By the various assumptions which may be made regarding the transition from $\vec{v}(\vec{R}, 0)$ to $\vec{v}(\vec{R}, T)$ as t varies from $t = 0$ to $t = T$, a variety of trajectory constructions arises.

In the following sections the constructions which appear to have the most merit will be discussed: 1) Petterssen's Method, 2) J. J. George's Method, which is a shortened version of Petterssen's Method, 3) Linear Interpolation Method, 4) Consecutive Streamline Methods, 5) the Central Tendency Method, 6) the Relative Trajectory Method, and 7) the General Mills' Standard Objective Method, which may be

considered as a version of the Relative Trajectory Method.

The operational aspects of these methods have already been described in Section I. In the following sub-sections some additional information of a more theoretical nature is given concerning some of the methods.

Method 4, 5, and 7 are exhaustively treated in Section I and will receive no further mention in this Section.

In addition to the methods listed above, a short paragraph on constant-vorticity trajectories has been included mainly for completeness although it does fit very well under the heading, Kinematic Methods.

All of these methods are kinematic since the trajectory is constructed by graphical integration of the known kinematic field

$$\vec{v} = \vec{v}(\vec{R}, t)$$

to obtain the trajectory:

$$\vec{R} = \vec{R}_o + \int_o^t \vec{v}(\vec{R}, \zeta)\, d\zeta$$

where $(\vec{R}, t)$ now is a point on the trajectory (see Figure 21).

Several of these methods are discussed in some detail because none of them can be singled out and recommended as the optimum method under all conditions. The selection of the optimum method depends on such factors as: accuracy of the chart representation of the flow, length of period between synoptic charts, the flow patterns themselves, the time available for trajectory construction, the desired accuracy of the trajectory, and possibly other factors.

The selection of the optimum method is discussed in sub-section 1.15.

2.2.2. Petterssen's Method. It is assumed that the acceleration of the air parcel is constant during the time interval T. With reference to Figure 21

$$\frac{d}{dt}\vec{v}(\vec{R}, t) = \text{const.} = \vec{a} \text{ for } 0 \leq t \leq T$$

(18) or $$\vec{v}(\vec{R}, t) = \vec{v}(\vec{R}_o, 0) + \vec{a}\, t$$

$$\vec{a} = \frac{1}{t}\left[\vec{v}(\vec{R}, t) - \vec{v}(\vec{R}_o, 0)\right] = \frac{1}{T}\left[\vec{v}(\vec{R}_1, T) - \vec{v}(\vec{R}_o, 0)\right].$$

Writing $\vec{r} = \vec{R} - \vec{R}_o$, and since $(\vec{R}, t)$ is a point on the trajectory:

$$\vec{r} = \int_o^t \vec{v}(\vec{R}, \zeta)\, d\zeta$$

and from equation (18):

(19) $$\vec{r} = \frac{t}{2}\left[\vec{v}(\vec{R}_o, 0) + \vec{v}(\vec{R}, t)\right].$$

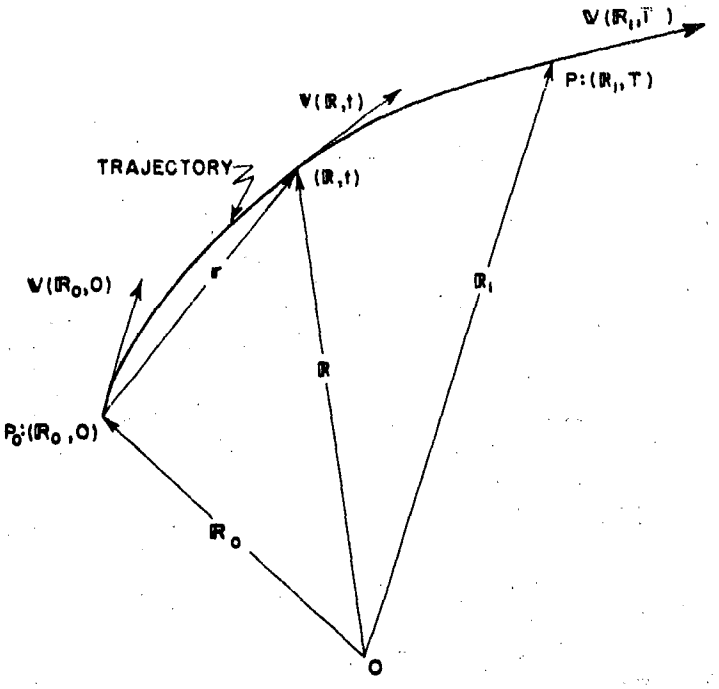

Figure 21. Illustration of Notations Used in Sub-Sections 2.2 – 2.2.5.

Thus, when t = T,

$$\vec{r} = \frac{T}{2}\left[\vec{v}(\vec{R}_0, 0) + \vec{v}(\vec{R}_1, T)\right]. \tag{20}$$

The trajectories are second degree curves. Equation (19) is a corollary of Equation (18). The end point of the trajectory is determined implicitly by Equation (20) and can be found by a successive approximation method suggested by Petterssen.*

Choosing the origin of the vector $\vec{R}$ at the starting point of the trajectory, P_0 in Figure 21, we have $\vec{R}_0 = 0$, $\vec{R}_1 = \vec{r}$, and we can write Equation (20) as follows:

$$\vec{r} = \frac{T}{2}\left[\vec{v}(0, 0) + \vec{v}(\vec{r}, T)\right]. \tag{21}$$

The vector succession,

---

*In the first edition of Petterssen's book [25] a typographical error occurs in the text. This has been corrected in the Second Edition (1956).

$$\vec{r}_o = T\,\vec{v}(0,\,0)$$

$$\vec{r}_1 = \frac{T}{2}\,[\vec{v}(0,\,0) + \vec{v}(\vec{r}_o,\,T)]$$

(22)
$$\vec{r}_2 = \frac{T}{2}\,[\vec{v}(0,\,0) + \vec{v}(\vec{r}_1,\,T)]$$

$$\vdots$$

$$\vec{r}_n = \frac{T}{2}\,[\vec{v}(0,\,0) + \vec{v}(\vec{r}_{n-1},\,T)]$$

$$\vdots$$

has $\vec{r}$ as its limit

$$\vec{r} = \lim \vec{r}_n$$

as $n \to \infty$

provided certain convergence criteria are met. Ertel [7] studied the convergence of this series and found that the convergence condition is:

$$T < \frac{2}{\sqrt{(\frac{\partial \vec{v}}{\partial x})^2 + (\frac{\partial \vec{v}}{\partial y})^2}}\,.$$

For magnitude, $\frac{\partial \vec{v}}{\partial x} = \frac{\partial \vec{v}}{\partial y} = 0.5 \times 10^{-4}$ sec^{-1}, the limiting value of T is about 8 hours.

To find the trajectory going through point P_o on Chart 0, the graphical construction in Figure 1 is equivalent to Equations (22). When T is given in hours and $\vec{v}$ in knots, distances $T\vec{v}$ are in nautical miles.

We set off vectors $\vec{r}_o = T\,\vec{v}(0,\,0) = \overrightarrow{P_oA}$ and $T\,\vec{v}(\vec{r}_o,\,T) = \overrightarrow{P_oB_o}$ from P_o. The point P_1 bisects connecting line AB_o between the vectors' end points. Vector $\overrightarrow{P_oP_1} = \vec{r}_1 = \frac{T}{2}\,[\vec{v}(0,\,0) + \vec{v}(\vec{r}_o,\,T)]$. The velocity at P_1 on Chart T, $\vec{v}(\vec{r}_1,\,T)$ multiplied by T is set off from P_o; this is vector $\overrightarrow{P_oB_1}$. P_2 bisects connecting line AB_1, and P_2 is the second approximation to the end point of the trajectory. If now the velocity at P_2, $\vec{v}(\vec{r}_2,\,T)$, is close enough to the velocity at P_1, the construction can cease at this stage. If not, the procedure is carried on until a point P_n is located on Chart T whose velocity is equal to the velocity at point P_{n-1} within the accuracy of the chart representation. The convergence of the procedure is expressed by the points P_1, P_2, P_3 steadily approaching a final point P. The second approximation usually suffices.

When the point P has been located, the trajectory is drawn in by

fitting a smooth curve through P_o and P, tangent to $\vec{v}(0, 0)$ at P_o and tangent $\vec{v}(\vec{r}, T)$ at point P.

2.2.3. J. J. George's Method. J. J. George [10] suggests that the first approximation $\vec{r}_1$ of (22) will give good results for low-level trajectories for chart intervals of 6 hours. He uses this in low-level advection problems (fog forecasting):

$$\vec{r}_o = T\,\vec{v}(0, 0)$$

$$\vec{r}_1 = \frac{T}{2}\,[\vec{v}(0, 0) + \vec{v}(\vec{r}_o, T)]$$

He does not pursue the higher approximations. If the series is continued as Petterssen's, it will converge toward the same point. An illustration of J. J. George's construction is given in Figure 22.

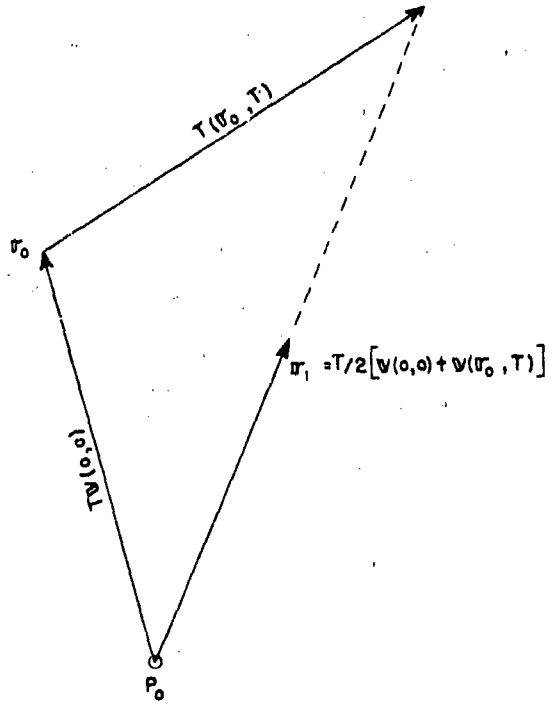

Figure 22. J. J. George's Construction.

2.2.4. The Linear Interpolation Method. It is assumed that

$$\vec{v}(\vec{r}, t) = \vec{v}(\vec{r}, 0) + \frac{t}{T}\,[\vec{v}(\vec{r}, T) - \vec{v}(\vec{r}, 0)] \tag{23}$$

for $0 \leq t \leq T$ for all points $\vec{r}$ on the trajectory. In other words, the local wind acceleration, $\partial\vec{v}/\partial t$, is constant for a point but may vary from point to point.

$$\partial\vec{v}/\partial t = \frac{1}{T}\,[\vec{v}(\vec{r},\ T) - \vec{v}(\vec{r},\ 0)]$$

The trajectory is given by

$$\vec{r} = \int_0^t \left[\frac{T-\zeta}{T}\,\vec{v}(\vec{r},\ 0) + \frac{\zeta}{T}\,\vec{v}(\vec{r},\ T)\right] d\zeta. \tag{24}$$

In practice the integral (24) must be evaluated stepwise. We divide the period, T, into n equal intervals of length $\frac{T}{n}$. Let $\vec{r}_k$ denote the position at the end of the k-th interval, i.e., at time t = kT/n. The velocity at this point is $\vec{v}(\vec{r}_k,\ 0)$ on Chart 0 and $\vec{v}(\vec{r}_k,\ T)$ on Chart T. The displacements during the interval (k + 1) is found by adding $\frac{T}{n}\,\vec{v}(\vec{r}_k,\ 0)$ and $\frac{T}{n}\,\vec{v}(\vec{r}_k,\ T)$, each weighted by the factors $\frac{(T-t)}{T}$ and $\frac{t}{T}$, respectively, of the integral (24). Using the weighting factors at the <u>midtime</u> of the interval (k + 1), i.e., at time $t = \frac{T}{n} \times (k + \frac{1}{2})$ the weighting factors become:

a. For displacement $\frac{T}{n}\,\vec{v}(\vec{r}_k,\ 0)$: $\frac{T-t}{T} = \frac{2n-2k-1}{2n}$

b. For displacement $\frac{T}{n}\,\vec{v}(\vec{r}_k,\ T)$: $\frac{t}{T} = \frac{2k+1}{2n}$

The displacement during the interval (k + 1) then becomes:

$$\frac{T}{n}\left[\frac{2n-2k-1}{2n}\,\vec{v}(\vec{r}_k,\ 0) + \frac{2k+1}{2n}\,\vec{v}(\vec{r}_k,\ T)\right] \tag{25}$$

The total displacement is:

$$\vec{r}_{k+1} = \vec{r}_k + \frac{T}{n}\left[\frac{2n-2k-1}{2n}\,\vec{v}(\vec{r}_k,\ 0) + \frac{2k+1}{2n}\,\vec{v}(\vec{r}_k,\ T)\right] \tag{26}$$

The displacements at the end of the 1st, 2nd,. . . ., n-th interval may be written:

$$\vec{r}_1 = \frac{T}{n}\left[\frac{2n-1}{2n}\,\vec{v}(0,\ 0) + \frac{1}{2n}\,\vec{v}(0,\ T)\right]$$

$$\vec{r}_2 = \vec{r}_1 + \frac{T}{n}\left[\frac{2n-3}{2n}\,\vec{v}(\vec{r}_1,\ 0) + \frac{3}{2n}\,\vec{v}(\vec{r}_1,\ T)\right]$$

$$\vec{r}_3 = \vec{r}_2 + \frac{T}{n}\left[\frac{2n-5}{2n}\,\vec{v}(\vec{r}_2,\ 0) + \frac{5}{2n}\,\vec{v}(\vec{r}_2,\ T)\right]$$

$$\vec{r}_n = \vec{r}_{n-1} + \frac{T}{n}\left[\frac{1}{2n}\,\vec{v}(\vec{r}_{n-1},\ 0) + \frac{2n-1}{2n}\,\vec{v}(\vec{r}_{n-1},\ T)\right]$$

The displacement (25) may be found by dissecting the connecting line between the end points of vectors $\frac{T}{n}\,\vec{v}(\vec{r}_k,\ 0)$ and $\frac{T}{n}\,\vec{v}(\vec{r}_k,\ T)$ in the proportions $\frac{2k+1}{2n}$ to $\frac{2n-2k-1}{2n}$ as shown in Figure 23. From this Figure:

$$\overrightarrow{BD} = \frac{2k+1}{2n}\,\overrightarrow{BC} = \frac{2k+1}{2n}\,(\overrightarrow{AC} - \overrightarrow{AB})$$

$$\overrightarrow{AD} = \overrightarrow{AB} + \overrightarrow{BD} = \left(1 - \frac{2k+1}{2n}\right)\overrightarrow{AB} + \frac{2k+1}{2n}\,\overrightarrow{AC}$$

$$= \frac{T}{n}\left[\frac{2n-2k-1}{2n}\,\vec{v}(\vec{r}_k,\ 0) + \frac{2k+1}{2n}\,\vec{v}(\vec{r}_k,\ T)\right]$$

Figure 4 shows the construction of a trajectory of T = 12 hours, n = 4,

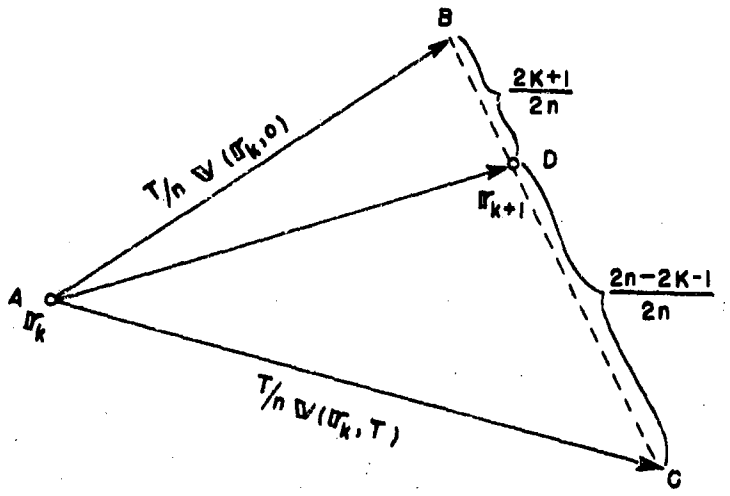

Figure 23. Construction of the Displacement During the Interval (k + 1) by Proportionate Parts.

and $\frac{T}{n}$ = 3 hours, following Equation (27).

2.2.5. The Relative Trajectory Method. This method applies strictly only to flow patterns that are translated across the map without changing shape and intensity.

If the flow at t = 0 is $\vec{v}(\vec{r}, 0)$, we have for time t by definition

(28) $$\vec{v}(\vec{r}, t) = \vec{v}(\vec{r} - \vec{c}t, 0)$$

where $\vec{c}$ is the translational velocity of the pattern, $\vec{c}$ might be a function of t, but in practical applications the assumption that $\vec{c}$ is a constant is probably as good as any other on the average. The trajectory may be constructed directly by

(29) $$\vec{r} = \int_0^t \vec{v}(\vec{r} - \vec{c}\,\zeta, 0)\,d\zeta$$

Figure 24 illustrates a case of the construction.

We may also compute the trajectory by an alternate method. In cases where the field of $\vec{v}(\vec{r}, 0)$-$\vec{c}$ is easily obtained as a continuous field, this alternate method is more rapid and gives more accurate results. This happens, for example, when $\vec{v}(\vec{r}, 0)$ is given by a stream function, $\vec{v}(\vec{r}, 0) = G\vec{k} \times \nabla\psi$ where G is a constant. We then form the auxiliary stream function η defined by $\vec{c} = G\,\vec{k} \times \nabla\eta$. Since $\vec{c}$ is a constant, η = const will be straight lines parallel to $\vec{c}$. The field of $\vec{v}(\vec{r}, 0)$-$\vec{c}$ is then obtained by graphical addition of the ψ and η fields: $\vec{v}'(\vec{r}) = \vec{v}(\vec{r}, 0)$-$\vec{c} = G\,\vec{k} \times \nabla(\psi + \eta)$. $\vec{v}'(\vec{r})$ is the relative velocity field, as appearing to an observer that moves with velocity $\vec{c}$.

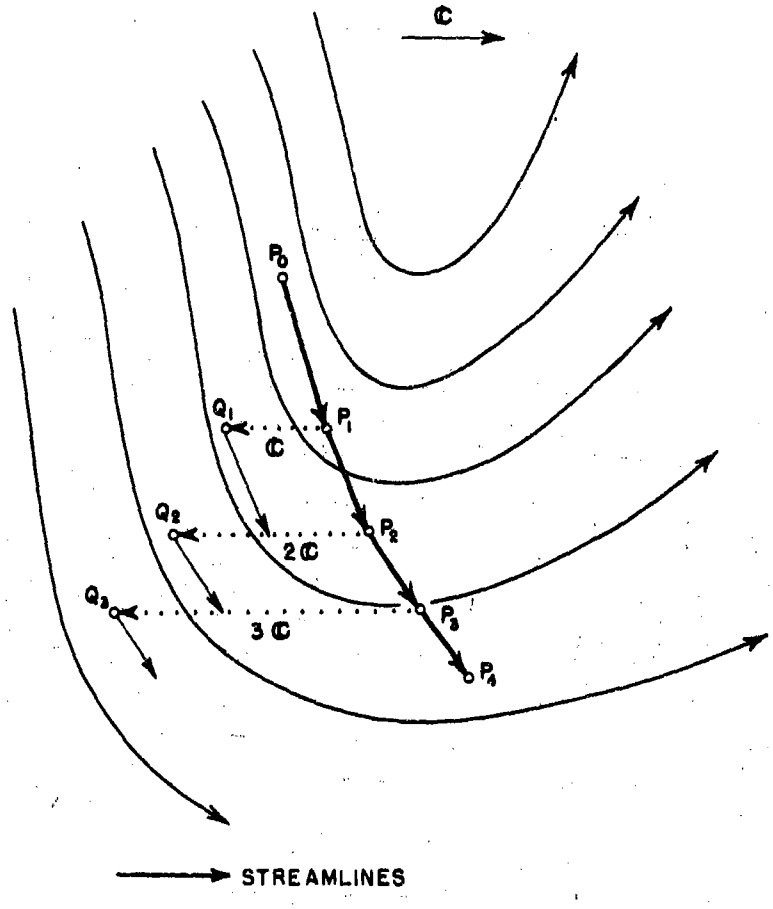

Figure 24. Construction of a Trajectory in a Flow Pattern that Moves Across the Chart with Velocity $\vec{c}$. P_0, P_1, P_2, etc., are the objective positions at $t = 0, 1, 2$, etc.

This field is stationary and the trajectories in this field (the relative trajectories) coincide with the streamlines (the relative streamlines). The relative trajectories are obtained from

$$\vec{r}' = \int_0^t \vec{v}'(\vec{r})\,d\zeta ; \tag{30}$$

and since $\vec{r} = \vec{r}' + \vec{c}t$, the chart trajectory ("absolute" trajectory) is obtained from

$$\vec{r} = \int_0^t \vec{v}'(\vec{r})\,d\zeta + \vec{c}t. \tag{31}$$

Denoting the stream function of the relative velocity $\vec{v}'$ by γ, $\gamma = \psi + \eta$, the relative trajectory is parallel to the γ lines. The object's positions on the relative trajectory as a function of time may

be found by measuring the distances between adjacent γ lines in the same way as done when computing geostrophic winds from contour charts. A useful relation is found by noting that the area swept by a normal to the trajectory and following the object (the normal being bounded by the two adjacent γ lines) is proportional to the time of travel. This relationship follows from Figure 25. Referring to this Figure, we can write:

$$v' = \frac{\Delta s}{\Delta t} = G \frac{\Delta \gamma}{\Delta n} \tag{32}$$

where Δs is distance measured along the relative trajectory. Hence,

$$\Delta t = \frac{1}{G \Delta \gamma} \Delta n \Delta s = \frac{1}{G \Delta \gamma} \Delta A$$

where ΔA is an area element. Summed over the trajectory:

$$t = \frac{1}{G \Delta \gamma} A \tag{33}$$

We can locate the object at any time from Formula 33 by measuring the area between two adjacent γ lines from the normal through the initial point P_o to the normal through the end point.

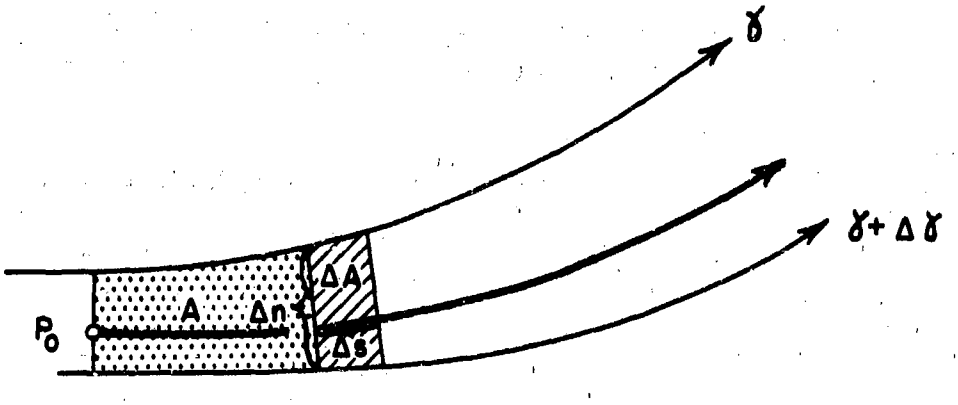

Figure 25. A Relative Trajectory in the Contour Field of the Relative Velocity. The relative trajectory (thick line) starts at P_o. Travel time of the object is proportional to the area A between the adjacent contour lines, γ and $\gamma + \Delta\gamma$.

Figures 5 and 6 of sub-section 1.10 show some trajectories computed by the method of relative trajectories. In these constructions it is assumed that the velocity is geostrophic, so that the ψ field is identical with the contour field. The variation of G with latitude ($G = g/f$) may be taken into account by introducing the same variation in the η field; the η lines are then no longer strictly parallel or equidistant.

The relative trajectory method is often advantageous near pressure centers and troughs and ridges with appreciable curvature. Often the best estimate we can make of the behavior of such flow patterns between synoptic charts is a straight translation from one map to another in the limited area of the chart occupied by these features. The Relative Trajectory Method applied to the parts of the trajectory which approach these features will give a more realistic trajectory than, for example, the Central Tendency Method. To illustrate this by an extreme example, take the trajectory from point A in Figure 6. The Central Tendency Method (see sub-section 1.7) would keep the object stationary at point A for a period of 6 hours before and 6 hours after map time. Since the circulation center moves, however, the object will be caught by the northwesterly winds behind the center and start to move southeastward as shown by the trajectory.

2.2.6. Constant Vorticity Trajectories. Constant vorticity trajectories have been discussed previously in AWS TR 105-99, December 1952.

The trajectories are computed from

$$(34) \qquad \begin{cases} f + k_t v_o = f_o \\ v = v_o \end{cases}$$

where v_o and f_o are initial values of speed and Coriolis parameter, and k_t is the curvature of the trajectory.

The conditions imposed upon the atmosphere by (34) are only very infrequently met satisfactorily on constant-pressure charts at any level.

In tests the method has been found to be less satisfactory than other standard methods [18].

Since the method requires only data at the initial point, it may be considered as a method for forecasting the trajectory when little or no data are available downstream. This leads into the realm of forecasting for no-data-areas, which is beyond the scope of this Manual.

2.3. Effect of Eddies on the Trajectory.

The atmospheric motion that we can chart and predict is a smoothed motion, i.e., the motion is a space and time average of the actual motion. The space scale and the time scale of this averaging process is (in a not too definite manner) determined by the distances between observing points in the flow analysis, and also by the frequency and accuracy of the observations. Of necessity in the prognostic flow

charts these scales become enlarged, since our ability to predict becomes poorer as the space scale and time scale of the motion diminish.

The motions of smaller dimensions than these averaging scales (at present perhaps 100-200 nautical miles and 6-12 hours for the high-level flow over the U. S.) will for our purpose be called eddies. The eddies represent a random component of motion unobservable and, therefore, in principle unpredictable. The eddies of a magnitude equal to or larger than the balloon are the ones which will affect its trajectory. The extent to which the trajectory is affected will determine an upper limit for the accuracy with which we can forecast the trajectory.

Our knowledge of the eddies of the high-level flow is very limited. However, a few experiments have been conducted which throw some light on the eddy effect along a trajectory.

C. B. Moore et al [22] studied the trajectories of balloons released simultaneously to float at 300 mb. The balloons were tracked by aircraft. Table VII gives the observed horizontal separation of the balloons. Most of the time the vertical separation was less than 150 feet.

TABLE VII

Separation of Balloon Pairs at 300 mb.

Pair No.	Flight Distance when Compared (mi)	Flight Time when Compared (hr)	Separation (mi)	Separation in % of Flight Distance	Across Track Separation (mi)
1	850	14.5	20	2.3	8
2	775	18.0	13	1.7	6
3*	1200	20.2	1	.08	1
4*	1200	20.2	5	.4	1
5*	1200	20.2	5	.4	1
6	1640	27.5	18	1.1	5

*Pairs 3, 4, and 5 are internal comparisons of a cluster of three balloons.

These separations, presumably mainly due to eddy motions, appear surprisingly small. The mean vector error of hindcast trajectories is about 20% of the distance travelled. Compared to that error the effect of eddy motions on the trajectory appears negligibly small. We might be tempted to draw the conclusion that the unpredictable eddy motions contribute very little to the error in the trajectory hindcasts. This

conclusion is probably not correct. Owing to the various sizes of eddies encountered, the rate at which two balloons separate is a function of the distance between them (Richardson [26], Sutton [30], Durst and Gilbert [5]). This is illustrated in Figure 26 where two eddies of scale S are indicated. The two particles B_1 and B_2, a distance s ($s \ll S$) apart, will separate very little in a given time; whereas, the two particles B_1 and B_3, a distance S apart, will change distance rapidly.

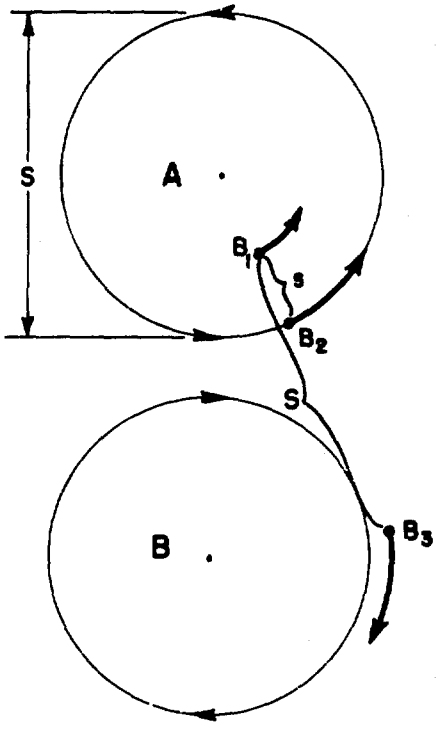

Figure 26. Illustration of the Effectiveness of Eddies in Separating Two Air Parcels as a Function of the Initial Separation and the Scale of the Eddies.

The separation of the balloons in Table VII only reached a magnitude of the order of 10-20 miles. This magnitude is much smaller than the averaging scale of the upper-level synoptic flow fields; hence, Table VII shows only the effect of the lower end of the eddy spectrum.

When we make a trajectory hindcast or forecast, we may think of the computed position and the verifying position as representing positions of a balloon pair. The separation between them is the forecast

error. The "computed balloon is not affected by eddies; the actual balloon is. The larger-scale eddies are particularly effective in causing large errors, but are much less effective in separating an actual balloon pair as long as their distances apart are of smaller scale than the eddies we consider. Hence, we cannot conclude from Table VII that eddy motion contributes only little to the error of computed trajectories. It should be recalled here that eddies were defined as motions of scales less than the averaging scales. The error in a computed trajectory is due to the errors in the smoothed motion as well as to eddies. In just what proportions these two enter is not possible to say at the present time. The smoothed flow is only very loosely defined in synoptic analysis practice, and we also have no ready means of obtaining the errors of analysis of this smoothed flow. We can state only that their combined effects is of the order of 15-20% of the distance travelled (see sub-section 1.13).

REFERENCES

[1] Anderson, A. D., "A Study of the Accuracy of Winds Derived from Transosonde Trajectories," NRL Memorandum Report 498, 1955.

[2] [Anon], "Tracking the Cross-Country Balloons," Air Weather Service Bulletin, November 1952.

[3] Brunt, D. and Douglas, C. K. M., Mem. Roy. Met. Soc., Vol. 3, No. 22, 1928; see also Brunt, D., Physical and Dynamical Meteorology, Cambridge University Press, 2d Ed., 1944, p. 195.

[4] Durst, C. S. and Davis, N. E., "Constant-Height Balloons — Calculation of Geostrophic Departures," Quart. Jn. Roy. Met. Soc., Vol. 76, 1950, pp. 75-86.

[5] Durst, C. S. and Gilbert, G. H., "Accuracy of Geostrophic Trajectories," MRP 574, Meteorological Office, London, 1950.

[6] Emmons, G., "Calculations of Geostrophic Deviations by Means of Balloon Trajectories," Res. Div., N. Y. Univ., Tech. Rept. 121.05, Contract AF 19(122)-45, June 1950, pp. 15-20.

[7] Ertel, H., "Ein neues Verfahren zur Konstruktionen von Trajektorien in Strömungsfeldern," Zeit. f. Angew. Math. u. Mech., Vol. 28, 1948, pp. 270-274.

[8] Forsythe, G. E., "Exact Particle Trajectories for Nonviscous Flow in a Plane with Constant Coriolis Parameter," Jn. Met., Vol. 6, No. 5, 1949, pp. 337-346.

[9] Franceschini, G. A., and Freeman, J. C., "Computation of Horizontal Trajectories in the Atmosphere," Texas A and M Research Foundation, Sci. Report No. 5, Contract AF 19(604)-559; Sci. Report No. 1, Contract AF 19(604)-1302, A and M Proj. 57 and 108, ref. 55-13T. Mimeo., January 1955, 18 pp.

[10] George, J. J., Bull. Amer. Met. Soc., Vol. 21, April 1940, p. 147.

[11] Godson, W. L., "A Study of the Deviations of Wind Speeds and Directions from Geostrophic Values," Quart. Jn. Roy. Met. Soc., Vol. 76, 1950, pp. 3-15.

[12] Gustafson, A. F., "Final Report on the Upper-Level Winds Project," UCLA Report on Contract W28-099-ac-403, 26 June 1949, mimeo. 7 pp. plus five Appendices.

[13] [Gustafson, A. F.], "The Computation of Air Trajectories," AWS TR 105-62, June 1950.

[14] Gustafson, A. F., "A Test of Perkin's Formula for the Central Wind Solution," Headquarters Air Weather Service, Washington, D. C. (in manuscript).

[15] Hesselberg, Th., "Über oszillatorische Bewegungen der Luft," Ann. Hydr. u. Mar. Met., Jg. 33, 1915, pp. 311-317.

[16] Hughes, L. A, Jordan, E. S., and Renard, R. D., "On the Computation of Winds from Constant Pressure Charts," Dept. of Meteorology, Univ. of Chicago, Report prepared under Navy Contract N6ori-02036, August 1953, 14 pp. Lithoprint.

[17] Lotz, K., "Über Trajektorien der Luft und deren Divergenz," Ann. Hydr. u. Mar. Met., Jg. 68, Heft VII, 1940, pp. 227-248.

[18] Machta, L., "Meteorological Trajectories," S.S. Div., USWB, (in manuscript), 1951.

[19] Machta, L., "A Mathematical Verification of Trajectory Methods," S.S. Div., USWB, (in manuscript), 1954.

[20] Mastenbrook, H. J., and Anderson, A. D., "Evaluation of the Transosonde System," NRL Memorandum Report No. 240.

[21] Meisinger, C. L., "The Constant Elevation Free-Balloon Flights from Fort Omaha," Mon. Wea. Rev., Vol. 47, 1919, pp. 535-538.

[22] Moore, C. B., Smith, J. R., and Gaalswyck, A., "On the Use of Constant-Level Balloons to Measure Horizontal Motions in the Atmosphere," Jn. Met., Vol. 11, 1954, pp. 167-172.

[23] Neiburger, M., and Angell, J. K., "Meteorological Applications of Constant-Pressure-Balloon Trajectories," Dept. of Met. UCLA, Report on work sponsored under ONR Contract Nonr 233 (21), 1955, ozalid 100 pp.

[24] Perkins, D. T., "On the Solution of the Equations of Motion for Linear Fields," Jn. Met., Vol. 7, 1950, pp. 291-303.

[25] Petterssen, S., Weather Analysis and Forecasting, McGraw-Hill, New York, 1940, pp. 221-223, (2nd Edition 1956).

[26] Richardson, L. F., "A Search for the Law of Atmospheric Diffusion," Beitr. z. Ph. fr. Atm., Vol. 15, 1929, pp. 24-29.

[27] Shaw, W. N., and Lempfert, R. G. K., "The Life History of Surface Air Currents," Meteorological Office, London, 1906.

[28] Stewart, H. J., "Kinematics and Dynamics of Fluid Flow," Handbook of Meteorology, McGraw-Hill, New York, 1945, p. 143.

[29] Sutcliffe, R. C., and Sawyer, J. S., "Forecasting Winds Up to the 100-mb Level by the Contour Chart Technique," Proc. Toronto Met. Conf., London, 1953.

[30] Sutton, O. G., "A Theory of Eddy Diffusion in the Atmosphere," Proc. Roy. Soc., London, Vol. A 135, 1932, p. 143.

[31] Wexler, H., "The Great Smoke Pall, September 24-30, 1950," Weatherwise, Vol. 3, pp. 129-134.

[32] AWS TR 105-139, "The Black Sheep System of Forecasting Winds for Long-Range Jet Aircraft," March 1956.

GPO 916188

DEPARTMENT OF THE AIR FORCE
AIR FORCE COMBAT CLIMATOLOGY CENTER (AFWA)
ASHEVILLE, NORTH CAROLINA 28801-5002

19 April 2005

MEMORANDUM FOR DTIC-OQ

ATTENTION: LARRY DOWNING
8725 JOHN J. KINGMAN ROAD
FORT BELVOIR, VA 22060-6218

FROM: Air Force Weather Technical Library
151 Patton Ave, Rm 120
Asheville, NC 28801-5002

SUBJECT: CHANGE CLASSIFICATION AND DISTRIBUTION STATEMENTS

1. AD873241 – A model of ionospheric total electron content.
2. AD117710 – Constant-pressure trajectories.
3. AD265052 – List of translations on meteorology and atmospheric physics, vol.II.
4. AD284757 – List of translations on meteorology and atmospheric physics, vol.III.
5. AD862101 – Meteorological resources and capabilities in the '70's. Proceedings of the 5th AWS Technical Exchange Conference, Air Force Academy, 14-17 July 1969.
6. AD227459 – List of translations on meteorology and atmospheric physics, vol.I.

All the above documents need to be changed to "Approved for Public Release, Distribution Unlimited" please.

Susan A. Tarbell

SUSAN A. TARBELL
Librarian, Classified Custodian,
DTIC Point of Contact

Attachment:
1. 6 copies of front covers